Dissertation
submitted to the
Combined Faculties for the Natural Sciences and for Mathematics
of the Ruperto-Carola University of Heidelberg, Germany
for the degree of
Doctor of Natural Sciences

presented by

Corinna Wagner, M.Sc.
born in Schwerte (Ruhr)

Oral-examination: July 17th 2014

Characterizing mitochondrial function and structure – Mitochondrial regulation of apoptosis and visualization of mitochondria - endoplasmic reticulum interactions

Referees:

PD Dr. Karsten Rippe (DKFZ, Heidelberg)

Prof. Dr. Ana J. García Sáez (Universität Tübingen)

Eidesstattliche Erklärung

Ich erkläre hiermit, dass ich die vorliegende Dissertation selbst verfasst und mich keiner anderen als der von mir ausdrücklich bezeichneten Quellen und Hilfsmittel bedient habe. Diese Dissertation wurde in dieser oder anderer Form weder bereits als Prüfungsarbeit verwendet, noch einer anderen Fakultät als Dissertation vorgelegt. An keiner anderen Stelle ist ein Prüfungsverfahren beantragt.

Heidelberg, den 20.05.2014

Corinna Wagner

Table of Contents

Abbreviations

5-FU	5-fluoruracil
ACAT	Acyl-CoA:cholesterol acyltransferase
APAF-1	Apoptotic protease activating factor-1
ATP	Adenosine triphosphate
Bap31	B-cell receptor-associated protein 31
BH	Bcl-2 homology
CCCP	Carbonyl cyanide *m*-chlorophenyl hydrazone
CD95L	CD95 ligand
DcR3	decoy receptor 3
DIABLO	Direct IAP binding protein with low pI
DMEM	Dulbecco's Modified Eagle Medium
DR	Death receptor
Drp 1	Dynamin-related protein 1
EGFR	Epidermal-growth-factor receptor
ER	Endoplasmic reticulum
FACL4	Fatty acid-CoA ligase type 4
FADD	Fas-Associated protein with Death Domain
$FADH_2$	Flavin adenine dinucleotide
FCS	Fetal calf serum
Fis1	Fission-1 homolog
FLICE	FADD-like interleukin-1 ß-converting enzyme
FLIP	FLICE-like protease – inhibitory protein
Grp75	Glucose regulated protein 75
Grp78	78-kDa glucose regulated protein
HPV	Human papillomavirus
IAP	Inhibitor of apoptosis protein
IM	Inner (mitochondrial) membrane
IMS	Intermembrane space
IP_3R	Inositol triphosphate receptor
MAM	Mitochondria associated membrane
MCU	Mitochondrial calcium uptake
Mfn	Mitofusin

MOM	Mitochondrial outer membrane
MOMP	Mitochondrial outer membrane permeabilization
NADH	Nicotinamide adenine dinucleotide
PACS-2	Phosphofurin acidic cluster sorting protein 2
PBS	Phosphate buffered saline
PDGFR	Platelet-derived growth-factor receptor
PSS-1	Phosphatidylserine synthase-1
Rb	Retinoblastoma protein
sCD95	soluble CD95
SDS -PAGE	SDS-polyacrylamide gel electrophoresis
Sig-1R	Sigma-1 receptor
SMAC	Second mitochondria-derived activator of caspase
STED	Stimulated emission depletion
TNF	Tumor-necrosis factor
TNF-R1	TNF receptor 1
TRAIL	TNF-related apoptosis-inducing ligand
VDAC	Voltage dependent anion channel

Abstract

Mitochondria are the powerhouse of the cell generating most of the energy for cellular mechanisms in form of ATP (adenosine triphosphate). Another important role of mitochondria is the regulation of programmed cell death, apoptosis. Apoptosis, in turn, is regulated by a complex protein network, the Bcl-2 protein family. There is a fine balance within the about 25 Bcl-2 proteins between pro- and antiapoptotic proteins. If control gets lost, cells may gain resistance to apoptosis, they can divide in an uncontrolled manner resulting in tumors and diseases like cancer may develop. The second leading cause of cancer deaths in women is cervical cancer. For proving that human papillomaviruses (HPV) are the causative agents of cervical cancer, Harald zur Hausen, a scientist of the German Cancer Research Center, Heidelberg, was awarded the Nobel Prize in 2008. In this study, one aim is to find out which antiapoptotic proteins are responsible for cervical cancer cells to become resistant to apoptosis. Using a specific method called BH3 profiling, Bcl-xL upregulation in cervical cancer cells is suggested to be responsible for apoptosis resistance. This data is supported by knock-down of Bcl-xL in cervical cancer cells finding them to regain apoptosis sensitivity. Furthermore, Bcl-2 proteins have been shown to control Ca^{2+} influx from ER (endoplasmic reticulum) into mitochondria and thus regulate apoptosis since high mitochondrial Ca^{2+} levels lead to the induction of apoptosis. Ca^{2+} transfer takes place at very tight interaction sites between mitochondria and ER called ER-mitochondria contact sites or mitochondria associated membranes (MAMs). More and more proteins are becoming evident to play a role in keeping those two organelles in close contact. However, the structural organization of those proteins is unknown. Since the distance between mitochondria and ER at their contact sites is only between 10 and 25 nm, it is impossible to resolve those structures with conventional confocal microscopy. This is why in this study the high resolution microscopy technique STED (stimulated emission depletion) is used to visualize MAMs. Thus, the second aim of this thesis is to image ER-mitochondria contact sites via STED microscopy to gain a deeper structural insight of these sites. A labeling strategy was established for the used STED microscopy setup to image ER, mitochondria and, as an example for a MAM protein of interest, Grp78. High resolution images could be obtained for mitochondria and Grp78 and the distribution of Grp78 with respect to the ER could be visualized. Using the here established MAM labeling strategy for STED microscopy and studying further MAM proteins in the future will enable the structural analysis of ER-mitochondria contact sites in more detail.

In summary, this study provides insights into mitochondrial function and structure. 1) apoptosis regulation in cancer cells via the Bcl-2 protein network is studied, and 2) the interaction of mitochondria and the ER is visualized via high resolution STED microscopy to gain a deeper insight into the structural organization of the MAMs.

Zusammenfassung

Mitochondrien sind das Kraftwerk der Zelle. Dort wird der Hauptteil der Energie für zelluläre Mechanismen in Form von ATP (Adenosintriphosphat) gebildet. Eine andere wichtige Rolle nehmen Mitochondrien in der Regulierung des programmierten Zelltods, der Apoptose, ein. Apoptose wird durch ein komplexes Proteinnetzwerk, das Bcl-2 Netzwerk mit circa 25 Bcl-2 Proteinen, reguliert. Die Bcl-2 Proteine sind genau aufeinander abgestimmt, sodass pro- und antiapoptotische Proteine im Gleichgewicht stehen. Wird dieses Gleichgewicht gestört, können Zellen resistent gegen Apoptose werden und sich dann unkontrolliert teilen, was zu der Entstehung von Tumoren und letztendlich zu Krankheiten wie Krebs führen kann. Die zweithäufigste Todesursache der Krebserkrankungen bei Frauen ist Gebärmutterhalskrebs. Für den Beweis, dass humane Papillomviren (HPV) die Ursache der Entstehung von Gebärmutterhalskrebs sind, erhielt Harald zur Hausen, Wissenschaftler am Deutschen Krebsforschungszentrum, Heidelberg, 2008 den Nobelpreis. Ein Ziel der vorliegenden Arbeit besteht darin herauszufinden, welche antiapoptotischen Proteine dazu führen, dass Gebärmutterhalskrebszellen apoptoseresistent werden. Dazu wurde in dieser Studie eine spezifische Methode, genannt BH3 Profiling, angewendet. Sie zeigte, dass die Hochregulierung von Bcl-xL in Gebärmutterhalskrebszellen die mögliche Ursache hierfür sein könnte. Dieses Ergebnis wird durch weitere Experimente gestützt, in denen Bcl-xL in Gebärmutterhalskrebszellen herunterreguliert wurde. Dieser knock-down von Bcl-xL führte dazu, dass die Zellen ihre Apoptosesensitivität zurückerlangten. Unabhängig davon besitzen Bcl-2 Proteine außerdem die Eigenschaft den Ca^{2+} - Einfluss vom ER (endoplasmatischen Reticulum) in die Mitochondrien zu kontrollieren. Dies ist eine weitere Möglichkeit der Apoptoseregulation, da hohe Ca^{2+} - Konzentrationen in den Mitochondrien zur Apoptoseinduktion führen. Der Ca^{2+} - Transfer findet an Kontaktstellen zwischen Mitochondrien und ER statt, die MAMs (mitochonria associated membranes) genannt werden. Die Zahl der identifizierten Proteine, die bedeutend für den Zusammenhalt der zwei Organellen sind, steigt stetig. Allerdings ist die strukturelle Anordnung dieser Proteine unbekannt. Da der Abstand zwischen Mitochondrien und ER and den MAMs nur zwischen 10 und 25 nm beträgt, ist es nicht möglich diese Strukturen mit konventioneller Konfokalmikroskopie aufzulösen. Deshalb wird in dieser Studie die hochauflösende Mikroskopietechnik STED (stimulated emission depletion) eingesetzt. Dahingenend ist das zweite Ziel dieser Arbeit MAMs mithilfe der STED Mikroskopie zu visulaisieren um einen tieferen Einblick in den Aufbau dieser Strukturen zu ermöglichen. Dafür wurden Markierungsverfahren etabliert, um ER, Mitochondrien und, als ein Beispiel für ein MAM-

Protein, Grp78 an dem verwendeten STED Mikroskopieaufbau zu visualisieren. Das Ergebnis sind hochaufgelöste, zweifarbige Bilder von Mitochondrien und Grp78 und die Proteinverteilung von Grp78 konnte in Bezug zum ER visualisiert werden. Mithilfe der hier etablierten Markierungsstrategie von MAMs für die STED Mikroskopie und indem weitere MAM Proteine analysiert werden, wird es zukünftig möglich sein einen tieferen Einblick in die Struktur von MAMs zu bekommen.

Zusammenfassend gibt die vorliegende Arbeit einen Einblick in Mitochondrienfunktion und –struktur. 1) Die Apoptoseregulierung von Krebszellen durch das Bcl-2 Proteinnetzwerk wird untersucht und 2) die Interaktion von Mitochondrien und ER wird mithilfe von hochauflösender STED Mikroskopie visualisiert, um einen tieferen Einblick in die Struktur von MAMs zu bekommen.

I.Introduction

1. Mitochondria: Structure and Function

Mitochondria are membrane-bound organelles, which are found in nearly all eukaryotic cells. They range from 0.5 to 1 µm in diameter and vary in number and location according to cell type. Those organelles often form a complex 3D branching network inside the cell [1] (Figure 1A).

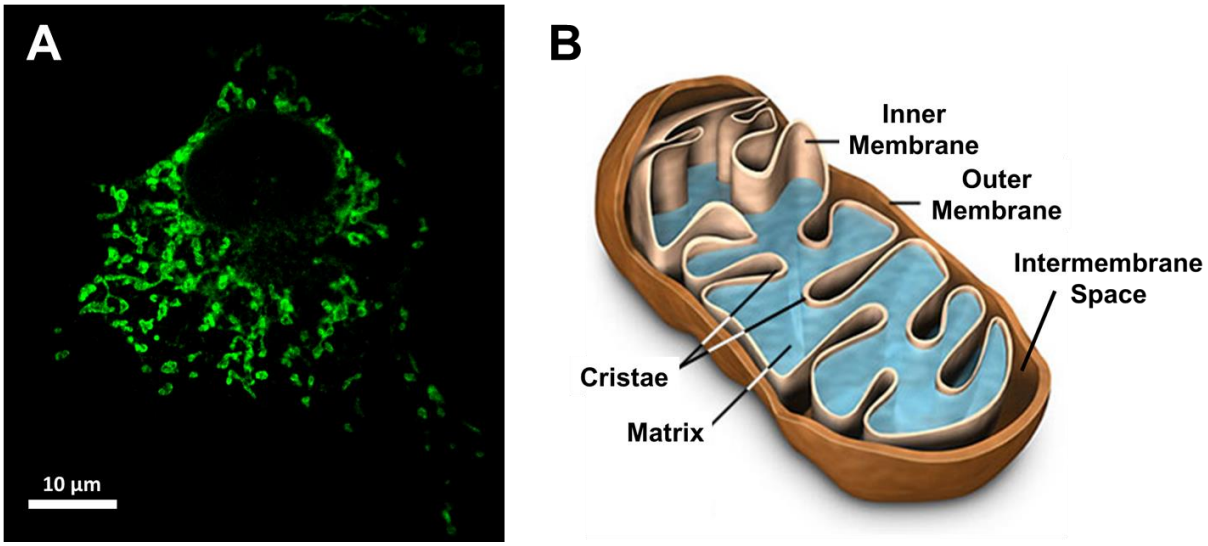

Figure 1: (A) Mitochondrial staining of Cos-1 cell: Tom20 – Atto565 immunocytochemistry staining. (B) Mitochondria structural features (adapted from [2]).

Mitochondria are often described as the "energy powerhouse of the cell" because they generate most of the cell's supply of adenosine triphosphate (ATP). Another important function of these organelles is the regulation of programmed cell death (apoptosis - described in chapter 3) [3].

1.1. Mitochondrial Structure

Mitochondria are composed of several compartments, which carry out distinct functions: These compositionally and functionally distinct regions include the outer mitochondrial membrane (MOM), the intermembrane space (IMS), the inner membrane (IM), the cristae and the matrix (Figure 1B).

The MOM contains large channel-forming proteins, called porins, which enable molecules up to 5000 Daltons to freely diffuse through the MOM. Larger proteins can enter the mitochondrion if they contain a mitochondrial signaling sequence, which binds to the so-called translocase in the MOM actively importing proteins. Furthermore, this membrane contains enzymes involved in mitochondrial lipid synthesis [1, 4]. Another important fact about the MOM is that it is an important site during apoptosis, during which it is

permeabilized by the proapoptotic proteins Bak and Bax. This event is called mitochondrial outer membrane permeabilization (MOMP). MOMP can be antagonized by proteins also located in the MOM. Thus the MOM is an important location for apoptosis regulation [5]. (Detailed description in chapter 3.)

The intermembrane space is the compartment between the outer and inner mitochondrial membrane. It contains several enzymes, which phosphorylate molecules using the ATP produced in the mitochondria [1]. The inner membrane (IM) is folded into many cristae, which hugely expand the surface area of the IM. It contains many different proteins with several functions: Firstly, it incorporates proteins, which carry out the redox reactions of oxidative phosphorylation (for details see below). Secondly, the ATP synthase is localized to the IM, which generates ATP. Thirdly, the IM contains transport proteins that regulate the transport of metabolites into and out of the matrix. Furthermore, an electrochemical gradient of protons is established across the IM, which drives the ATP synthase. The matrix is the compartment enclosed by the IM. It contains a high number of many different enzymes. They are mainly required for ATP synthesis, oxidation of pyruvate and fatty acids, and for the citric acid cycle. Additionally, there are enzymes for the expression of mitochondrial genes since the matrix contains the mitochondria's own DNA genome and thus also mitochondrial ribosomes and tRNAs [1]. Mitochondrial DNA (mtDNA) is a circular, double-stranded DNA molecule with a size of about 16 kb. Cells contains between 100 and 10 000 copies of mtDNA. MtDNA codes for 37 genes. 13 genes encode components of the respiratory chain, 22 for mitochondrial tRNA molecules, and two for rRNA molecules. Human mtDNA lacks introns, thus being very efficient with about 93% representing a coding region. Furthermore, the mitochondrial genetic code is slightly different from nuclear DNA. Mitochondria use different stop codons and the codon for isoleucine in nuclear DNA encodes for methionine in mitochondria [6].

1.2. ATP generation

One of the most important functions of mitochondria is the production of ATP. They produce ATP via oxidative phosphorylation. Pyruvate and fatty acids are transported from the cytosol across the IM and are converted into acetyl CoA in the matrix. Acteyl CoA is oxidized in the matrix via the citric acid cycle into CO_2 and the cycle generates high-energy electrons carried by the activated carrier molecules NADH and $FADH_2$. These high-energy electrons are transferred to the IM where they enter the electron-transport chain (Figure 2) [1].

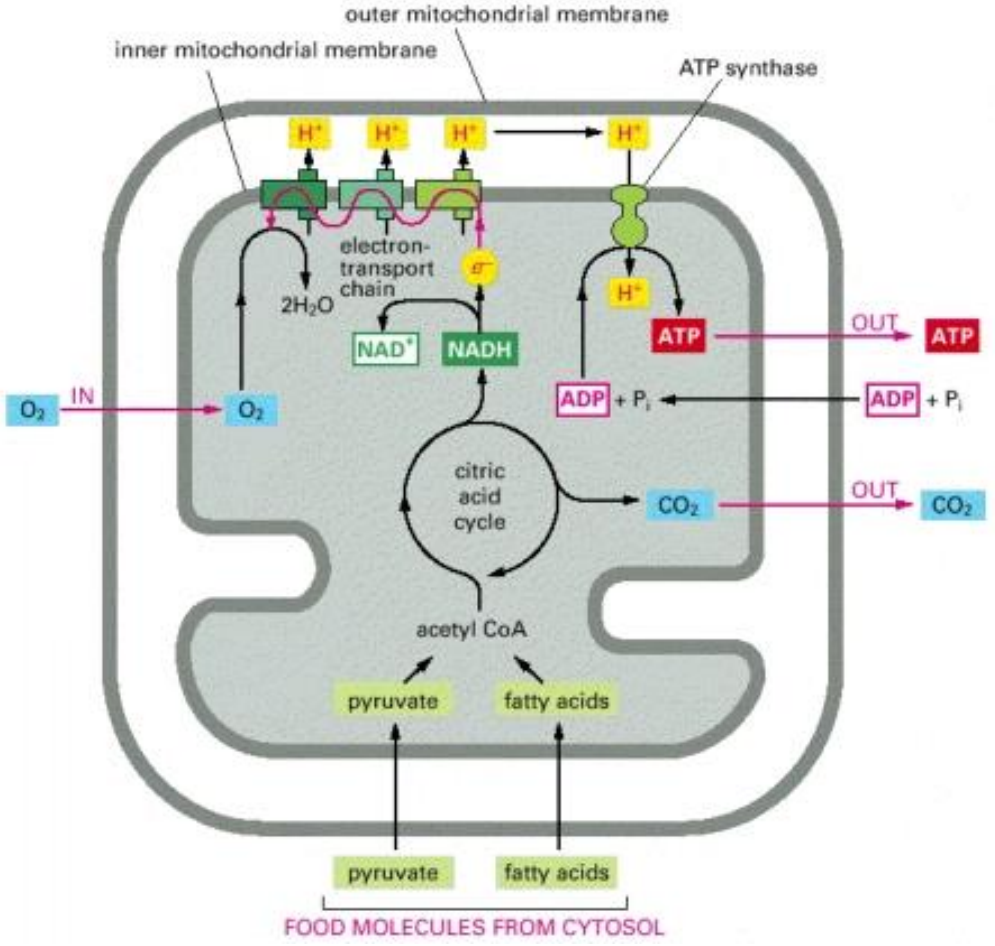

Figure 2: Energy-generating metabolism in mitochondria. Fatty acids and pyruvate enter the mitochondrion and are turned into acetyl CoA. Acetyl CoA is metabolized by the citric acid cycle generating NADH from NAD^+ (and FADH2 from FAD, not shown). NADH (and FADH2) then transfer high-energy electrons to the electron-transport chain in the inner mitochondrial membrane in the process of oxidative phosphorylation. Here electrons are passed along onto finally oxygen. The electron transport chain generates a proton gradient across the inner mitochondrial membrane, which drives ATP production by the ATP synthase. (From [1].)

The electron transport chain (also termed respiratory chain) embedded in the IM performs sequential redox reactions resulting in proton pumping from the matrix into the IMS. Electrons are transported along electron carriers in the respiratory chain. Those electron carriers can be metal ions embedded in porphyrin rings like heme groups bound to cytochromes. The embedded iron atom changes from the ferric oxidation state (Fe^{3+}) to the ferrous oxidation state (Fe^{2+}) whenever it accepts an electron. Other examples for electron carriers are iron-sulfur proteins, small hydrophobic molecules like ubiquinone, and flavin.

There are three complexes, which all act as an electron-transport-driven proton pump (Figure 3) [1].

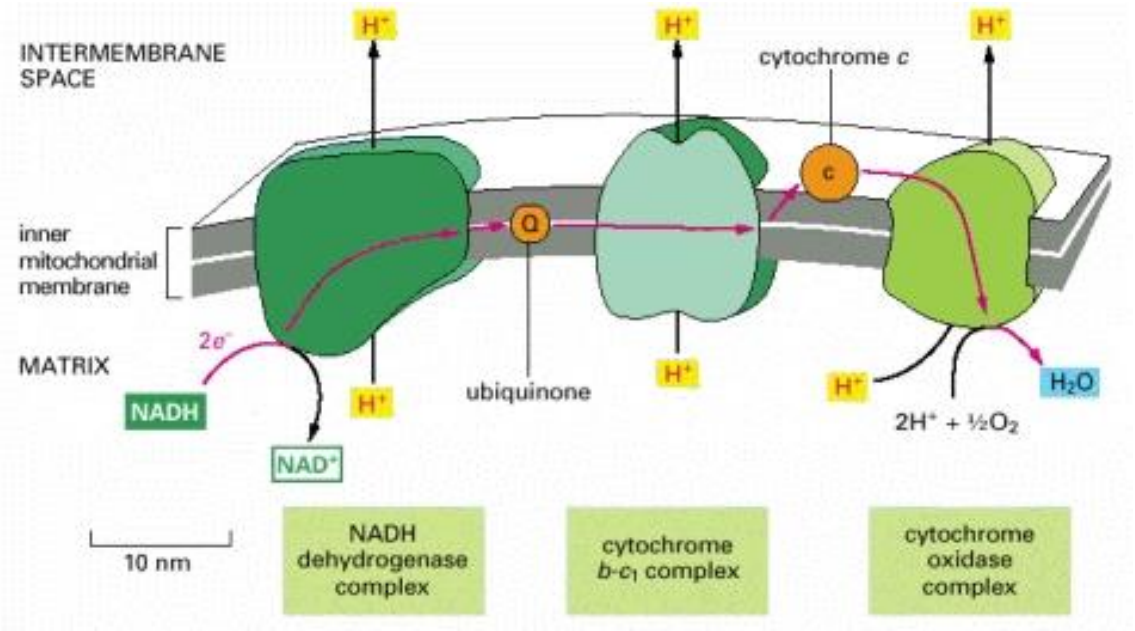

Figure 3: The three respiratory enzyme complexes. Electrons are transferred from NADH to oxygen (red lines). Ubiquinone and cytochrome c serve as mobile carriers ferrying electrons from one complex to the next. During electron transfer, protons are pumped across the inner mitochondrial membrane by each respiratory complex. (From [1].)

Complex I, the NADH dehydrogenase complex, is the largest of the respiratory enzyme complexes. It accepts electrons from NADH and passes them through a flavin and iron-sulfur centers to ubiqinone. Ubiquinone transfers the electrons to comlex II, the cytochrome b-c_1 complex. Electrons are passed through hemes bound to cytochromes and an iron-sulfur protein on to cytochrome c, which carries its electron to complex III, the cytochrome oxidase complex containing two cytochromes and two copper atoms. This complex finally passes electrons to oxygen. The transfer of electrons along the respiratory chain is coupled to a transfer of H^+ across the IM from the matrix to the intermembrane space. Electron carriers are closely associated with protein molecules transporting protons by allosteric changes in protein confirmation caused by electron transport. Thus a pH gradient across the IM and a voltage gradient (mitochondrial membrane potential) is generated together constituting a so-called electrochemical proton gradient. This proton gradient is released through the ATP synthase machine, which drives oxidative phosphorylation from ADP to ATP. The ATP synthase consists of a rotating head facing the matrix and a transmembrane stator consisting of a narrow channel. Protons pass through the narrow channel causing the head to spin. Thus mechanical energy is produced by the proton flow. The enzyme head contains binding sites for ADP and inorganic phosphate, which are driven to form ATP as mechanical energy is converted into chemical bond energy [1].

1.3. Mitochondrial dynamics

Mitochondrial structure and their cellular location are important for the function of these organelles. Mitochondria are mobile and very dynamic organelles, which constantly fuse and divide. Thus motility, division and fusion, and tethering determine mitochondrial shape, connectivity, and location of mitochondria within cells. Mitochondria are for example transported on microtubules to sites of synaptic activity where ATP is required for synaptic vesicle release. This mitochondrial transport is mediated by the MOM protein Miro, which links the mitochondrial surface with the microtubule motor protein Milton [7].

Mitochondrial division and fusion is mediated by dynamin-related GTPases: Drp1 (Dynamin-realted protein 1) mediates division and Mfn (Mitofusin) 1/2 and Opa1 mediate fusion. In healthy cells fusion is balanced by division, which creates organelles of the appropriate size for transport along actin or the microtubule network. However, during apoptosis mitochondria fragment due to increased recruitment of Drp1 to the mitochondria. Contrarily, mitochondrial fusion protects the cell from apoptosis.

Mitochondrial distribution and dynamics are influenced by physical connections between the MOM and diverse intracellular membranes such as the plasma membrane, peroxisomes, ER, autophagosomes, and lysosomes. Those mitochondria associated membranes play a role in processes, which involve more than one organelle such as Ca^{2+} homeostasis and lipid biosynthesis. An example for a physical connection between mitochondria and another intracellular membrane, which has been shown to be important for many housekeeping functions of the cell, is the association between the MOM and the ER. Those ER-mitochondria contact sites have also been shown to play an important role in mitochondrial dynamics since ER tubules wrap around mitochondria during mitochondrial division and likely constrict mitochondria. Thus ER-mitochondria contact sites mark the points of mitochondrial division [8].

2. ER – Mitochondria Contact Sites

ER-mitochondria contact sites were identified by the observation that some ER membranes co-purified with mitochondria in velocity sedimentation experiments. These close contact sites between ER and mitochondria were called MAMs (mitochondria associated membranes) [9]. The direct molecular contact between ER and mitochondria could also be inferred from their proximity assessed by electron microscopy [8]. However, only a small area of the MOM (12%) is estimated to associate with the ER. Furthermore, electron tomography results have

shown that the minimum distance between ER and mitochondria is 10 – 25 nm. Such a short distance enables ER proteins to directly associate with proteins and lipids of the MOM [10]. The mitochondria co-sedimenting ER fraction contained lipid biosynthesis enzymes. Thus it was inferred that the MAMs are sites of lipid exchange and biosynthesis [10]. Another indirect inference was the Ca^{2+} trafficking function of the MAM [11].

2.1. Organization of ER-mitochondria contact sites (MAMs)

ER-mitochondria contact sites have been studied extensively during the last years and more and more proteins have been identified to be involved in the structural and functional link of the MAMs. Some of the proteins involved in ER-mitochondria contact sites are depicted in Figure 4.

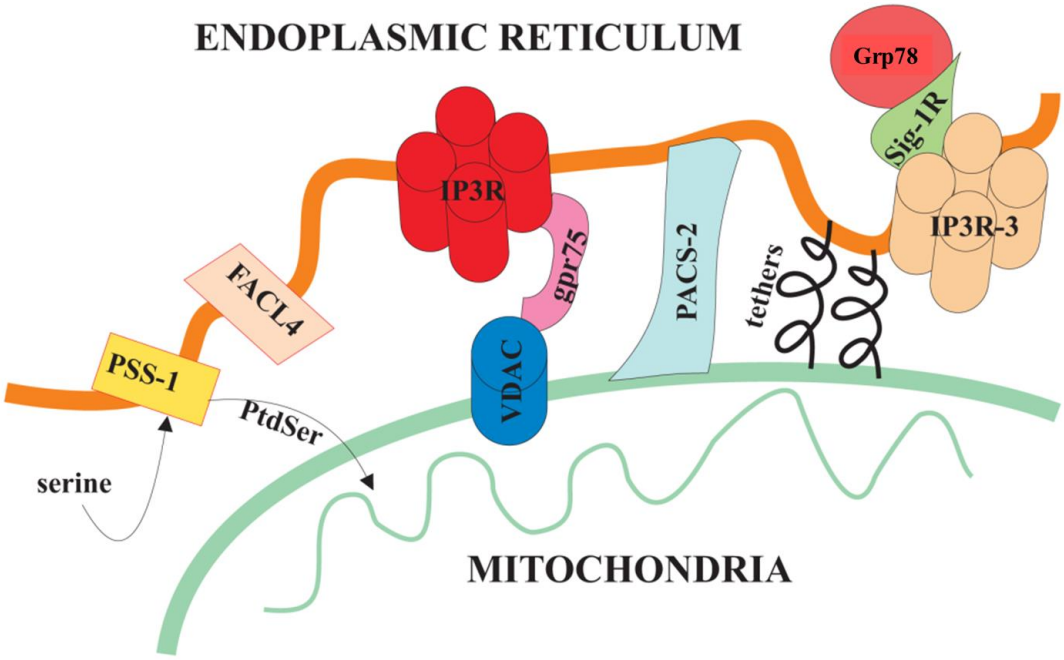

Figure 4: Schematic representation of the structural organization of the MAM with key players in lipid metabolism (PSS-1, FACL4), Ca^{2+} signaling (IP3R, VDAC), chaperones (PACS-2, Grp75 and 78, Sig-1R), and peptidic tethers keeping ER and mitochondria in close contact (adapted from Giorgi *et al.* 2009 [12])

The physical connection of ER and mitochondria is mediated by proteins and protein complexes. But the exact nature of the ER-mitochondria contact domain is still unclear. The core components of ER-mitochondria contact sites are not conserved between yeast and metazoans. In Metazoa the composition of those sites is quite complex and many proteins may participate in ER-mitochondria tethering. One example is the connection between the nonselective porin VDAC (voltage dependent anion channel) in the mitochondria and the Ca^{2+} channel IP_3R (inositol triphosphate receptor) in the ER via the cytosolic chaperone Grp75 (glucose regulated protein 75) (Figures 4 and 6). This interaction may participate in

tethering and positions the Ca^{2+} channel opposite to the porin for optimal Ca^{2+} transfer [11]. Besides Ca^{2+} exchange, another important function of ER-mitochondria contact sites is lipid biosynthesis and the direct transfer of lipids between ER and mitochondria. Examples for lipid synthesizing enzymes found at the MAMs are FACL4 (fatty acid-CoA ligase type 4) and PSS-1 (phosphatidylserine synthase-1). In addition, the chaperone PACS-2 (phosphofurin acidic cluster sorting protein 2) has been found at the MAM, a multifunctional sorting protein, which e.g. controls the apposition of mitochondria and ER and the formation of ER lipid-synthesizing centers [12]. Other examples for MAM proteins are the homo- and heterotypic interactions of ER-bound Mfn2 (mitofusin-2) with mitochondrial Mfn2 and Mfn1, and the interaction of Bap31 (B-cell receptor-associated protein 31) with Fis1 (Fission-1 homolog) in the mitochondria [11].

2.2. Functions at the MAM

The physiological role of ER-mitochondria contact sites was first thought to be limited to lipid and calcium exchange between the two organelles. But it is becoming more and more obvious that these contact sites also play an important role in mitochondria dynamics [11].

2.2.1. Lipid exchange and biosynthesis

Lipid exchange and biosynthesis is the first function described for ER-mitochondria contact sites [9]. Nevertheless, most membrane lipid bilayers are assembled in the ER and nearly all of the major classes of lipids are synthesized in the ER membrane including phospholipids like phosphatidylcholine and cholesterol. Lipids forming mitochondrial membranes need to be imported form the ER [1]. Besides biosynthesis of phosphatidylcholine in the ER there is another biosynthesis pathway including mitochondria (Figure 5): phosphatidylcholine (PC), which is present in the inner and outer mitochondrial membrane, can be synthesized by traveling between ER and mitochondria involving several enzymes residing in mitochondria and ER: The starting product of this PC synthesis pathway is serine. It is converted into phosphatidylserine (PS) in the ER by the PS synthase (PSS). PS is transported to mitochondria and converted into phosphatidylethanolamine (PE) by the mitochondrial enzyme PS decarboxylase (PSD). PE is transported back into the ER and reacts to PC by three successive methylation steps, which are performed by PE methyl transferases (PEMT) located in the ER. PC then needs to travel back to mitochondria. The exchange of the products between ER and mitochondria is probably catalyzed by lipid transporter proteins, but their identity remain elusive [11].

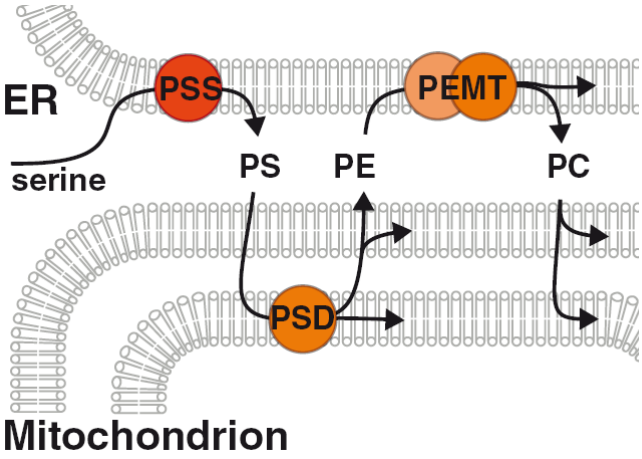

Figure 5: De novo phosphatidylcholine (PC) biosynthesis pathway starts with serine converted to phosphatidylserine (PS) by the PS synthase (PSS) in the ER. PS is changed into phosphatidylethanolamine (PE) by the mitochondrial PS decarboxylase (PSD). PE is transported back into the ER and methylated by PE methyl transferase (PEMT) into PC. (Adapted from Kornmann [11].)

2.2.2. Ca^{2+} exchange

The second main function of ER-mitochondria contact sites is the exchange of Ca^{2+}. This exchange serves several purposes: Firstly, it regulates cellular bioenergetics since some mitochondria matrix-localized citric acid cycle enzymes involved in ATP-production are Ca^{2+}-dependent. Secondly, the Ca^{2+} exchange is cytoprotective: by uptaking Ca^{2+}, released from the ER, mitochondria may prevent a cytotoxic cytosolic Ca^{2+} accumulation. Thirdly, Ca^{2+} exchange may also be cytotoxic because Ca^{2+} accumulation in the matrix can trigger the opening of the mitochondrial permeabilization transition pore, which leads to the release of cytochrome c and other proapoptotic factors into the cytosol to induce apoptosis [11].

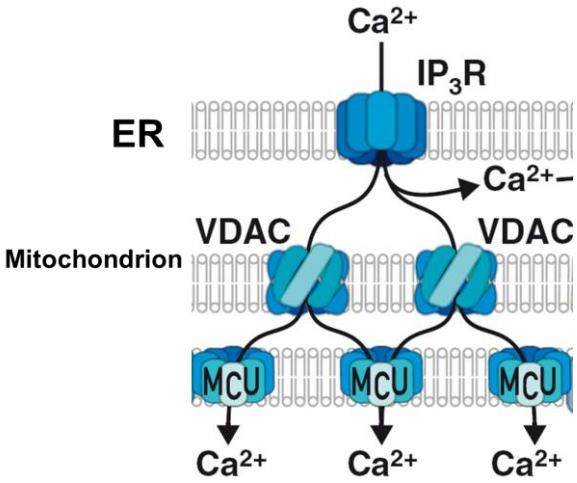

Figure 6: Ca^{2+} transfer from ER to mitochondria. Ca^{2+} is released from the ER through the IP_3R channel and taken up into the mitochondria by the nonselective MOM porine VDAC and the inner membrane Ca^{2+} uniport MCU. (Adapted from Kornmann [11].)

As mentioned above, Ca^{2+} is transported from the ER via IP_3R through the nonselective porins VDACs in the MOM (Figure 6). Ca^{2+} crosses the IM through a Ca^{2+} uniport (MCU) [11]. The cytosolic chaperone Grp75 regulates IP_3R-mediated Ca^{2+} signaling since it physically links IP_3R and VDAC (Figure 4). The resulting association probably enhances the Ca^{2+} accumulation in mitochondria by stabilizing the coupling of the two receptors [13]. For Ca^{2+} transfer the Sig-1R (Sigma-1 receptor) chaperone has also been shown to play an interesting role: Sig-1Rs associate with IP_3R-3 at the MAM, form a Ca^{2+} -sensitive chaperone machinery together with Grp78 (78-kDa glucose-regulated protein, also referred to as the immunoglobulin binding protein BiP) (Figure 4), and prolong Ca^{2+} signaling from ER to mitochondria by stabilizing IP_3R-3 at the MAM [14]. This association between Sig-1Rs and Grp78 takes place under normal conditions in which the ER luminal Ca^{2+} concentration is 0.5 – 1.0 mM. However, upon the activation of IP3 receptors, which causes a decrease of the Ca^{2+} concentration at the MAM, Sig-1Rs dissociate from Grp78 to chaperone type-3 IP_3 receptors, which would otherwise be degraded by proteasomes. The Sig-1R thus ensures proper Ca^{2+} signaling from ER into mitochondria [14].

2.2.3. Regulation of mitochondrial dynamics by MAM residing proteins

The interactions between ER and mitochondria seem to be modulated by mitochondria-shaping proteins like the mitochondrial fusion proteins Mitofusin 1 and 2 the fission protein Drp-1. Friedman et al. observed that mitochondrial division takes place at ER-mitochondria crossovers. ER tubules may mediate physical constriction before Drp1 recruitment. Thus, ER may be important for defining mitochondrial fission sites [8]. In addition, Miro, a MOM protein that is involved in microtubule-based mitochondrial movement, localizes at ER-mitochondria contact sites. Thus, it has been suggested that mitochondrial movement occurs in synchrony with that of specific ER regions [15].

In yeast ER-mitochondria contact sites are involved in the inheritance of mitochondria of budding yeast. Mitochondria are transported to the yeast bud, and anchor to the cortical ER, which is associated with the plasma membrane, that prevents reverse movement of mitochondria back into the mother [16].

2.3. Ca^{2+} transfer between ER and mitochondria regulates apoptosis

During normal signaling conditions there is a continuous flow of Ca^{2+} between mitochondria and ER. The bulk amount of Ca^{2+} inside the ER functions as a reservoir of signal Ca^{2+} and is important for maintaining chaperone activity, which is essential for protein processing. An

alteration of ER-mitochondria contact sites provides a pathway for activating apoptosis [17]. Apoptosis can be triggered upon ER stress. This can lead to an alteration of Ca^{2+} homeostasis at the MAM resulting in an increase of the mitochondrial Ca^{2+} concentration. When a critical threshold is reached, apoptosis is induced by the translocation of the proapoptotic proteins Bax and Bak from the cytosol to the MOM leading to permeabilization of the MOM resulting in cytochrome c release. This leads to mitochondrial potential loss followed by caspase-9 activation [12] (details described below).

As mentioned above, the mitochondrial fission protein Drp1 localizes to the MAM. Drp 1 has been shown to colocalize with Bax at mitochondrial constriction sites during apoptosis. At these ER-mitochondria contact sites Bax-dependent MOMP takes place initiating apoptosis [18]. Cytochrome c, which is released from mitochondria during the apoptotic process, can bind IP_3 receptors (IP_3Rs) located at the MAM, further activating Ca^{2+} flux enhancing apoptotic signaling [19]. In agreement, cells, which are deficient of IP_3Rs, are resistant to apoptosis [20]. Furthermore, IP_3 receptor 1 (IP_3R-1) has been shown to physically interact with the antiapoptotic protein Bcl-2 at the ER surface. Here, Bcl-2 family members may regulate IP_3R-1 phosphorylation and thus control the rate of ER Ca^{2+} leak from intracellular stores regulating apoptosis [21, 22]. For example Bcl-2 overexpression has been shown to decrease the steady-state Ca^{2+} content of the ER. This results in a lower Ca^{2+} signal-release and less cytosolic and mitochondrial Ca^{2+} response. Thus Bcl-2 can protect from Ca^{2+} -dependent apoptotic stimuli [23]. Besides, it has been shown that the knock-down of proapoptotic Bax and Bak also leads to a reduction of the steady-state Ca^{2+} concentration of the ER. Those knock out cells were more resistant to apoptosis [24]. In contrast, overexpression of Bax resulted in a higher ER Ca^{2+} content and those cells were more susceptible to apoptosis [25]. In conclusion, manipulating ER Ca^{2+} levels has an influence on the amount of mitochondrial Ca^{2+} exposure regulating apoptosis.

Besides influencing mitochondrial apoptosis, the MAM has also been shown to be involved in death receptor induced, namely Fas-signaling-induced apoptosis. Upon this signaling-cascade IP3 production is increased. As a consequence increasing amounts of Ca^{2+} are released from IP3 receptors inducing apoptosis [26].

3. Apoptosis

Apoptosis is the form of cell death, which is also known as programmed cell death, because during apoptosis a “suicide” program is activated within the cell. Apoptosis is necessary to

control the number of cells in a multicellular organism: The rate of cell death and cell division needs to be exactly balanced to maintain tissue homeostasis. Furthermore, apoptosis plays an important role in developing animal tissues since, for example, in the developing vertebrate nervous system about half of the nerve cells die soon after they are formed. In a healthy adult human, billions of cells die in the intestine and bone marrow due to apoptosis every hour. Defects in apoptosis can lead to many different diseases, e.g. insufficient apoptosis results in uncontrolled cell proliferation and cancer may develop [1].

Execution of apoptosis

A cell undergoing apoptosis dies without lysing or damaging neighboring cells. This form of cell death is contrary to necrosis, which is a result of acute injury. During necrosis cells typically swell and burst spilling their contents all over their neighbors causing a potentially damaging inflammatory response. Thus, in comparison to necrotic cells, apoptotic cells die neatly. They undergo organized degradation of cellular organelles and show a characteristic morphology: Cells shrink and round because of the breakdown of the cytoskeleton. The cytoplasm condenses and the organelles are tightly packed. Chromatin condenses and the nuclear envelope disassembles. Nuclear DNA is fragmented and the nucleus breaks into chromatin bodies. The cell membrane forms blebs, which are irregular buds. Finally, the cell breaks apart into vesicles called apoptotic bodies, which are rapidly phagocytosed by neighboring cells or macrophages before any leakage of the cellular contents occurs. Thus the organic components of dead cells become recycled [1, 27].

Apoptosis is mediated by an intracellular proteolytic cascade

The intracellular machinery responsible for those apoptotic changes depends on so-called caspases. These are proteases that have a cysteine at their active site and cleave their target proteins at specific aspartic acids. There are two types of apoptotic caspases in the cell: initiator and effector caspases. Both caspases exist in the cell as so called procaspases, which are inactive precursors. Those procaspases are activated by cleavage by other caspases. Initiator caspases cleave inactive pro-forms of effector caspases thereby activating them. Effector caspases are the effectors of the apoptotic program in the cell cleaving key proteins, which leads to the degradation of the cell as described above [1]. Apoptotic stimuli cause the clustering of initiator caspases enabling them to cleave each other, which leads to the activation of initiator caspases enabling them to activate the effector caspases. Caspase activity is tightly regulated inside the cell to ensure that cell death is only carried out when needed. In principle, there are two alternative pathways to activate caspases and initiate

apoptosis: One is called the “extrinsic pathway”, which is mediated by death receptors on the cell surface and the other one is referred to as the “intrinsic pathway”, which is mediated by mitochondria (Figure 7) [27]. Both pathways will be described in the following.

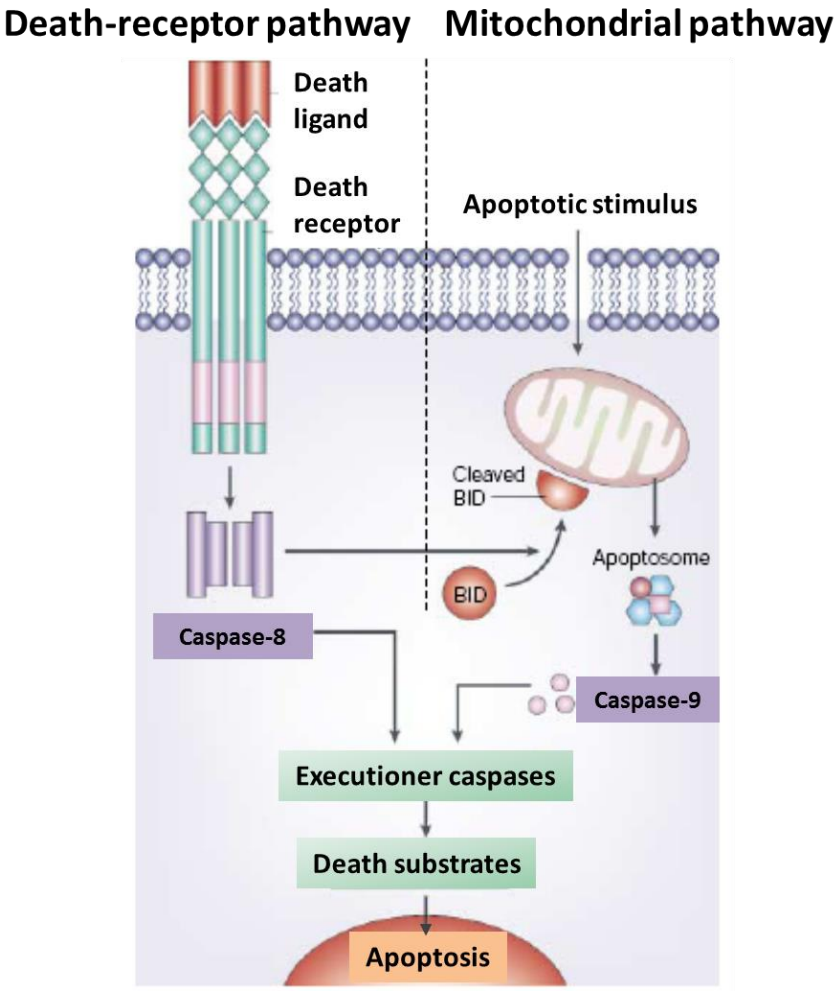

Figure 7: The two pathways of apoptosis. Apoptosis can be initiated by two different pathways: either by death receptors on the cell surface (extrinsic pathway) or through mitochondria (intrinsic pathway). Both pathways lead to the activation of an initiatior caspase (Caspase-8 or -9), which is activated via death receptors during the extrinsic pathway or at the multiprotein complex called apoptosome during the intrinsic pathway. The initiator caspases activate executioner caspases, which cleave death substrates ultimately leading to apoptotic disassembly of the cell. Both pathways are connected via the proapoptotic protein Bid, which is cleaved by caspase-8 activating the mitochondrial pathway to amplify the apoptotic signal of the death receptor pathway. (Adapted from Igney and Krammer [27].)

3.1. The Extrinsic Pathway

The extrinsic pathway of apoptosis is also called the death receptor pathway because it is triggered by the activation of death receptors at the cell surface. Death receptors are members

of the TNF-(tumor-necrosis factor) receptor superfamily, which is characterized by a sequence of 2 – 5 cysteine-rich extracellular repeats. Death receptors have an intracellular domain, the death domain, which is essential for transduction of the apoptotic signal. Death receptors are activated by their natural ligands called the TNF family. Death ligands are mainly transmembrane proteins of which a soluble form can be produced by metalloprotease cleavage [28]. Examples for death receptors and their corresponding ligands are the TNF receptors 1 and 2 (TNF-R1 and 2), which bind to TNF-alpha, Fas ligand binding to Fas (CD95), and TRAIL (TNF-related apoptosis-inducing ligand) binding to Death Receptors (DR) 1 – 5. When those ligands bind to their corresponding death receptor, the death domain recruits adaptor molecules from the cytosol such as FADD (Fas-Associated protein with Death Domain), which in turn attracts the inactive proform of an initiator caspase, caspase-8 or caspase-10 (Figure 8) [27].

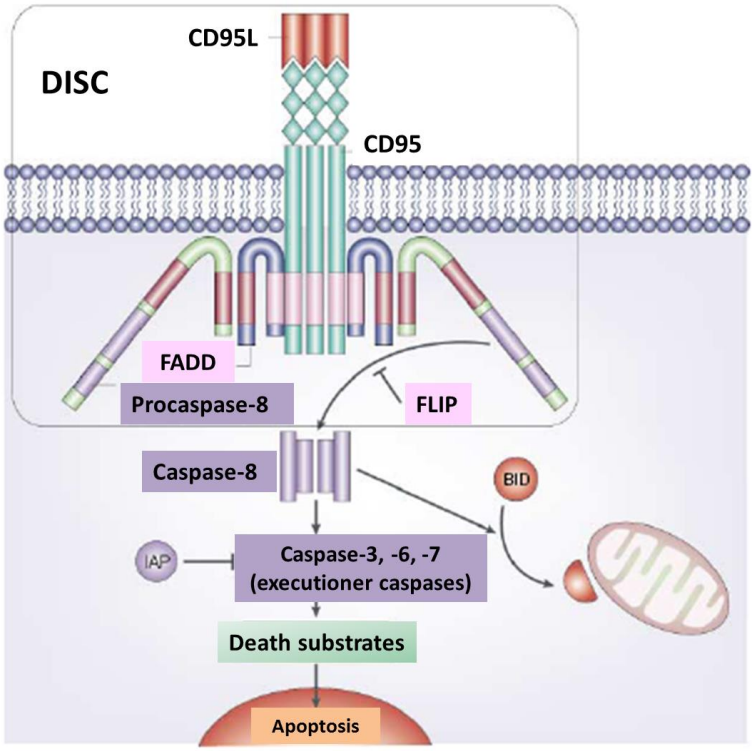

Figure 8: Apoptosis signaling through death receptors. Binding of death ligands like CD95L to their receptor leads to the generation of the death-inducing signaling complex (DISC). The DISC consists of the death ligand and receptor, which recruits FADD (FAS-associated death domain protein) binding to procaspases-8, which is cleaved autocatalytically. This extrinsic pathway of apoptosis can be inhibited by FLIPs (FADD-like interleukin-1 ß-converting enzyme-like protease inhibitory proteins), which bind to the DISC preventing the activation of caspase-8. Furthermore, inhibition of the death receptor pathway can be performed by IAPs (inhibitors of apoptosis proteins), which bind to and inhibit caspases. (Adapted from Igney and Krammer [27].)

The multi-protein complex formed by a death receptor, FADD and the initiator caspase is called death-inducing signaling complex (DISC). The procaspase becomes activated by

aggregation of 2 or more procaspase molecules. When procaspases are in close proximity to each other, they can cleave each other into their active form [29]. Thus, the active tetramer of caspase-8 is formed and the apoptosis signal is initiated. In some cells, called type I cells, the amount of active caspase-8 formed at the DISC is enough to induce apoptosis directly. In contrast, in type II cells DISC formation is reduced, less amounts of caspase-8 are activated and apoptosis activation involves the mitochondrial (intrinsic) apoptotic pathway (described in detail below) to amplify the caspase cascade. In type I cells the caspase cascade is directly activated by large amounts of active caspase-8, which cleave and activate the executioner caspases directly, mainly caspase-3, -6, and -7. Activated executioner caspases cleave each other and thus amplify the proteolytic caspase cascade. Finally, the executioner caspases cleave cellular substrates, referred to as "death substrates", which leads to the characteristic biochemical and morphological changes described above resulting in degradation of the cell [27].

Regulation of apoptosis

Cells also contain natural inhibitors of apoptosis so that the apoptotic self-destruction machinery can be tightly controlled. One example of apoptosis controlling proteins are FLIPs (FADD-like interleukin-1 ß-converting enzyme-like protease (FLICE/caspase-8) – inhibitory proteins), which inhibit apoptosis directly at the death receptor level (Figure 8). FLIPs are structurally homolog with procaspase-8 but lack its catalytic site. Thus they can bind to the DISC competing for binding sites and inhibiting the activation of initiator caspase-8. Another class of apoptosis regulatory proteins are the IAPs (inhibitor of apoptosis proteins). IAPs inhibit caspases and might also function as ubiquitin ligases, leading to the degradation of caspases. IAPs are inhibited by SMAC/DIABLO (second mitochondria-derived activator of caspase/direct IAP binding protein with low pI). This protein is released from mitochondria along with cytochrome c upon apoptosis induction and promotes caspase activation by inhibiting IAPs. The third class of apoptosis regulators are the members of the Bcl-2 protein family (Figure 11). They regulate apoptosis at the intrinsic apoptotic pathway on the mitochondrial level, which is described below.

3.2. The Intrinsic Pathway

The key event of the intrinsic pathway is the permeabilization of the mitochondrial outer membrane (MOMP). In this process cytochrome c is released from the inter-membrane space of mitochondria into the cytosol. In the cytosol cytochrome c forms a complex with APAF1

(apoptotic protease activating factor-1), ATP and the inactive initiator caspase procaspases-9, known as the apoptosome (Figure 9). Within this complex caspase-9 is activated autocatalytically and initiates a caspase cascade downstream of the mitochondrion [27]. MOMP is controlled by members of the Bcl-2 family. The extrinsic pathway can intersect the intrinsic pathway through caspase-8 cleavage-mediated activation of the proapoptotic Bcl-2 protein Bid. The truncated form of Bid (tBid) translocates to mitochondria promoting Caspase-9 activation (Figure 8).

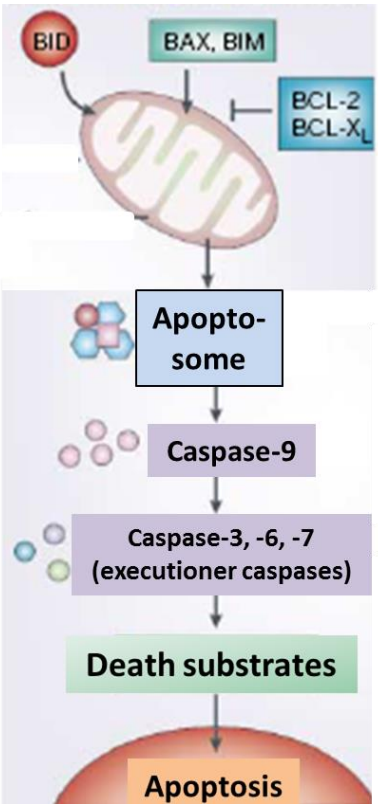

Figure 9: Apoptosis signaling through mitochondria. Apoptotic signals that lead to the activation of proapoptotic proteins Bid, Bim, Bax, and Bak initiate the intrinsic apoptotic pathway. Bax and Bak lead to MOM permeabilization releasing cytochrome c and other apoptotic factors from the mitochondria. Those lead to the formation of the apoptosome activating initiator caspase-9. Initiator caspases activate executioner caspases ultimately leading to apopotic disassembly of the cell. Antiapoptotic proteins like Bcl-2 and Bcl-xL can inhibit the mitochondrial apoptosis pathway. (Adapted from Igney and Krammer [27].)

3.2.1. The Bcl-2 Protein Family

Bcl-2 proteins can be either pro- or antiapoptotic. They share sequence homology in at least one Bcl-2 homology region (BH domains 1 - 4) (Figure 10). The Bcl-2 protein family is classified into three subgroups (Figure 11). The first group, the multidomain proapoptotic proteins Bax and Bak share homology in BH regions 1 – 3. They are also called effectors

because they mediate the critical step in apoptosis, MOMP. The second group, the antiapoptotic proteins include Bcl-2, Bcl-xL, Bcl-w, Mcl-1, and Bfl-1 and contain all 4 BH domains [30]. They inhibit the effectors by binding and antagonizing them. The third group is proapoptotic and called BH3-only proteins. They share only the BH3 domain [31].

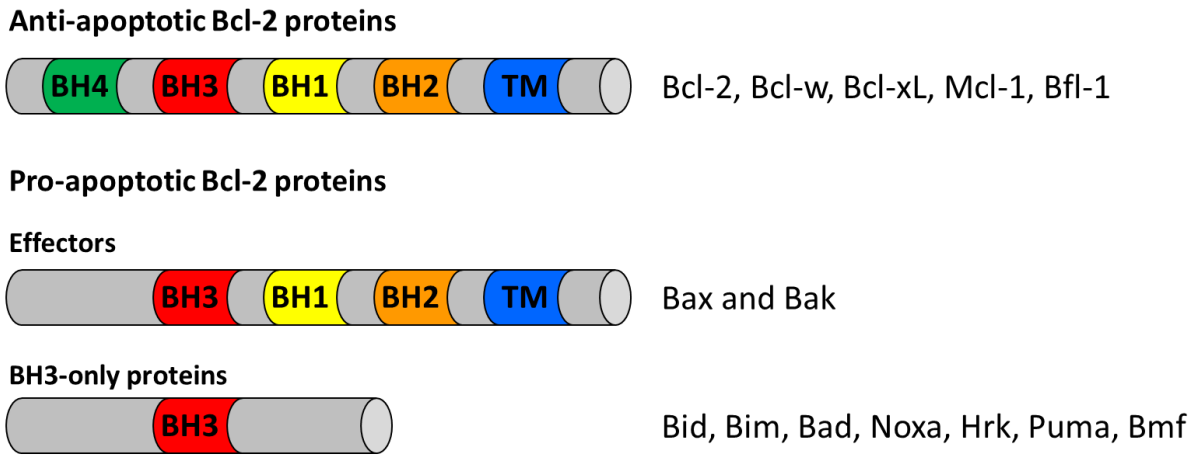

Figure 10: The Bcl-2 protein family is classified into three groups based on their Bcl-2 homology (BH) domain organization. Antiapoptotic proteins contain all four BH domains. Proapoptotic proteins can be subdivided into effectors, which share homology in BH domains 1 – 3, and BH3-only proteins, which only contain the BH3 domain. (Adapted from Tait and Green [5])

BH3-only proteins can be subdivided into activators and sensitizers. The activators Bim and Bid can directly activate the effectors Bak and Bax. The sensitizers (Bad, Bik, Noxa, Bmf, and Puma) bind the antiapoptotic Bcl-2 proteins preventing them from interacting with Bax and Bak or the activator BH3-only proteins [32] and thus inhibit apoptosis indirectly. BH3-only protein expression can be induced by transcription factors. For example, Noxa and Puma are induced by the tumor suppressor p53 in response to DNA damage. BH-3 only proteins can also be activated post-translationally. Bad for example can be activated by loss of phosphorylation in response to growth-factor deprivation. Also, as mentioned above, Bid is activated by caspase-8-mediated proteolysis. Furthermore, antiapoptotic protein expression level regulation is another way of regulating apoptosis. E.g. Bcl-xL can be transcriptionally induced via growth factors to promote cell survival. Mcl-1 can be rapidly degraded by the ubiquitin-proteasome pathway in response to death stimuli like UV radiation. The effectors Bax and Bak are mainly regulated post-transcriptionally by other members of the Bcl-2 family as described in

Figure **11**. However, the interaction between sensitizer BH3-only proteins and antiapoptotic Bcl-2 proteins is selective while Bim and Bid bind all antiapoptotic proteins [33] (Figure 15).

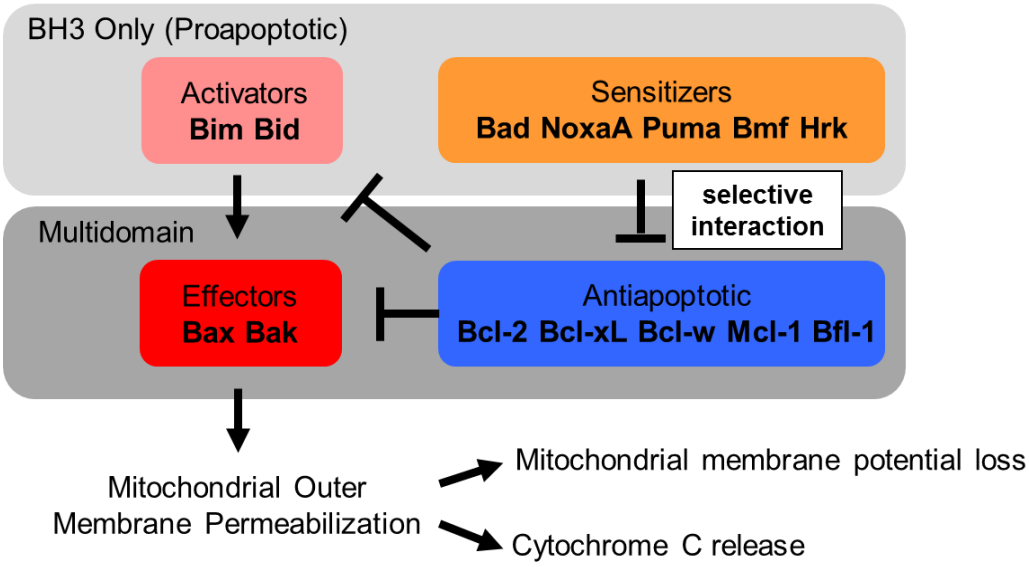

Figure 11: Bcl-2 protein family. The Bcl-2 protein family consists of three groups of proteins: the effectors, the antiapoptotic proteins and the BH3-only proteins. Activators activate the effectors while antiapoptotics inhibit activators and effectors. However, sensitizers inhibit the antiapoptotics and are thus proapoptotic themselves. (Adapted from Ryan *et al.* [34])

Cells in which the antiapoptotic proteins are loaded with Bim and Bid or Bax and Bak react differently towards death signals than cells with free antiapoptotic Bcl-2 proteins: Cells with loaded antiapoptotics are primed for death because additional cell death signals are more likely to provoke Bax or Bak activation. Once the multidomain proapoptotic proteins Bax and Bak get activated, they undergo a series of conformational changes including homo-oligomerization and induce pores in the mitochondrial outer membrane, which lead to cytochrome c release into the cytosol [31]. One very interesting fact about the Bcl-2 proteins is that some of them exist partly in the cytosol and translocate from the cytosol to mitochondria during apoptosis. The effector Bax is mostly cytosolic and sequesters its hydrophobic membrane anchor in its BH3-binding pocket. Bax exists as a monomer in the cytosol but during apoptosis induction, it translocates to mitochondria, where it inserts into the MOM with its membrane anchor. In contrast to Bax, the other effector Bak resides on the MOM in healthy cells, where it has been reported to be bound to Mcl-1 and to Bcl-xL. Mcl-1 binds to the BH3 pocket of Bak displacing the membrane anchor. The membrane anchor of Bcl-xL has been proposed to mediate binding to Bax. On apoptosis induction, Mcl-1 is degraded and the Mcl-1 – Bak and Bcl-xL – Bak interactions are disrupted by BH3-only proteins which frees Bak to promote apoptosis. Interestingly, some of the antiapoptotic Bcl-2 proteins can also exist in the cytosol. While Bcl-2 is constitutively membrane bound, Bcl-xL, Bcl-w and, Mcl-1 exist partly in the cytosol and translocate to mitochondria during apoptosis.

They bind to BH3-only proteins, which triggers apoptosis and leads to membrane insertion of those antiapoptotic proteins inhibiting MOM permeabilization by direct interactions with proapoptotic proteins. However, it is not completely clear if the antiapoptotic proteins mainly inhibit apoptosis by sequestering and blocking BH3-only proteins or mainly by binding to Bax and Bak inhibiting them from permeabilizing the mitochondrial outer membrane. In this context two models have been proposed: the indirect and direct model of activation of Bax and Bak. The indirect model suggests that Bax and Bak are constitutively inhibited by the interaction with antiapoptotic proteins. When BH3-only proteins are activated, they bind the antiapoptotic proteins leading to the liberation of Bax and Bak resulting in membrane permeabilization. In contrast, the direct activation model states that Bax and Bak have to be activated directly by the activator BH3-only proteins Bim and Bid and thus inducing MOM permeabilization. It is most probable that a combination of both models is true. This means that permeabilization of the MOM is controlled by complex interactions of the Bcl-2 network. However, both models do not pay enough attention to the role of the lipid membrane in Bcl-2 network regulation. The "embedded together" model does take it into account stating that MOM permeabilization is finally regulated in the lipid membrane and the inserted Bcl-2 proteins where the equilibrium is either shifted towards Bax and/or Bak oligomerization and MOM permeabilization or towards the formation of unproductive complexes resulting in the integrity of the MOM. However, membrane insertion of both pro- and antiapoptotic proteins comes with dramatic conformational changes during apoptosis. Bax conformational changes lead to oligomeric complex formation being coupled to membrane insertion. Bak also changes conformation and oligomerizes during apoptosis. One model for Bax and Bak activation is that they form large pores in the MOM, which allow cytochrome c release into the cytosol. However, the exact physiology of such pores is still investigated [33, 35, 36].

3.3. Tumor resistance to apoptosis

As described above, metazoans eliminate damaged or infected cells by apoptosis. Apoptosis is essential for embryogenesis, tissue homeostasis, and defense against pathogens. The deregulation of apoptosis can lead to autoimmune and degenerative diseases or cancer. It is widely accepted, that diminution of apoptosis is a critical step in tumorigenesis [37]. Hanahan and Weinberg defined the resistance to cell death as a hallmark of cancer [38]. Thus, cells whose cell cycle control is disrupted by oncogenic mutations, are not removed by apoptosis but are preserved which enables them to become neoplastic [37]. Tumor progression has been shown to require the expression of proteins, which promote cell proliferation and the expression of antiapoptotic proteins or the inactivation of essential proapoptotic proteins.

Cancer treatment by chemotherapy and ɤ-irradiation kills tumor cells mainly by the induction of apoptosis. Since the apoptotic pathway is often defective in cancer cells, only few tumors are sensitive to those therapies. That is why the development of resistance to therapy is an important clinical problem [27]. Therefore it is necessary to understand how cancer cells gain resistance to apoptosis in order to be able to design new cancer drugs.

3.3.1. Tumors express antiapoptotic proteins

One mechanism by which cancer cells gain resistance to apoptosis is the expression of antiapoptotic proteins. The first antiapoptotic protein identified was Bcl-2 (B-cell lymphoma (gene) 2) [39], an oncoprotein activated via a t(14; 18) translocation in human follicular lymphoma [40]. This translocation places the *bcl-2* gene under the control of the immunoglobulin heavy (IgH) chain gene enhancer, which results in a constitutive high level expression of Bcl-2. Bcl-2 overexpression causes cells to stay alive which may actually be programmed to dye. Thus it increases the risk of cells to acquire additional oncogenic mutations e.g. mutations that deregulate the control of cell proliferation. One mutation, which is often found in Bcl-2 overexpressing lymphomas is the *myc; IgH* chromosomal translocation [41]. Myc is a transcription factor that regulates proliferation, cell size, and differentiation. It seems to synergize with Bcl-2 by driving rapid proliferation of Bcl-2 overexpressing cells with downregulated apoptosis thereby contributing to tumorigenesis [27, 37]. High level Bcl-2 expression is associated with a higher malignancy of human tumors and thus seems to be predictive of shorter, disease-free survival. Furthermore, high level Bcl-2 expression often leads to a poor response to many kinds of chemotherapeutic drugs and irradiation [27]. Besides high level Bcl-2 expression in lymphomas, expression of antiapoptotic proteins has also been found in solid tumors e.g. lung, stomach, brain, and breast cancer. In addition to Bcl-2 they may also overexpress other antiapoptotic proteins like Bcl-xL and Mcl-1 [27, 41].

3.3.2. Proapoptotic genes are inactivated in cancer cells

Besides overexpression of antiapoptotic proteins, another mechanism by which tumors can acquire apoptosis resistance is the downregulation or mutation of proapoptotic molecules. One example is the mutation of the Bcl-2 family protein Bax. Bax may be mutated in the BH domains, which results in loss of function or may have frame shift mutations that lead to loss of expression. Frame shift mutated Bax in cancer cell lines leads to apoptosis resistance. Furthermore, reduced Bax expression correlates with a poor response to chemotherapy and a lower overall survival rate [27, 41]. Besides Bax, the other apoptosis effector Bak is also mutated e.g. in 16% of gastric and 20% of colorectal cancers [42]. Another example for the

downregulation of a proapoptotic protein is the lower Bim expression either due to homozygous deletion [43] or promoter hyper-methylation [44]. Low Bim levels have been associated with poor therapeutic response and early relapse. Besides the reduction of Bim, the BH3-only proteins Noxa and Puma have also been shown to be downregulated in some lymphomas [37, 41]. Another way to escape the mitochondrial pathway of apoptosis has been observed in metastatic melanomas: here APAF1, which forms part of the apoptosome, is often not expressed due to gene loss or methylation. APAF1 downregulation oftentimes leads to chemotherapy response failure [45]. Moreover, the death-receptor pathway of apoptosis has been found to be inhibited in cancer cells at several points: Firstly, death receptors like CD95, TRAIL-R1, and 2 are downregulated or inactivated in many tumors [27]. Additionally, some tumors have been found to express soluble receptors, which act as decoys for death ligands. Examples are soluble receptor sCD95 (soluble CD95) and decoy receptor 3 (DcR3). Both soluble receptors have been shown to competitively inhibit CD95 signaling by binding CD95L and thus inhibiting CD95L-induced apoptosis [41].

3.3.3. Alterations of the tumor suppressor functions of p53 in tumorigenesis

The molecular connection between cell death and cell cycle involves the p53 pathway [27]. Upregulation of the tumor suppressor protein p53 leads to cell-cycle arrest and apoptosis. In a normal, unstressed cell, p53 is inactivated by the ubiquitin ligase MDM2. MDM2 targets p53 for destruction by the proteasome. Thus p53 levels are kept low by continuous degradation. Upon cell stress, like DNA damage, MDM2 dissociates from p53. Activated p53 acts as a transcription factor in the nucleus and induces protein expression for cell cycle arrest and DNA repair. If DNA damage is irreparable, p53 induces apoptosis by driving expression of Bax, Noxa, Puma, CD95, TRAIL-R1 and 2. Mutation or deletion of p53 very likely leads to cancer development because cells may escape apoptosis and continue proliferation despite damaged DNA [1, 27, 46, 47]. Thus the ability of p53 to induce apoptosis is an important component of its tumor suppressor function. Tumors, which have a mutated or deleted p53 gene (called *TP53* in humans), are less sensitive to apoptosis and often show a poor response to chemotherapy and ɣ –irradiation. Furthermore, mutations in *TP53* have been linked to early relapse in breast cancer patients [27, 37].

3.3.4. Pharmacological strategies to overcome apoptosis resistance

As described above, there is a remarkable amount of knowledge about how tumors acquire resistance to apoptosis. However, the challenge is to translate this knowledge into clinical applications [27].

One promising strategy is to therapeutically target the Bcl-2 antiapoptotic proteins, which have been found to be upregulated in many types of cancer (see paragraph I.3.3.1). Targeting the expression or function of those pro-survival Bcl-2 proteins seems especially promising because there is strong evidence that these proteins are not only essential for the development but also for the growth of tumors [41]. One example of targeting Bcl-2 is by a Bcl-2 antisense oligonucleotide, which significantly reduced tumor growth in mice experiments and preliminary clinical studies. Oblimersen, a Bcl-2 antisense oligonucleotide, was used in combination with chemotherapy and improved overall survival significantly in phase I–II clinical studies. However, in a recent phase III clinical study overall survival did not significantly improve by the addition of oblimersen to standard chemotherapy [48]. Another antiapoptotic Bcl-2 protein having been downregulated by an antisense approach is Bcl-xL [27]. Besides the downregulation of antiapoptotic Bcl-2 proteins by the antisense strategy, another successful approach of targeting those proteins is by so called "BH3 mimetics". The aim of these molecules is to mimic the action of the BH3 domain by binding the groove of antiapoptotic Bcl-2 proteins and trigger apoptosis. BH3 mimetics can be effective because most tumors have a defective p53 pathway and overexpress antiapoptotic Bcl-2 proteins while the core apoptotic machinery remains intact [37]. BH3 mimetics are likely to kill tumor cells specifically without high cytotoxic effects in normal cells, because one could design BH3 mimetics that specifically target a certain antiapoptotic protein most important for maintaining survival of a particular tumor type due to the finding that the binding pattern between antiapoptotic and BH3-only proteins is selective meaning that particular BH3 domains preferentially bind particular antiapoptotic proteins [49]. BH3 mimetics can be BH3 peptides [50] or even more potentially small organic molecules binding the groove. One promising example is the small molecule ABT-737 [51]. ABT-737 strongly binds Bcl-2, Bcl-w, and Bcl-xL but not Mcl-1. It has been shown to successfully kill several kinds of cancer cells in phase I/II clinical trials [52]. Furthermore, it was found to be successful as an adjuvant in conjunction with conventional therapy. ABT-737 and another BH3 mimetic called A-385368, which predominantly targets Bcl-xL [53], sensitize cells to several chemotherapy agents [37]. Obatoclax, also called GX15-070, binds to all five prosurvival Bcl-2 proteins. Some phase I/II clinical trials have not proved convincing single-agent activity but phase III trials with obatoclax in combination therapies are ongoing [52].

Besides inducing the mitochondrial apoptosis pathway by inhibition of antiapoptotic proteins as described above, another strategy to induce apoptosis in tumor cells is by targeting the death receptor pathway of apoptosis. One therapy approach involves the CD95 system: CD95

is induced by a transcriptionally regulated mechanism by chemotherapeutic drugs like the nucleotide analogue 5-fluoruracil (5-FU). By also engaging other signaling pathways, those chemotherapeutic agents eventually lead to the upregulation of CD95 and CD95L, which results in apoptosis of the cell itself or of the neighboring cells. Another therapeutic strategy to induce death receptor mediated apoptosis in tumors is to treat cancer with the death ligands TRAIL or TNF. Those molecules have been shown to selectively kill malignant cell lines while normal cells were resistant [27].

A further cancer therapy concept is to influence the p53 signaling pathway directly: small molecules have been shown to be able to restore the activity of mutated p53 and induce apoptosis in tumor cells. Furthermore, the wild-type p53 gene *Trp53* was successfully transferred into tumor cells with mutated p53 by adenoviruses. This led to p53 induced apoptosis and suppression of tumor growth in mice [27].

All of those cancer therapy concepts aiming to induce apoptosis in tumor cells described face the challenge of macroscopic tumors being heterogeneous. This is why it is likely that different cells within the same tumor have acquired different or even multiple mechanisms of apoptosis resistance. Therefore it will probably be most effective to use combinations of various therapeutic strategies, which will selectively dispose tumor cells without affecting normal healthy cells [27].

4. Human papillomaviruses may lead to cancer

Cervical cancer is one of the most well studied malignancies and is the second leading cause of cancer deaths in women worldwide. An association between cervical cancer and human papillomavirus (HPV) infection was initially reported over 30 years ago and today it is well known that HPVs are the causative agents of cervical cancer. For this discovery Harald zur Hausen, a scientist of the German Cancer Research Center, Heidelberg, was awarded the Nobel Prize in Physiology or Medicine in 2008. HPVs are also associated with many anal, penile, and vulvar cancers and contribute to over 40% of oral cancers [54]. Human papillomaviruses are small double-stranded DNA viruses that infect squamous epithelia. These viruses are tissue-tropic and very species-specific. They are classified by the genome sequence of their major capsid protein L1. Thus over 120 types of HPV have been identified. Despite of their phylogenetic diversity, the genome structure of HPVs is highly conserved.

HPVs possess a genome with a size of about 8 kb (Figure 12). It can be divided into three domains: the noncoding LCR (long control region), the early region, and the late region [55].

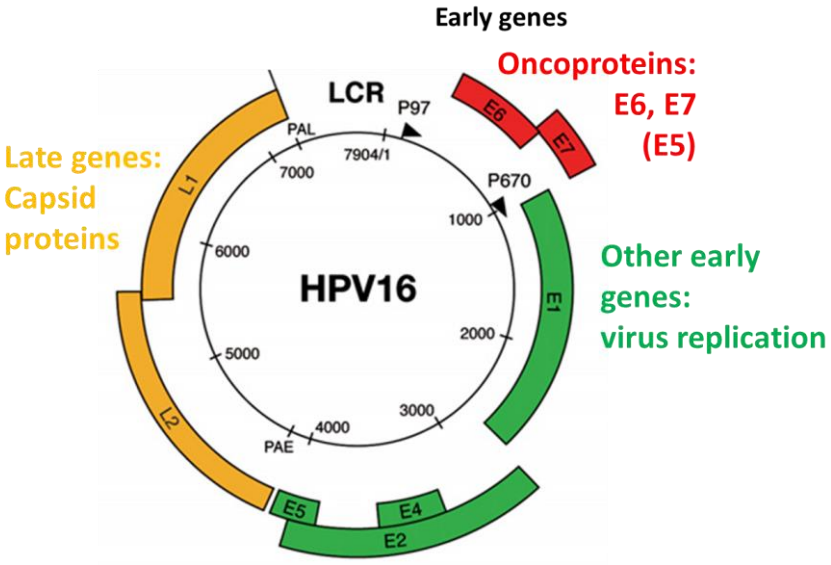

Figure 12: The HPV-16 genome. Viral gene expression is controlled by the LCR (long control region). The open reading frames (ORFs) of early and late genes are shown. Early (p97) and late (p670) promoters are marked by arrows. PAE: early polyadenylation site; PAL: late polyadenylation site. (Figure adapted from Doorbar [56].)

HPVs are classified into high- and low-risk types, depending on their oncogenic potential: High-risk HPVs are associated with the development of cancer while low-risk types are not. Low-risk HPVs are primarily found in genital warts and non-malignant lesions [57]. HPV high-risk types 16 and 18 are the most important genotypes as they are responsible for about 70% of cervical cancer cases [54]. However, high-risk genital HPV infection is very common. Infection is commonly transmitted by sexual contact and in the majority of individuals the infection is cleared within 6 – 12 months by the immune system. But approximately 15% of women cannot effectively clear the virus and persistence of a high-risk HPV infection is the major risk factor for the development of ano-genital cancer [55, 57].

4.1. HPV life-cycle and carcinogenesis

HPV's unusual life cycle is the key to understand how virus infection results in malignant development. Other than most viruses, which infect a target cell and produce progeny virus from that same cell, HPVs synthesize new virions only after the infected cell has divided and one of the infected daughter cells has differentiated [54]. HPVs infect basal layer cells of epidermal or mucosal epithelia, which are cells that are still able to proliferate (Figure 13).

These basal cells can be reached by the virus due to mircowounds. After infection, HPV genomes exist as extrachromosomal elements or episomes in the host cells. In these cells, viral gene expression is mostly suppressed. However, the low expression of the specific early viral oncogenes E6 and E7 leads to enhanced proliferation of the infected cells. After cell division, one daughter cell migrates into the suprabasal layer, excites the cell cycle, and undergoes differentiation. HPV DNA replication depends on the cellular DNA synthesis machinery. But cellular DNA polymerases and replication factors are only made in mitotically active cells. Thus the virus encodes proteins that reactivate cellular DNA synthesis in non-cycling cells, inhibit apoptosis, and delay differentiation of infected keratinocytes. E6 and E7 are important for these functions. Thus viral DNA is replicated in the top epithelial layer cells that normally would have exited the cell cycle. Then late viral gene expression is initiated and the late-phase L1 and L2 structural proteins encapsidate viral genomes and virions are shed from the upper layers of the epidermis or mucosa and might then infect additional tissues. An unfortunate but rare by-product of this role in high-risk HPV replication is the deregulation of growth and cell cycle control in the infected cell and the development of cancer.

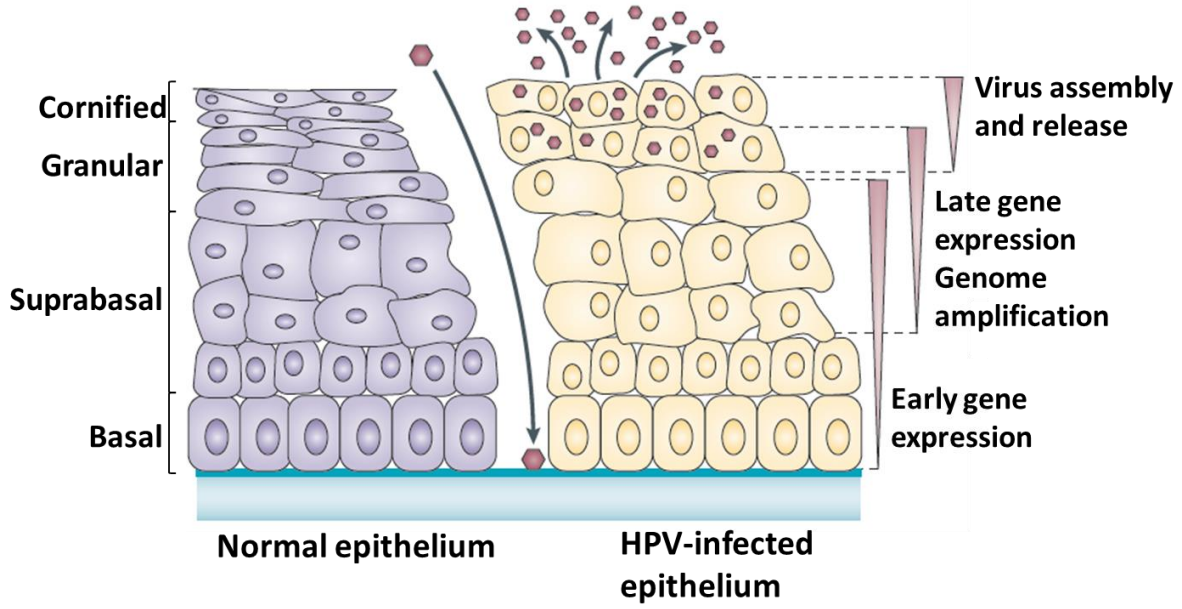

Figure 13: The life cycle of human papillomaviruses. HPVs infect keratinocytes in the epithelial basal layer exposed through microwounds. After infection, the viral genomes are established in the nucleus as low-copy episomes and early viral genes are expressed. Viral genomes get amplified by the cellular DNA machinery. When HPV-positive cells move away from the basal layer and differentiate the viral oncogenes E6 and E7 deregulate cell cycle control and push the cells into S-phase leading to genome amplification. Late-phase L1 and L2 proteins encapsidate viral genomes and virions are shed from the uppermost layers of the epithelium. (Adapted from Moody and Laimins [54].)

Three HVP genes are able to stimulate proliferation: E5, E6, and E7. E5 is important early on during infection. It stimulates cell growth by forming complexes with growth factors (like EGFR, PDGFR) [58]. E5 has also been shown to prevent apoptosis after DNA damage [59] and promote hyperproliferation [60]. However, E5 is not necessary for late events in HPV-mediated carcinogenesis because a substantial part of the viral genome, including E5, is often deleted when the episomal viral DNA becomes integrated into the host-cell DNA [57]. In contrast, the HPV oncoproteins E6 and E7 are more significant for malignant transformation and are consistently expressed in cancer tissue. They can immortalize tissue culture cells independently from each other but are more efficient when expressed together [61]. E6 has been shown to interact with p53 [62] and E7 with proteins of the retinoblastoma family (Rb) [63] to block the activity of these tumor suppressors (Figure 14). By binding Rb, E7 leads to its degradation, which in turn results in the release of Rb's binding partner E2F. E2F is a transcription factor, which activates the expression of S phase genes finally driving cell proliferation of the HPV infected cells [54]. The resulting high activity of E2F may lead to apoptosis in E7-expressing cells by the accumulation of p53. But E6 prevents E7-generated apoptosis by degrading the apoptosis-inducing proteins BAK [64] and p53.

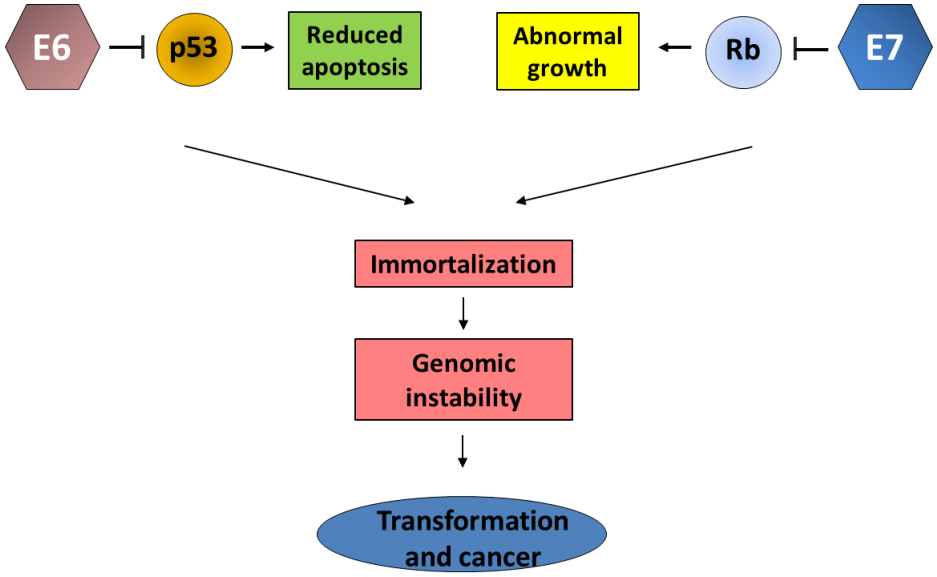

Figure 14: Molecular mechanisms by which the HPV oncoproteins E6 and E7 cooperate to induce cervical cancer. E6 leads to the ubiquitination and degradation of p53 which leads to reduced levels of apoptosis. E7 binds and inhibits the retinoblastoma protein (Rb) which leads to abnormal growth signaling. Thus cells are immortalized which may lead to genomic instability and mutations ultimately resulting in the formation of cancer.

The combined action of E6 and E7 in targeting cell cycle regulators to maintain S phase in differentiating cells also leads to the abolishment of several cell cycle checkpoints. This results in genetic instability and mutations over time and thus to cancer progression [65].

4.2. How HPV escapes apoptosis

One of the most powerful strategies of host organisms to clear viral infections is the ability to induce apoptosis, and thus eliminate infected cells. Human papillomaviruses have developed several strategies to escape apoptosis. E6 can inhibit apoptosis mainly through the p53 pathway. E6 binds to p53 and prevents p53 from inducing apoptosis by targeting it for degradation via the ubiquitin-proteasome pathway. Furthermore, HPV has found ways to inhibit both the intrinsic and extrinsic pathway of apoptosis [66]. The extrinsic apoptotic pathway is activated by inflammatory cytokines, e.g. TNF-alpha, which are produced by the host cells upon viral entry. To escape apoptosis the HPV oncoprotein E6 can block the initiation of apoptosis at several points, e.g. by directly binding to TNF receptor-1, FADD, or caspase-8 blocking TNF, FAS, and TRAIL stimulated apoptosis [54, 66, 67]. Furthermore, E6 can interfere with these processes by binding to Bak leading to its ubiquitination and degradation [66]. E6 has also been shown to interact with Bax [54] and inhibit its activity [68]. Moreover, there are hints in the literature that HPV may inhibit the mitochondrial pathway by interacting also with other members of the Bcl-2 protein family [67]. Thus HPV is able to interfere with both apoptotic pathways.

5. Aims of this work

The main function of mitochondria is the generation of the cell's energy by synthesizing ATP. However, mitochondria also play a very important role in apoptosis. They are the key organelles in the intrinsic apoptotic pathway. More and more connections between apoptosis and other functions of mitochondria are becoming evident like mitochondrial dynamics as mitochondrial fusion and division proteins interact with the executers of apoptosis, the Bcl-2 family proteins. An imbalance in the Bcl-2 network has been shown to result in disease like cancer. For apoptosis, calcium homeostasis has also been found to be critical. Ca^{2+} is imported into mitochondria from the ER. This transfer takes place at tight ER-mitochondria contact sites. Many proteins have been identified to participate in those mitochondria-associated membranes but mainly by biochemical studies isolating those MAMs. Because the distance between ER and mitochondria at the contact sites is very small, only between 10 and 25 nm, it is not trivial to image those interaction sites.

To gain a better insight into mitochondrial functions with respect to the impact of the Bcl-2 protein network during cancer progression and in mitochondrial interactions with the ER, the following objectives were proposed:

1) Characterization of the role of the Bcl-2 proteins in cervical cancer progression. To find out which antiapoptotic Bcl-2 proteins are responsible for cervical cancer cells to gain resistance to apoptosis, in this study a method called BH3 profiling was applied, which takes advantage of the specific interactions of antiapoptotic proteins and BH3 only proteins.

2) High-resolution imaging of mitochondria-ER contact sites. To gain a deeper insight into the structural organization of ER-mitochondria contact sites, this study aimed to image those sites labeling ER, mitochondria, and proteins involved in the interaction sites fluorescently. Since the distance between ER and mitochondria is only between 10 and 25 nm, the high-resolution microscopy technique STED (stimulated emission depletion) was applied.

II. Results and Discussion

6. Bcl-2 network studies in HPV induced carcinogenesis

6.1. Experimental strategy: BH3 Profiling in a cell line-based model system representing HPV induced cancer progression

To study the influence of the oncoproteins E6 and E7 on cervical cancer cells in gaining resistance to apoptosis, an established keratinocyte model system [69-71] (Table 1) was used. With this cell model the aim was to study cancer progression by comparing primary cells on the one hand to non-tumorigenic oncogene transduced cells and carcinoma cell lines on the other hand. As primary cells, and thus as an HPV-negative genital cell control, human neonatal primary foreskin keratinocytes (pK) were used. These cells were immortalized by amphotropic retroviruses carrying the HPV-16 oncogenes E6, E7 or both (referred to as E6/E7) in order to investigate the role of individual viral oncoproteins [69]. Primary and oncogene immortalized keratinocytes were compared to the two HPV-16-positive cervical cancer cell lines CaSki and SiHa [72].

Table 1: Cell lines of the model system used in this study representing HPV induced cancer progression.

Name of cell line	Source	Details
pK (primary keratinocytes)	Invitrogen (Cat. no. C-001-5C)	Human epidermal keratinocytes isolated from neonatal foreskin.
E6	Whitaker and zur Hausen, unpublished [69]	Human foreskin keratinocytes, transduced with recombinant retrovirus carrying retrovirus expression vector containing the open reading frames (ORFs) of HPV-16 E6 or E7 oncogene or the contiguous region encoding E6 and E7 from HPV-16 controlled by a long terminal repeat (LTR) promoter.
E7	Whitaker and zur Hausen, unpublished [69]	
E6/E7	Whitaker and zur Hausen, unpublished [69]	
CaSki	Pattillo *et al.* (1977) [73]	Cervical carcinoma cell line, isolated from epidermoid cervical carcinoma, copy number: 60 - 600 HPV-16 genome copies.
SiHa	Friedl *et al.* (1970) [74]	Cervical carcinoma cell line, isolated from squamous cell carcinoma, copy number: 1 - 2 HPV-16 genome copies.

To study the influence of E6 and E7 on Bcl-2 proteins, a method called BH3 profiling was used. This method takes advantage of the fact that not every sensitizer BH3-only protein can bind to every antiapoptotic protein but their interaction pattern (Figure 15) is rather selective [32].

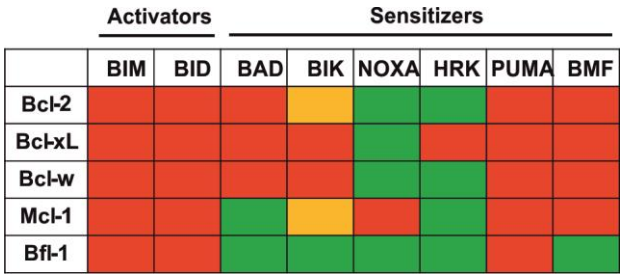

Figure 15: Interaction pattern between antiapoptotic Bcl-2 proteins and BH3 peptides (according to Deng *et al.* 2007). Red represents high-affinity binding, orange represents low-affinity binding, and green represents undetectable binding.

Peptides with the sequence of BH3-only sensitizers are sufficient to perform proapoptotic functions. Thus, so called BH3 peptides can be used as probes for antiapoptotic protein function making use of the interaction pattern to find out which antiapoptotic proteins are mainly responsible for cell survival. This strategy can help to determine how cancer cells evade apoptosis [75]. In BH3 profiling, mitochondria are exposed to a panel of the different BH3 peptides to find out which sensitizer BH3-only peptide leads to the permeabilization of the mitochondrial outer membrane. Healthy mitochondria have an intact membrane potential whereas mitochondrial membrane potential is lost during apoptosis when Bak and Bax lead to permeabilization of the mitochondrial outer membrane. To study this, originally mitochondria were isolated, treated with peptides and cytochrome c release was measured via ELISA as a measurement of MOMP [32]. But a faster read-out, which fewer cells are needed for is reading out membrane potential loss using the fluorescent probe JC-1 [34]. The red fluorescence signal is highest when JC-1 is concentrated in the matrix of intact mitochondria. Red fluorescence is lost upon membrane potential loss. JC-1 data indicate which of the BH3 peptides induce MOMP and which do not. When a peptide induces MOMP one can conclude that Bak and Bax are present and active. Since sensitizer BH3 peptides are not able to activate Bak and Bax directly the ability of sensitizer BH3 peptides to induce MOMP indicate the presence of antiapoptotic proteins loaded with proteins able to induce MOMP that are freed upon the interaction of the sensitizer BH3 peptide with the antiapoptotic protein. By comparing which sensitizer BH3 peptide leads to JC-1 fluorescence loss (this is called the

BH3 profile) to the interaction pattern of BH3-only proteins and antiapoptotic proteins (Figure 15) it is possible to conclude which antiapoptotic protein is necessary for maintaining cell survival [30, 75].

As described above, the intrinsic pathway of apoptosis is controlled by the quite complex network of Bcl-2 proteins. So far only the proapoptotic proteins Bak and Bax have been shown to be affected by the HPV oncoprotein E6. Thus HPV inhibits cytochrome c release. This is one strategy how HPV induced cancer cells gain resistance to apoptosis. In summary, here the aim was to find out which antiapoptotic proteins are responsible for maintaining survival of HPV induced cancer cells. Therefore the BH3 profiling method was used (Figure 16). In order to investigate the Bcl-2 protein network during HPV infection the cancer progression cell model described above was chosen.

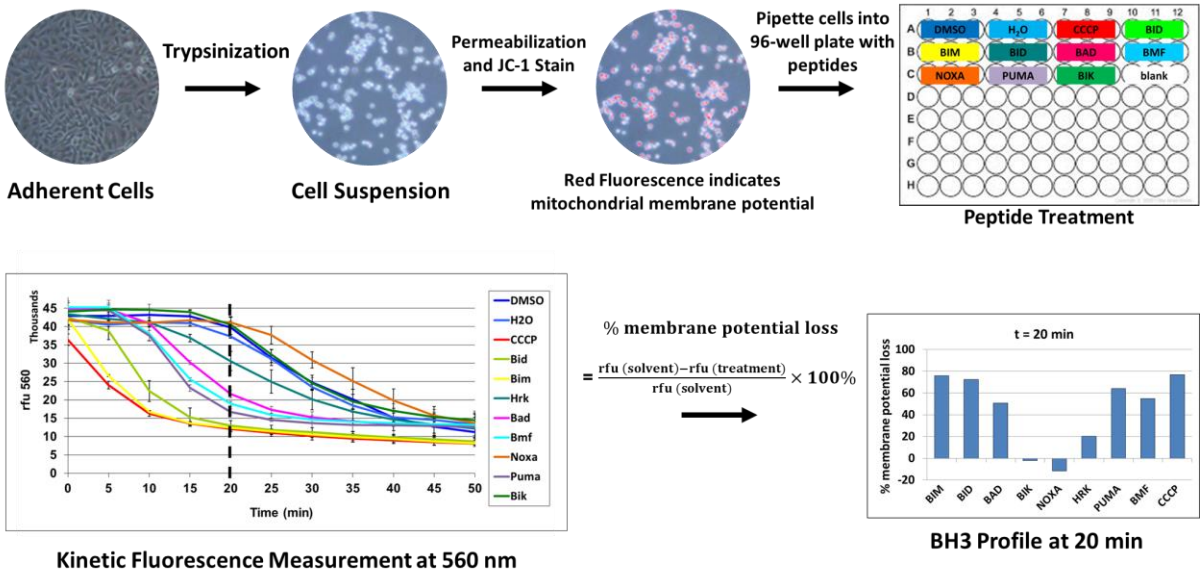

Figure 16: BH3 profiling assay using JC-1 fluorescence dye as an indicator for mitochondrial membrane potential measuring MOMP. Adherent cells were trypsinized to obtain a single-cell suspension. Cells were permeabilized via digitonin and stained with JC-1. Then cells were pipetted into 96-well plates already containing peptide treatments. JC-1 fluorescence loss was measured in a plate reader at 560 nm. From those kinetic measurements BH3 profiles meaning the percentage of membrane potential loss for each peptide were calculated 20 min after treatment addition.

6.2. Alterations in Bcl-2 expression levels upon E6/E7 oncogene expression

To get an overview of the abundance of Bcl-2 family proteins in the cell line-based model system representing HPV induced cancer progression, Western blot analysis on Bcl-2 protein expression was performed (Figure 17).

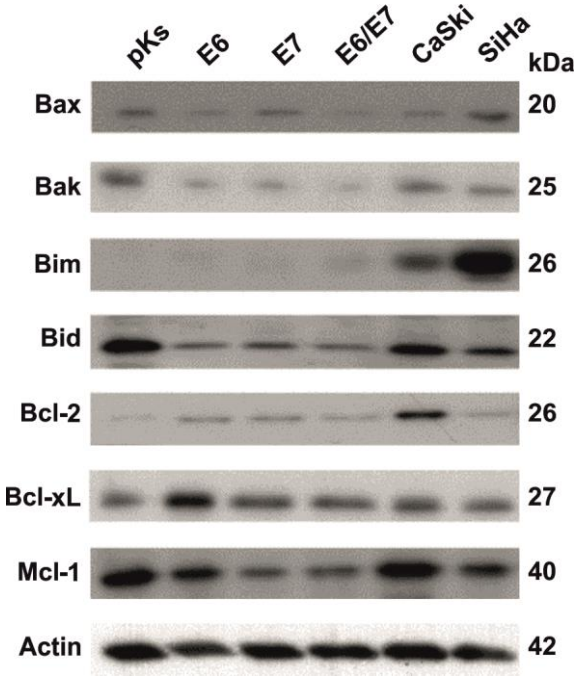

Figure 17: Western blot analysis of total protein lysates of the HPV induced cancer model cell lines. Proteins were separated by SDS-gel electrophoresis and transferred to PDVF membranes. Membranes were incubated with antibodies against Bcl-2 family proteins as indicated. To confirm equal loading, an Actin antibody was used. Molecular weights are shown on the right. (Western blot analyses were performed by my colleague Raquel Salvador Gallego.)

In agreement with the fact that apoptosis is inhibited upon HPV infection, proapoptotic protein levels of Bak and Bid are lower in all cell lines compared to the primary keratinocytes. Moreover, in line with prior results, Bax gets downregulated upon E6 but not E7 expression [69] but surprisingly, Bax seems to be upregulated in the cancer cell line SiHa. On the contrary, proapoptotic Bim is upregulated in the cancer cell lines and nearly not present in primary and immortalized keratinocytes.

The expression levels of the antiapoptotic proteins are slightly changed upon oncogene expression: Bcl-2 and Bcl-xL are upregulated in all cell lines in comparison to the primary keratinocytes, while Mcl-1 is slightly downregulated with respect to the primary keratinocytes. Taken together, the Bcl-2 family protein levels seem to be different in the model cell lines but do not give a clear answer about how the HPV oncoproteins lead to apoptosis inhibition.

6.3. BH3 profiling of model cell lines for HPV induced cancer progression

In this study the interest was to find out which antiapoptotic proteins are responsible for the inhibition of apoptosis upon HPV infection. Therefore the BH3 profiling method was used. Ryan *et al.*, who developed BH3 profiling using the fluorescence dye JC-1 as an indicator for

mitochondrial potential loss [34], used thymocytes, meaning suspension cell lines, for their studies. However, the cell model used here consists of epithelial cell lines, thus adherent cell lines. This means, that first the JC-1 assay protocol had to be adapted to the cell model used here.

6.3.1. Establishment of JC-1 assay in HPV infection model cell lines

Performing JC-1 assay with adherent or trypsinized cells

First of all, it was tested, if one could perform the BH3 profiling assay in adherent cells directly or if the cells had to be brought into suspension by trypsin. For the assay with adherent cells, 20 000 cells were seeded in 96-well plates and let adhere over night. For the assay with trypsinized cells, cells were trypsinized from culture dishes, washed with T-EB buffer, and counted. From the adherent cells, medium was removed and cells were also washed with T-EB. Then JC-1 staining solution was added to the cells also containing digitonin to permeabilize the cell membrane. The cell/dye solution was either added to the peptides already prepared in 96-well plates or peptides were added to cells respectively. Fluorescence loss was measured at 560 nm (Figure 18).

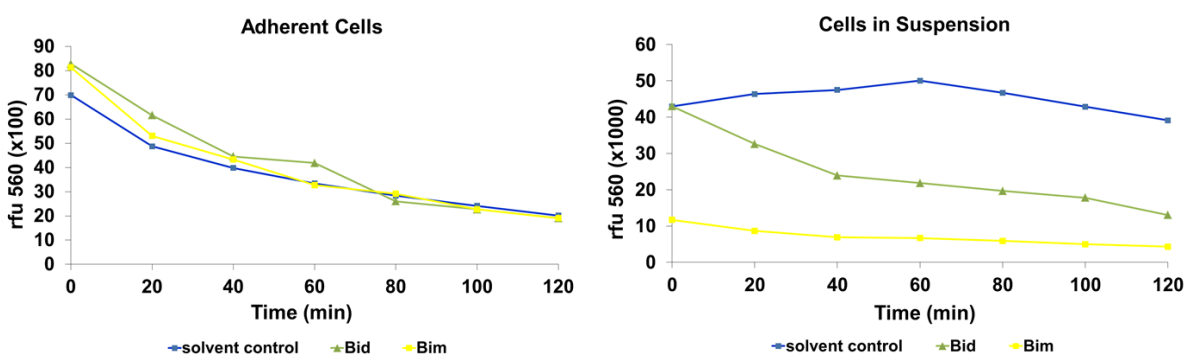

Figure 18: JC-1 fluorescence of SiHa cells treated with Bid-, Bim- BH3 peptides, or without treatement (solvent control) in adherent cells (left) or trypsinated cells in suspension (right).

Using adherent cells, the mitochondrial membrane potential measured in JC-1 fluorescence does not differ between solvent control treated cells and activator peptide (Bid or Bim) treated cells. In contrast, the assay with trypsinized cells shows clear differences in the mitochondrial membrane potential between solvent control treated cells and activator peptide treated cells: While cells only treated with solvent keep their mitochondrial membrane potential almost constant over 120 min, the membrane potential is lost immediately when treating cells with Bim peptide and lost over time when treating cells with Bid peptide as expected from the

literature [34]. Consequently, it was decided to perform further assays with trypsinized cells. However, since assay conditions were now different from the conditions used by Ryan *et al.*, other staining parameters also had to be optimized: JC-1 dye concentration and ß-Mercaptoethanol concentration used in the cell staining solution.

Optimization of JC-1 concentration

As explained above, for the JC-1 assay cells were trypsinized, washed with T-EB, counted with a Neubauer hemocytometer and then cells were resuspended in T-EB at 4 times their final densitiy (1 Million cells per ml). Then one volume of the 4x cell suspension was added to one volume of a 4x dye solution containing different JC-1 concentrations, 40 µg/ml oligomycin, 0.02% digitonin, and 10 mM 2-mercaptoethanol in T-EB and stained for about 20 min before treatments were added. JC-1 concentration during the staining procedure ranged from 1 to 4 µM. Cells were treated with either DMSO as a solvent control or the positive control CCCP (Carbonyl cyanide *m*-chlorophenyl hydrazone), a ionophore, which uncouples the proton gradient of the mitochondrial membrane and thus leads to mitochondrial membrane potential loss.

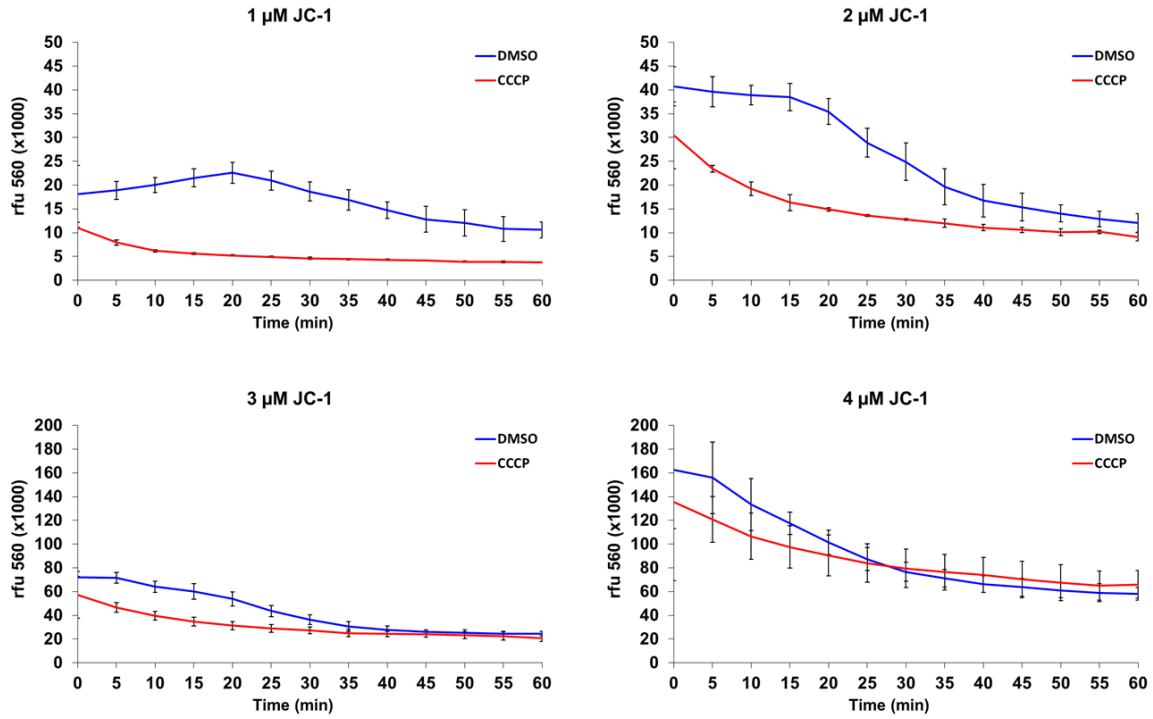

Figure 19: JC-1 fluorescence of non-treated E6/E7 cells (DMSO-negative/solvent control) and CCCP positive control treated cells. Cells were stained with four different JC-1 concentrations.

When comparing the timecourses of JC-1 fluorescence loss (Figure 19) of cells after staining with different JC-1 concentrations, one can observe obvious differences: Firstly, starting JC-1 fluorescence is higher the more JC-1 was used. More importantly, the difference between the curves of solvent control treated cells and CCCP treated cells is decisive. In all graphs fluorescence loss drops faster in cells treated with CCCP compared to DMSO solvent control treated cells, as expected. However, curve shapes are different and also differences between CCCP and DMSO curves are more significant when using 1 and 2 µM JC-1 than 3 or 4 µM. Looking at curves in the publication by Ryan *et al.*, one can see how curves should look like to be able to determine if a certain peptide treatment leads to mitochondrial membrane potential loss or not. Ideally, one is looking for assay conditions, which provide the greatest stability of mitochondrial membrane potential in control treated cells, while providing the greatest dynamic range of mitochondrial membrane potential loss in response to BH3 peptide-induced MOMP [76]. This means that it is important to be able to distinguish between solvent control treated cells and cells, which lose their mitochondrial membrane potential due to treatment with a certain agent. Thus fluorescence curves of DMSO treated cells would be expected to stay constant indicating that those cells keep their mitochondrial membrane potential for a significant amount of time compared to cells losing their membrane potential here due to CCCP treatment. Thus, using 3 or 4 µM JC-1 does not seem to be appropriate because fluorescence difference between DMSO and CCCP treated cells is not as strong as when using 1 or 2 µM JC-1. Furthermore, the curves using 2 µM JC-1 seem to be useful to distinguish between agents, which cause mitochondrial membrane potential loss and those which do not, because JC-1 fluorescence stays constant for about 20 min while one can clearly see that cells treated with CCCP significantly lose their mitochondrial membrane potential. Therefore, it was decided to use 2 µM JC-1 to stain the cells before measuring mitochondrial membrane potential loss.

Optimization of ß-Mercaptoethanol concentration

ß-Mercaptoethanol is included in the assay to dissociate JC-1 aggregates, which are not associated with the mitochondria. Thus ß-Mercaptoethanol is required to reduce background fluorescence [76]. ß-Mercaptoethanol concentrations of 0, 5, and 10 mM during the 20 min staining procedure were tested. As in the JC-1 concentration tests, cells were then treated with CCCP or DMSO as a solvent control and mitochondrial membrane potential loss was measured at 560 nm in the plate reader.

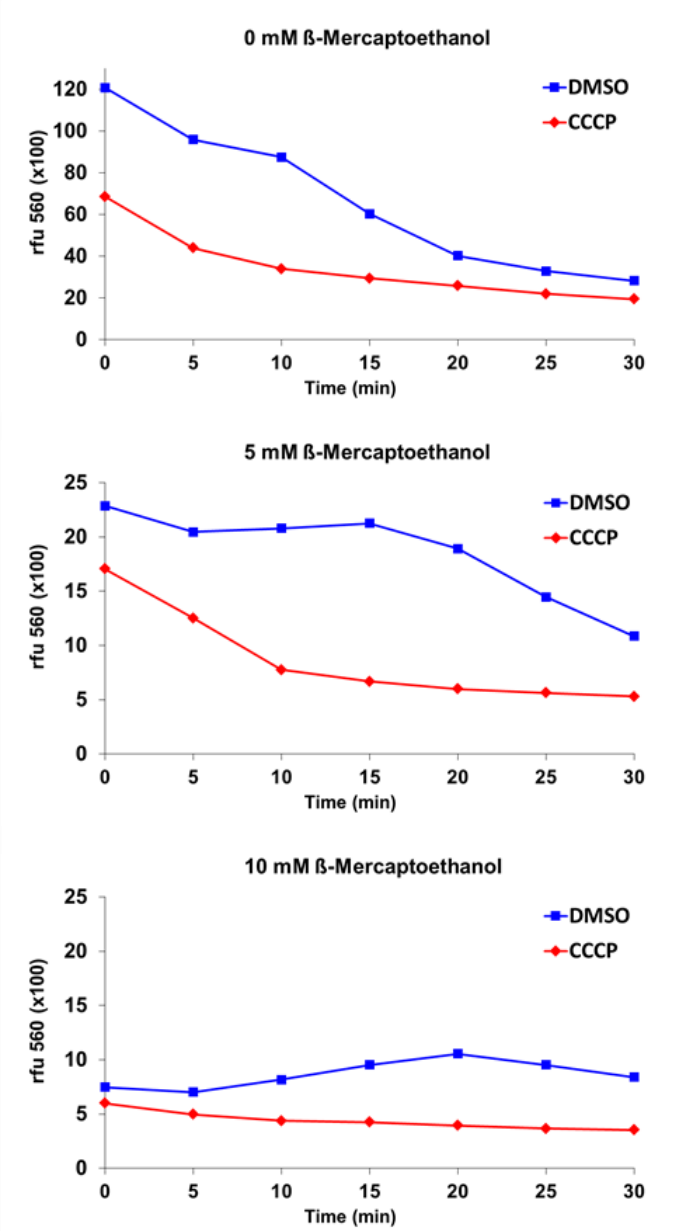

Figure 20: JC-1 fluorescence of E6/E7 cells treated with negative (solvent) control (DMSO) or positive control (CCCP) after staining cells with JC-1 dye solutions containing different ß-Mercaptoethanol concentrations.

The timecourses of JC-1 fluorescence (Figure 20) show that the more ß-Mercaptoethanol is used for the staining procedure the less fluorescence can be measured at 560 nm. Again, one is looking for a ß-Mercaptoethanol concentration, which provides the greatest dynamic range of mitochondrial membrane potential loss between non-treated (solvent control) cells and cells with depolarized mitochondria e.g. due to CCCP treatment. This is the case when using 5 mM ß-Mercaptoethanol. DMSO treated mitochondria keep their potential for about 20 min while CCCP treated mitochondrial show a clear drop in fluorescence loss. Thus it was decided to use 5 mM ß-Mercaptoethanol while staining our cells with JC-1.

Attaining BH3 profiles from JC-1 fluorescence measurements after BH3 peptide treatment

After optimizing JC-1 staining conditions, all of the 6 cell lines were treated with all of the BH3 peptides (Bid, Bim, Hrk, Bad, Bmf, Noxa, Puma, Bik) to finally obtain BH3 profiles. To correct for measuring inaccuracy, cells were treated with each peptide in triplicates on one 96-well plate. Thus error bars for standard deviation could be obtained (Figure 21). BH3 profiles are defined as the percentages of mitochondrial membrane potential loss for each peptide. Since the fluorescence (measured in relative fluorescence units, rfu) of solvent treated cells (either DMSO or H_2O, dependent on the peptide) is defined as 0% mitochondrial membrane potential loss, the potential loss of each peptide is calculated by comparing fluorescence values of peptide treated cells to solvent treated cells with the following formula

$$\%\ \text{membrane potential loss} = \frac{\text{rfu (solvent)} - \text{rfu (treatment)}}{\text{rfu (solvent)}} \times 100\%$$

.

To find out which time point is the best to calculate the BH3 profile, BH3 profiles were compared at different time points (Figure 21).

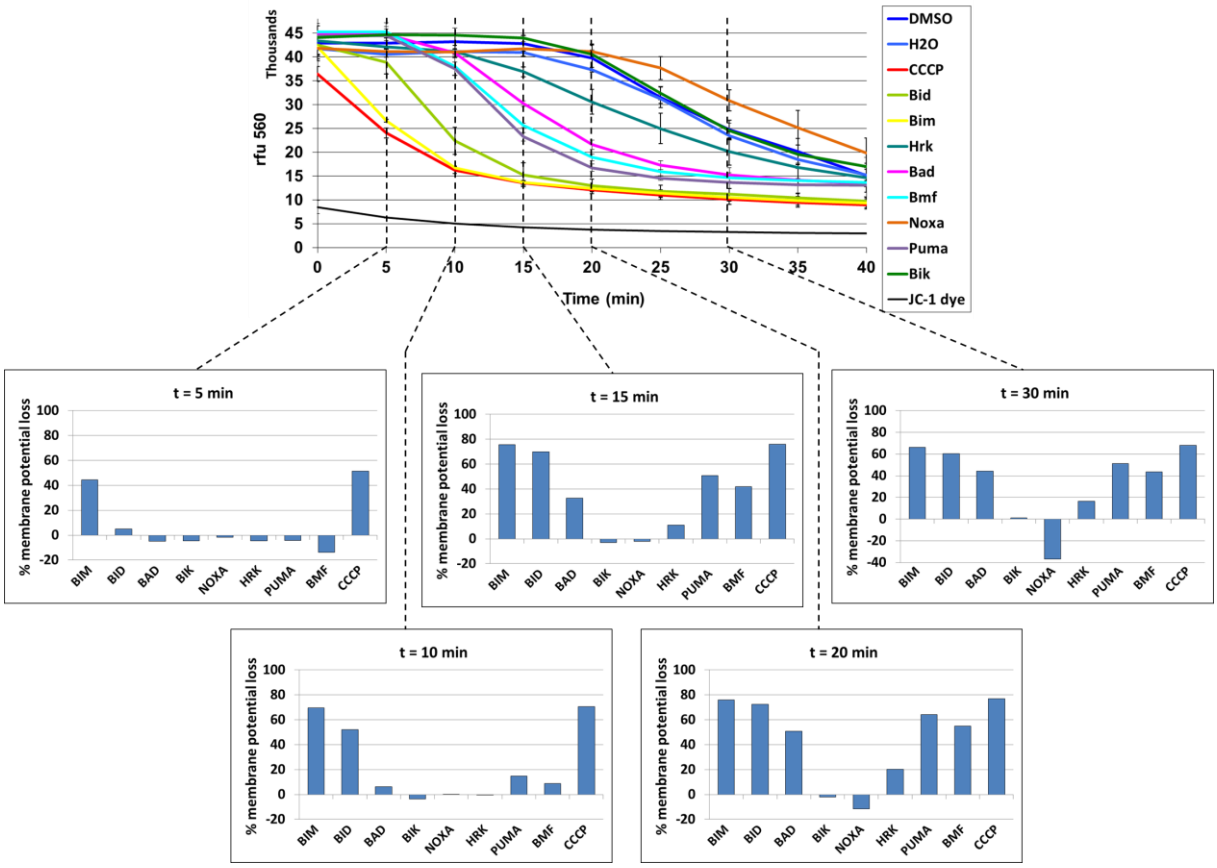

Figure 21: E6/E7 cells were treated with the panel of different BH3 peptides and JC-1 fluorescence loss was measured at 560 nm. To determine which treatment time would be the best for calculating a BH3 profiles, BH3 profiles were calculated at 5, 10, 15, 20, and 30 min after adding treatment and are displayed here.

Error bars for rfu's of technical replicates are of negligible size, which means that results are reproducible. As expected, there are some peptides, which do not lead to a mitochondrial membrane potential loss at all like Bik and Noxa, and the potential of cells treated by those peptides stays close to the potential of cells treated with DMSO or water. As one would expect, the calculated mitochondrial membrane potential of those peptides is about 0%, independent of the time point. As one can see, the potential of Noxa peptide treated cells is bigger (loss is smaller) than that of the solvent controls. This may be due to measuring mistakes as the error bars indicate and explains the negative membrane potential at 30 min. As also expected, the activator peptides Bim and Bid lead to mitochondrial membrane potential loss almost as fast as CCCP. The peptides Bad, Bmf, and Puma also lead to mitochondrial membrane potential loss. But in contrast to Bim and Bid the loss can only be seen after 15 min and peaks at 20 min. This is why it was finally decided to compare profiles of different cell lines at 20 min after peptide treatment because at this time point all peptides show their maximum effect if they show an effect at all. This is also the case for peptides like Hrk in this example which does almost not lead to any mitochondrial membrane potential loss at 5, 10, and 15 min but shows a little loss, namely about 20%, after 20 min. But in general, profiles look very similar at all time points after 10 min, which means that the data are quite robust after an initial reaction time of about 10 min. To finally obtain most solid data, the assay was repeated three times with independent biological samples each time measuring three technical replicates. The resulting 3 BH3 profiles of biological replicates were averaged, standard deviations were calculated and depicted as error bars. Results are shown in Figure 22.

6.3.2. BH3 profiling suggests that HPV induced cancer cells depend more on Bcl-xL for survival than primary keratinocytes

The aim was to find out which antiapoptotic proteins are responsible for the inhibition of apoptosis upon HPV infection. Therefore the BH3 profiling method was used, in which the mitochondrial membrane potential is monitored by staining cells with the fluorescent dye JC-1. As described above, cells were trypsinized and Digitonin was used to allow the BH3 peptides to enter the cell. In each reaction, cells were treated with 100 µM of one of eight BH3 peptides: Bim, Bid, Bad, Bik, Noxa A, Hrk, Puma, and Bmf. When the peptide interacts with a certain antiapoptotic protein that was previously interacting with an activator peptide (Bim or Bid) or an effector (Bax or Bak) Bcl-2 protein, those proapoptotic proteins are released from the antiapoptotic protein leading to activation of Bax/Bak followed by a rapid mitochondrial membrane potential loss, which in turn can be monitored by the fluorescence

loss of JC-1. The percentages of mitochondrial membrane potential loss compared to solvent-treated controls are shown for all peptides and all cell lines in Figure 22.

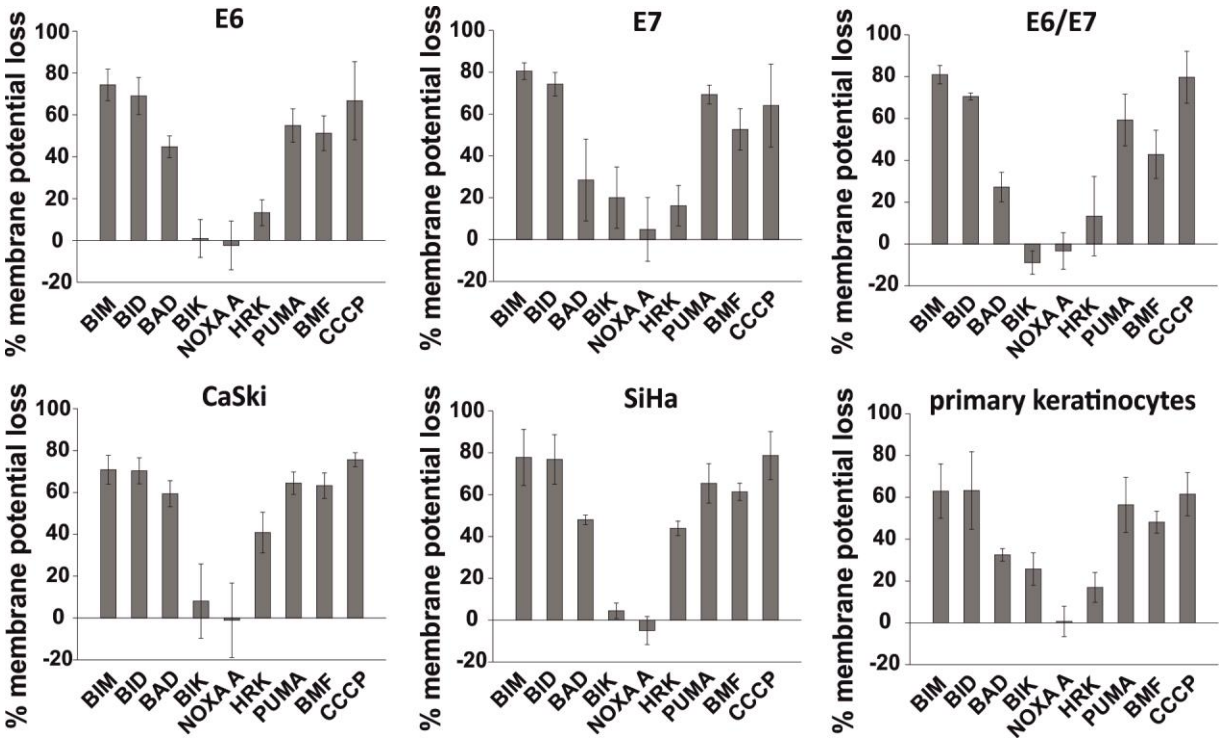

Figure 22: BH3 profiles of mitochondrial membrane potential loss at 20 min after treatment. Membrane potential loss is defined as the JC-1 fluorescence loss after 20 min of treatment in comparison to the fluorescence loss of cells without treatment, meaning the solvent control (DMSO or H2O). Cells are treated with BH3 peptides (BIM, BID, BAD, BIK, NOXA A, HRK, PUMA, or BMF) or as a positive control for the JC-1 assay with the chemical CCCP. The graphs show means of three biological and three technical replicates with error bars for standard deviation.

The BH3 profiles show that all of the cell lines lose their mitochondrial membrane potential almost completely upon treatment with the activator peptides Bim and Bid. The percentages were equally high compared to the positive control CCCP. This indicates that the effectors Bak and/or Bax are present and can be fully activated to permeabilize the mitochondrial outer membrane.

With the sensitizer BH3 only proteins more distinct results were found: All six cell lines show high mitochondrial membrane potential loss when treated with the sensitizer BH3 peptides Puma and Bmf and modest membrane potential loss when treated with Bad peptide. The ability of these BH3 peptides to induce mitochondrial membrane potential loss implies that they interact with antiapoptotic proteins, which in turn release Bim, Bid, Bax or Bak to induce MOMP [32]. Interestingly, Puma, Bmf and Bad all bind to Bcl-2, Bcl-xL and Bcl-w

(Figure 15) indicating that at least one of those three antiapoptotic proteins is active in all six cell lines and not altered by E6 or E7.

Noxa A and Bik peptide treatment showed almost no effect on the membrane potential in none of the cell lines. Contrarily, Hrk peptide induces a substantial membrane potential loss in the cervical cancer cell lines CaSki and SiHa, while the effect on the other cell lines is rather modest. Hrk peptide treatment seems to be indeed the sensitizer that differs the most between the cell lines. This is very interesting as according to the Bcl-2 protein interaction map (Figure 15) Hrk only interacts with Bcl-xL. Thus the difference in Hrk peptide sensitivity between the cell lines could indicate that HPV influences Bcl-xL expression/activity.

In conclusion, one can say that the mitochondrial membrane potential loss upon Hrk peptide treatment together with the fact that Hrk only interacts with Bcl-xL makes Bcl-xL an interesting candidate of being responsible for the survival of HPV infected cells. Western blot results for Bcl-xL show that Bcl-xL seems to be upregulated in the HPV oncogene immortalized and cervical cancer cell lines in comparison to primary keratinocytes (Figure 17). The fact that Bcl-xL is upregulated in the cancer cells in comparison to primary keratinocytes fits together with the BH3 profiling data because the cancer cells also show a stronger response to the Bcl-xL interacting peptide Hrk. Consequently, one could infer that the cancer cells depend more on Bcl-xL for survival than the primary keratinocytes. However, the oncogene immortalized keratinocytes also show upregulated Bcl-xL levels but respond to Hrk peptide as little as the primary keratinocytes. So despite a similar Bcl-xL expression of E6, E7, and E6/E7 cells in comparison to the cancer cell lines, their survival does not seem to depend as much on Bcl-xL as the survival of SiHa and CaSki. In summary, one can speculate that HPV induced cancer cells may gain resistance to apoptosis by the upregulation of Bcl-xL.

6.4. HPV cell lines are more resistant to Bid induced MOMP than primary keratinocytes

As described above, Bid and Bim peptide treatment induced a high mitochondrial membrane potential loss in all of the tested cell lines. However, one needs to consider that the cells were only treated with one peptide concentration (100 µM according to [34]). Since a concentration of 100 µM peptide may be too high to discover differences between the cell lines in their apoptotic behavior, cells were treated with decreasing peptide concentrations in the range of 0.4 – 100 µM. As a result typical dose-response curves were obtained for Bid peptide treatment (Figure 23) while for Bim peptide a strong mitochondrial membrane potential loss

could be observed even with a concentration of 0.4 µM. Since Bim peptide appeared to be a more potent apoptosis inducer, Bim peptide concentrations as low as 0.002 µM were used to receive dose-response curves (Figure 23).

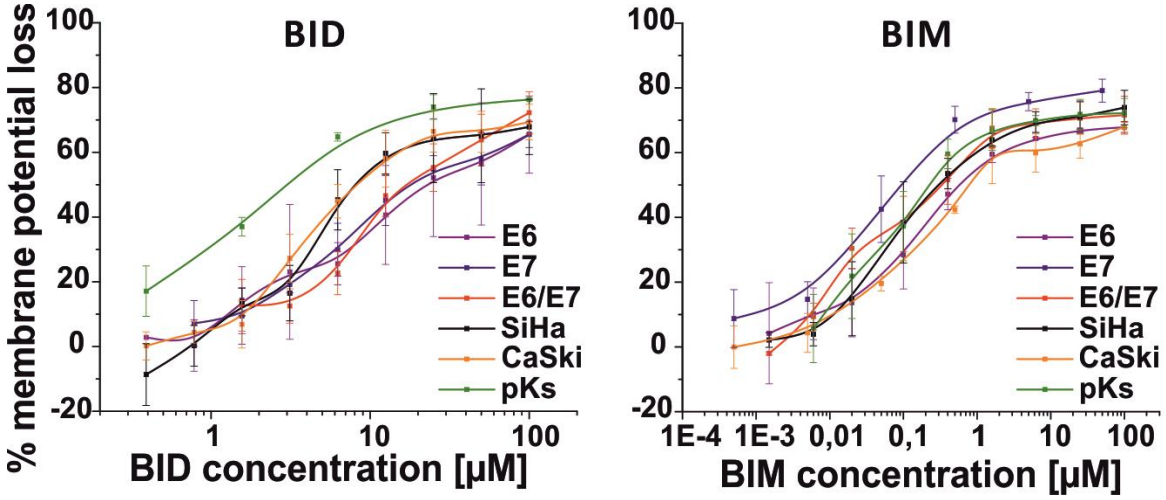

Figure 23: Dose-response curves of mitochondrial membrane potential loss treating the HPV induced cancer model cell lines for 20 min with different concentrations of the activator BH3 peptides Bid and Bim. As for the BH3 profiles, mitochondrial membrane potential loss was measured via JC-1 fluorescence. Results are plotted in semi-log scale. The graphs show means of three biological and three technical replicates with error bars for standard deviation.

But even at the lowest Bim peptide concentrations one could not observe significant differences in mitochondrial membrane potential loss between the cell lines. However, for Bid peptide treatment, a stronger mitochondrial membrane potential loss could be observed in primary keratinocytes with lower Bid peptide concentrations compared to the other cell lines. Consequently, the primary keratinocytes appear to be more sensitive to Bid peptide treatment meaning less resistant to Bid induced apoptosis in comparison to the oncogene immortalized and cervical cancer cell lines.

6.5. Cell death upon Bid peptide induced apoptosis is reduced in HPV oncogene expressing cells

Treating the HPV model cell lines with different Bid peptide concentrations and measuring mitochondrial membrane potential loss via JC-1 fluorescence loss as an indicator for apoptosis, it was concluded that primary keratinocytes are more sensitive to Bid induced apoptosis than the other cell lines. To confirm this data, additional methods to follow the apoptotic events downstream of mitochondrial membrane potential loss were used. Therefore other cell death assays were applied. The fluorescence probe SYTOX that detects dead cells was used. The probe does not cross intact cell membranes. It increases fluorescence upon

dsDNA binding entering cells with defective membranes binding to their nuclear DNA. Thus fluorescence signals indicate cell death at a later stage than JC-1 indicating only mitochondrial-membrane potential loss. The SYTOX cell death assay was compared to a caspase activity assay measuring caspase activity by luminescence signals (Caspase-Glo Assay, Promega) (Figure 24). Caspases get activated after MOMP but before the cell membrane gets permeable. Using the JC-1 assay and the two cell death assays, cell death could be detected at three different stages.

Apoptosis was induced using two different reagents. One the one hand apoptosis was induced with TNF. However, TNF has been shown to not cause cell death on its own because the TNF receptors lead to expression of apoptosis inhibitors in the cell. Thus, additionally to TNF, cells were treated with cycloheximide, which blocks new protein synthesis and thus the expression of inhibitors of apoptosis. Using this reagent combination, Bid has been shown to be essential for TNF-induced apoptosis [77]. Since JC-1 data suggested that primary keratinocytes are more sensitive to apoptosis induced by Bid, this hypothesis could be tested using TNF together with cycloheximide (Figure 24). To furthermore test the hypothesis, apoptosis was also induced with the drug Camptothecin, which has also been shown to induce apoptosis via Bid participation [78, 79] (Figure 25).

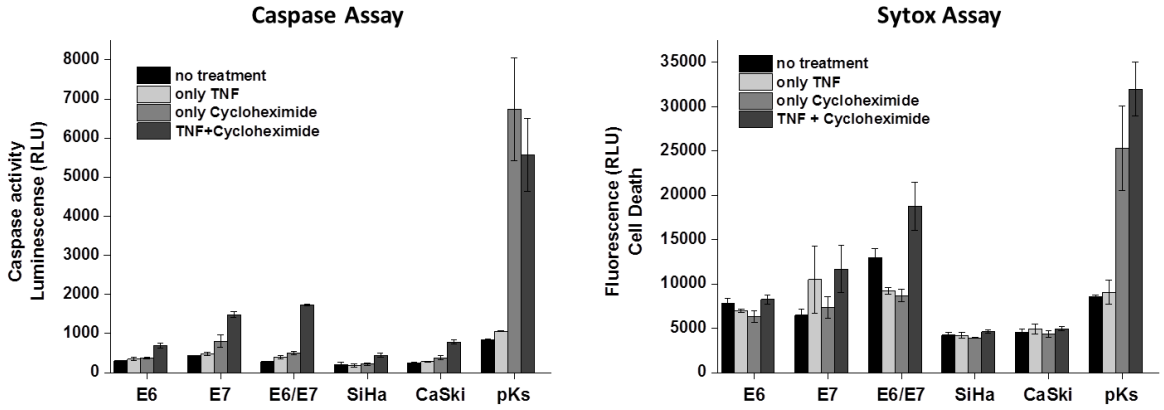

Figure 24: Cell death assays with TNF and Cycloheximide. Cell death was detected by measuring caspase activity with the luminescence based Caspase-Glo Assay (Promega) (left) or Sytox fluorescence (right). The graphs show means of triplicates with error bars for standard deviation.

Regarding Figure 24, both cell death assays imply that the primary keratinocytes are more sensitive to TNF/Cycloheximide induced apoptosis than all the other cell lines. This confirms the Bid dose-response data. However, one has to admit that the controls suggest that the assays may be error-prone: In the caspase assay the controls look rather fine since in all cell

lines except the primary keratinocytes no treatment, and single treatments with TNF and Cychloheximide show a lower death/caspase activity than the combined treatment with TNF and Cycloheximide. However, the primary keratinocytes show a higher caspase activity upon single Cycloheximide treatment than upon combined treatment with TNF. This result shows that primary keratinocytes are more sensitive to death signaling but this is not necessarily due to Bid induced apoptosis triggered by TNF. The controls of the Sytox assay do not look very convincing either: The primary keratinocyte results rather look as expected, although here Cycloheximide single treatment also show very high death response. However, the Sytox reagent itself seems to induce cell death in the immortalized keratinocytes (in E6 and E6/E7) or TNF single treatment also results in Sytox fluorescence comparably high to TNF in combination with Cycloheximide. In summary, the Caspase assay and the Sytox assay with TNF and Cycloheximide propose that the primary keratinocytes are more sensitive to apoptosis induced via Bid signaling but one has to consider that both assays do not show very reliable data because the controls do not behave as expected.

Since caspase assay results are more trustworthy because they were more reproducible and controls look fine in all cells except primary keratinocytes, Camptothecin treatment was read-out with the caspase assay (Figure 25).

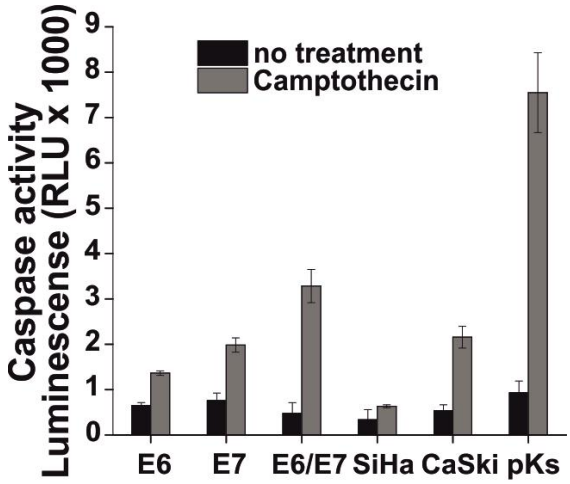

Figure 25: Caspase activity assay (Caspase-Glo Assay, Promega) with and without Camptothecin treatment for 24 hours. Caspase activity is measured in relative luminescent units (RLU). Luminescence is generated when active caspases react with the Promega substrate added. The graphs show means of triplicates with error bars for standard deviation.

In agreement with the Bid dose-response curves, primary keratinocytes show more caspase activity upon Camptothecin treatment than the other cell lines. This means that they are less resistant to apoptosis. Since Camptothecin induced apoptosis involves Bid activation, the observation that the drug treatment leads to less caspase activity in HPV oncogene immortalized and cancer cell lines supports the idea that Bid induced apoptosis is downregulated during HPV infection.

6.6. Experiments knocking-down Bcl-xL in cervical cancer cell lines are in agreement with the upregulation of Bcl-xL upon HPV infection being responsible for apoptosis resistance

One question was why the HPV model cell lines were more resistant to Bid induced mitochondrial membrane potential loss (Figure 23) and Camptothecin induced apoptosis (Figure 25) than primary keratinocytes. To answer this, one can take a look at the Western blots (Figure 17) and BH3 profiles (Figure 22) again. As described above, it was speculated that HPV induced cancer cells may gain resistance to apoptosis by upregulation of Bcl-xL. If cancer cells were more resistant to apoptosis because of the upregulation of Bcl-xL, they should get more sensitive to apoptosis stimulation if Bcl-xL is downregulated. To test this hypothesis, Bcl-xL was knocked down in the cervical cancer cell lines CaSki and SiHa by siRNA treatment.

6.6.1. Optimization of knock-down with siRNA

At first siRNA knock-down conditions had to be optimized. Validated siRNA (Silencer Select, Ambion) was used. This siRNA has been verified experimentally to reduce the expression of their target gene. Off-target effects are certified to be negligible. In the first knock-down experiment, only SiHa cells were used and two different transfection reagent (Lipofectamine) concentrations and three different siRNA concentrations were tested. To show that the siRNA treatment procedure does not have an effect on the experimental results themselves, cells were also treated with a negative control siRNA using the same reagents as for the Bcl-xL siRNA treatment (Figure 26). One can see that the knock-down was considerably more effective when using 1 µl Lipofectamine per 6-well than 0.3 µl. However, the siRNA concentration does not seem to affect the knock-down efficiency: Bcl-xL seems to be just as well downregulated with 2 nM siRNA as with 5 or 10 nM. Thus, 1 µl Lipofectamine per 6-well was used for knock-down experiments from now on. Furthermore, it was decided to only use 2 nM siRNA to reduce possible side effects of siRNA treatment.

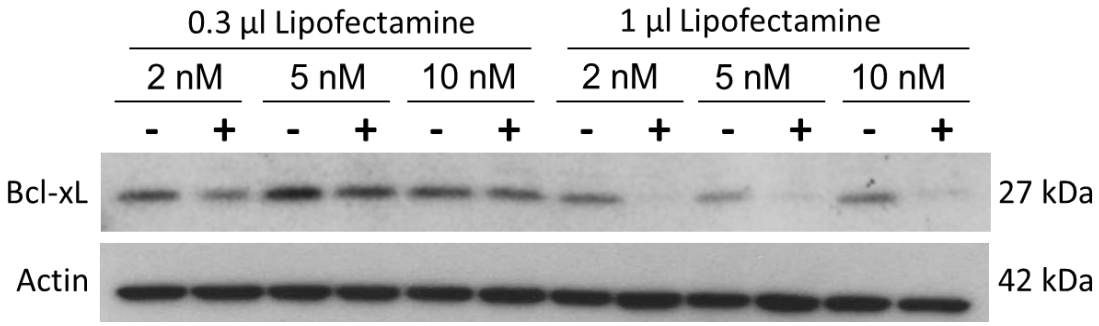

Figure 26: Western blot analysis of total protein lysates of SiHa cells treated with Bcl-xL siRNA (+) or negative control siRNA (-). Cells were incubated for 48 h after siRNA treatment before lysis. To optimize knock-down conditions three different siRNA concentrations and two different transfection reagent (Lipofectamine) amounts per 6-well were used. Western blots were performed with antibodies against Bcl-xL and Actin as loading control. Molecular weights are shown on the right.

Furthermore, it was tested if knock-down efficiency would increase when the incubation time was increased from 48 hours, as used before, to 72 hours. This time CaSki cells were used to test if the knock-down also functions under the same conditions in those cells as in SiHa but only the two lower siRNA concentrations were tested.

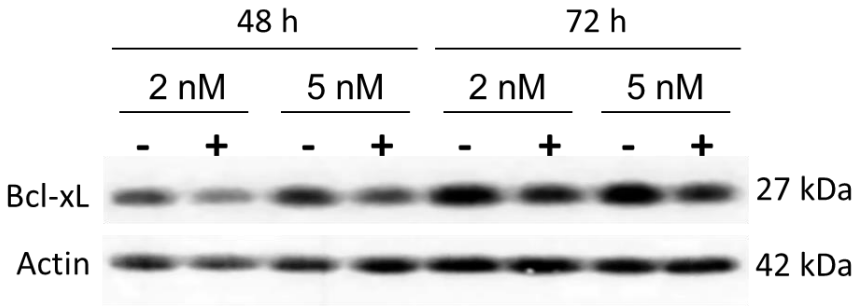

Figure 27: Western blot analysis of total protein lysates of CaSki cells treated with Bcl-xL siRNA (+) or negative control siRNA (-). Cells were incubated for 48 h or 78 h after siRNA treatment before lysis. Furthermore, two different siRNA concentrations were tested. Western blots were performed with antibodies against Bcl-xL and Actin as loading control. Molecular weights are shown on the right.

Observing the Western blot, one can see that the knock-down worked with both concentrations and both incubation times, although it needs to be admitted that the results are not as clear as in the previous Western blot. However, siRNA concentration again does not seem to influence results neither does incubation time. Thus, it was decided to keep the conditions as optimized in our first siRNA experiment using 2 nM siRNA, 1 µl Lipofectamine per 6-well and incubating cells for 48 hours after treatment. To test if these conditions lead to

reproducible results in both SiHa and CaSki cells, Bcl-xL Western blots were performed for three independent experiments.

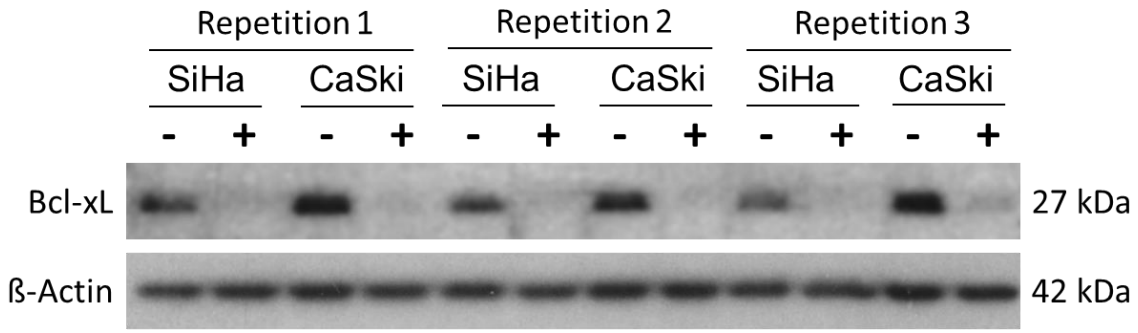

Figure 28: Western blot analysis of total protein lysates of SiHa and CaSki cells treated with Bcl-xL siRNA (+) or negative control siRNA (-). Cells were incubated for 48 h after siRNA treatment before lysis. To test reproducibility, three independent experiments were carried out. Western blots were performed with antibodies against Bcl-xL and Actin as loading control. Molecular weights are shown on the right.

Figure 28 clearly shows that Bcl-xL knock-down is reproducible for three different experiments in both SiHa and CaSki cells.

6.6.2. Bim and Bid dose-response curves in SiHa and CaSki with downregulated Bcl-xL

After optimizing Bcl-xL knock-down conditions, the hypothesis if HPV induced cancer cells gain apoptosis resistance by upregulation of Bcl-xL was tested. If cancer cells were more apoptosis resistant because of the upregulation of Bcl-xL, they should get more sensitive to apoptosis stimulation if Bcl-xL is downregulated. To test if this is true, the cells were treated with different Bid and Bim activator peptide concentrations and mitochondrial membrane potential loss was measured as an indicator for apoptosis via JC-1 fluorescence. To show that the siRNA treatment procedure does not have an effect on mitochondrial membrane potential loss, cells were also treated with a negative control siRNA using the same reagents as for the Bcl-xL siRNA treatment. As another reference, the experiments were also performed with non-treated cells (Figure 29). As expected, there is almost no difference between the dose-response curves of cells treated with negative control siRNA or non-treated cells. Comparing Bid dose-response curves (Figure 29A) one can see that both SiHa and CaSki cells with knocked-down Bcl-xL are more sensitive to Bid treatment than cells with original Bcl-xL content: In the range of Bid concentrations between 1.6 and 12.5 µM Bcl-xL knock-down cells lose their mitochondrial membrane potential considerably more than cells with original

Bcl-xL levels. This result supports the hypothesis that cervical cancer cell lines are more resistant to apoptosis because of the upregulation of Bcl-xL.

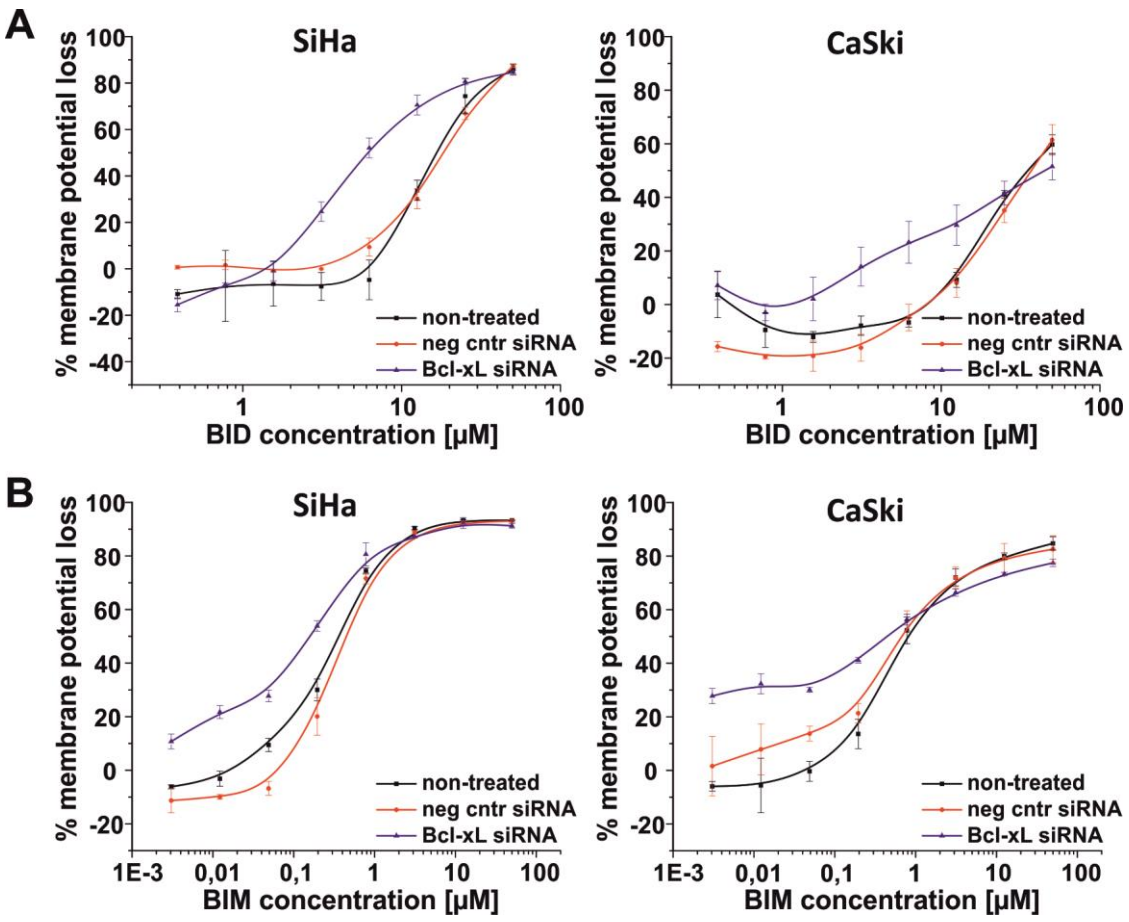

Figure 29: Bcl-xL knock-down causes cervical cancer cell lines to become less resistant to Bid induced apoptosis. Dose-response curves of mitochondrial membrane potential loss treating cells with different concentrations of Bid (A) and Bim (B). Both SiHa and CaSki cells (non-treated) were each analyzed in comparison to cells with knocked down Bcl-xL (Bcl-xL siRNA) and negative control siRNA (neg cntr siRNA) treated cells. Membrane potential loss was measured via JC-1 fluorescence as before. The graphs show means of triplicates with error bars for standard deviation.

Since there were no obvious differences in Bim dose-response curves between primary keratinocytes, HPV oncogene immortalized and cervical cancer cell lines (Figure 23), the effect of Bcl-xL knock-down on Bim dose response curves was also tested. But the difference between the dose-response curves of negative control siRNA/non-treated cancer cells and Bcl-xL knocked down cells is not as prominent for Bim as for Bid treatment. Consequently, the Bid – Bcl-xL interaction seems to be more important than the Bim – Bcl-xL interaction in the process of cervical cancer cells gaining resistance to apoptosis.

6.7. Discussion and Outlook

In this study the Bcl-2 protein network was investigated in an HPV infection cell model comparing primary keratinocytes with keratinocytes immortalized with the oncoproteins E6 or/and E7 and the cervical cancer cell lines SiHa and CaSki. Both cell viability assays and a Bid dose-response BH3 profiling assay showed that cells expressing the oncoproteins gain resistance to apoptosis in comparison to the primary keratinocytes. The antiapoptotic protein Bcl-xL was found to be upregulated upon expression of the HPV oncoproteins E6 and E7. Applying the BH3 profiling assay using all BH3 peptides, Bcl-xL upregulation was suggested to be responsible for HPV cancer cells becoming resistant to apoptosis. This hypothesis was supported by siRNA experiments: Knocking down Bcl-xL in the cervical cancer cell lines SiHa and CaSki, these cell lines became more sensitive to Bid induced apoptosis.

Differences between primary keratinocytes and all the other cell lines could be observed in Bcl-xL expression, in response to Bid treatment, and in caspase activity upon Camptothecin treatment. But no differences could be detected between oncogene immortalized and cancer cell lines or between the different oncogene immortalized cells. This observation suggests that expression of one oncogene seems to be sufficient to cause cells to become more resistant to apoptosis. The expression levels of Bak and Bid supported this hypothesis since Bak and Bid were downregulated upon the expression of one or both oncogenes. However, mitochondrial membrane potential loss in response to Hrk treatment, which was observed in the BH3 profiles, was higher in the cancer cell lines than in all the other cell lines. Since Hrk only interacts with Bcl-xL, the cancer cells seem to depend more on Bcl-xL for survival than all the other cell lines. Although Bcl-xL was expressed in higher amounts in the oncogene immortalized keratinocytes in comparison to the primary keratinocytes, Bcl-xL may not be loaded with activator and effector Bcl-2 proteins in the oncogene immortalized cells as much as the cancer cell lines. This may be an explanation for the lower response of immortalized keratinocytes to Hrk treatment in comparison to the cancer cells.

The equally high response to Bim and Bid peptide treatment in all cell lines in the BH3 profiles was rather unexpected since the expression of Bak and Bax was different. Additionally, it has been published that E6 but not E7 leads to downregulation of Bax. Therefore differences in the sensitivity to the activator peptides or generally differences in the BH3 profiles would have rather been expected. One can speculate that the available Bax is sufficient for apoptotic functions. Another explanation is that the Bid and Bim signals just get saturated very quickly because only small amounts of these peptides may be enough to induce

cell death. Furthermore, with respect to Sarosiek et al. [80] even another explanation could be possible: Sarosiek et al. state that Bid preferentially activates Bak while Bim preferentially activates Bax. If this holds true, Bax is not as important as Bak in the used model cell lines to initiate apoptosis because there was almost no Bim expressed in the primary and immortalized keratinocytes (Figure 17) to activate Bax. However, the Bak and Bid expression was downregulated in immortalized keratinocytes and cancer cells with respect to the primary keratinocytes. Assuming that Bid induces apoptosis by preferentially activating Bak explains the observations of higher caspase activity in primary keratinocytes compared to the other model cell lines. Furthermore, it also explains the Bid dose-response results since a higher membrane potential loss upon Bid peptide treatment could be observed in primary keratinocytes compared to the other model cell lines: With respect to Sarosiek et al. one would expect a higher membrane potential loss upon Bid treatment in primary keratinocytes because they have higher Bak levels compared to the other cell lines. However, the observation that there were no differences within the cell lines in Bim titrations cannot be explained by their activation model.

As stated in the introduction (I.4.2), researchers have seen a clear connection between apoptosis inhibition by E6 oncoprotein both of the extrinsic and intrinsic pathway of apoptosis. Thus E6 seems to play an important role in HPV induced cancer cells gaining resistance to apoptosis. However, E7 so far has been shown to inhibit or induce apoptosis depending on the cell model system being experimented on [66]. However, the experiments presented here, Bid dose-response curves and caspase assays, show that E7 by itself seems to be sufficient for cells gaining resistance to apoptosis.

Others have already studied die expression of Bcl-2 proteins during HPV infection. Du et al. observed that the resistance to apoptosis of HPV is associated with decreased Bak and increased Bcl-2 expression [81]. This is in agreement to the observations in this study since Bak was downregulated in immortalized and cancer cells and Bcl-2 was upregulated (Figure 17). However, others also obtained different results like Aguilar-Lemarroy et al. Their Western blots of primary keratinocytes, E6, E7, and E6/E7 cells show a downregulation of Bcl-2 in the immortalized cells compared to pK and similar expression of Bcl-xL in all cell lines with a slightly smaller amount in E6 cells [69].

Deng et al. state that via BH3 profiling it is possible to identify classes of apoptotic blocks in cells defining by which kind of molecular mechanisms cancer cells gain resistance to

apoptosis. They define three distinct classes: class A block cells inhibit upstream activation of BH3-only proteins; class B block cells lose Bax and Bak; class C block cells express antiapoptotic proteins preventing the activation of Bax and Bak [75]. All of the cells used in this study showed class C block BH3 profiles since they all lost their mitochondrial membrane potential upon Bim and Bid peptide treatment and selective membrane potential loss upon sensitizer BH3 peptide treatment (Figure 22).

It is striking that most of the observed differences were between the primary keratinocytes and all the other cell lines. This is in agreement with the fact that apoptosis seems to be inhibited upon HPV oncogene expression. However, critics may note that it may be possible that resistance to apoptosis is not developed in response to HPV oncogene expression but actually in cultured cells in contrast to primary cells since all the HPV infected cells are cell culture cell lines while pK are not. To rule this possibility out one could perform the experiments with primary cells freshly transformed or transfected with oncogenes. However, it is rather difficult to transfect primary cells. Another possibility would be to perform those experiments with the NIKS human keratinocyte progenitor cell line. This is a cell line, which can be cultivated but behaves as normal human keratinocytes [82]. Another possibility to confirm the data and take more physiological relevant assumptions would be to work on primary tissue from cancer and healthy patients.

If Bcl-xL can be confirmed to be responsible for HPV infected cells to gain resistance to apoptosis, strategies like BH3 mimetics could be applied for cervical cancer treatment to specifically target cancer cells regaining sensitivity for apoptosis. This could make it possible to treat patients, who may have acquired resistance against chemotherapy regaining sensitivity for those kinds of drugs.

All in all, the BH3 profiling method was applied successfully in the HPV infection cell model finding Bcl-xL as an interesting candidate to be responsible for gaining apoptosis resistance upon HPV oncoprotein expression and cervical cancer development.

7. Imaging the structural organization of ER-mitochondria contact sites by high resolution fluorescence microscopy

Mitochondria and ER have been shown to come into close contact at ER-mitochondria contact sites called MAMs (mitochondria associated membranes). These contact sites are important for several housekeeping functions of the cell like Ca^{2+} transfer from ER to mitochondria and the transfer of lipids and lipid biosynthesis. More and more proteins are identified to be important for keeping those two organelles in close contact but little is only known about the structural organization of those proteins.

7.1. Experimental strategy: High resolution microscopy – STED

The distance between ER and mitochondria at their interaction sites is very small and has been estimated to be between 10 and 25 nm [12]. This is why an in depth visualization of MAMs is not possible with conventional confocal microscopy [83]. However, several groups have published images simultaneously labeling ER, mitochondria and a MAM protein of interest, but these images do not give an insight into the structural organization of MAMs but rather visualize the MAM as a point of colocalization of all three labels [8, 84]. Thus, a promising approach to study ER-mitochondria interaction sites are high-resolution microscopy techniques like STED [85] to gain a deeper insight into the structural organization of proteins at the contact sites. This study was conducted in collaboration with Dr. Jasmin Zahn from the Division of Optical Nanoscopy, German Cancer Research Center (Prof. Stefan Hell). A microscopy setup established by Dr. Thorsten Staudt was used, with which one can simultaneously image two fluorescence dyes by STED microscopy (DY485XL (DY: Dyomics), and Atto565) and additionally the fluorescent protein GFP by confocal microscopy. Other groups mainly used fluorescent proteins to label ER, mitochondria and MAM proteins of interest or Mitotracker, a fluorescent dye localizing to mitochondria. But neither fluorescence proteins nor Mitotracker are photostable enough for high resolution STED microscopy. Consequently, it was not possible to apply those fluorescence labels used by other groups to visualize MAMs with STED. Therefore, another strategy for visualization of ER-mitochondria contact sites had to be established. After having tested two antibodies against the ER protein Calnexin without obtaining high quality images, the well-established ER-GFP construct was used for ER visualization and hence the ER was visualized only confocally at the setup. In this construct GFP is linked to the ER protein Sec61beta [86]. Sec61beta is a protein in the ER membrane and thus exactly marks the site of ER-mitochondria interaction. Therefore, mitochondria and MAM proteins of interest had to be

imaged using the fluorescence dyes Atto565 and DY485XL. Both dyes are available as secondary antibodies and in this way can be used for immunostaining. Atto565 can be resolved slightly better with STED microscopy at the used microscopy setup than DY485XL. Consequently for two-color images Atto565 was combined with ER-GFP. Aiming for 3-color images, the MAM protein of interest was stained with Atto565 to resolve its unknown distribution and mitochondria were stained with DY485XL. Two primary antibodies were tested to visualize mitochondria because in some publications a matrix targeted dsRed fluorescent protein was used in combination with Sec61beta-GFP to identify MAMs [8, 87] and other publications used a primary antibody directed against Tom20, the translocase of the mitochondrial outer membrane, as a mitochondrial marker [88]. Thus, Tom20 was tested as one possible mitochondrial marker in combination with ER-GFP to identify MAMs. Mitochondrial matrix targeted dsRed cannot be used for STED at the used microscopy setup. Therefore an antibody directed against a mitochondrial matrix protein was chosen to be tested as the second possibility to label mitochondria. An antibody, which was described to function well for immunocytochemistry, was an antibody against the matrix protein Acat1 (Acyl-CoA:cholesterol acyltransferase).

As an example of a MAM protein, the chaperone Grp78 was chosen to be visualized in this study. Grp78 is a molecular chaperone important for Ca^{2+} transfer (chapter I.2.2 Functions at the MAM). Imaging a MAM protein with respect to ER and mitochondria, the aim is to get an insight into the structural organization of the ER-mitochondria contact sites.

In this study COS-1 cells were used because their lamellipodia stretch out widely so that the ER can be visualized nicely as a tubular network and ER-mitochondria interaction sites are visible. It should be mentioned that COS-1 cells are about 50 µm in diameter on average, which is too large for taking STED images of whole cells with the used setup. This would take about 1 h and within this time cells may shift in z-direction making an overlay of mitochondrial and ER images impossible. This is why images of whole cells are all only confocal images and details are shown as STED images.

7.2. Visualization of ER-mitochondria contact sites

7.2.1. Imaging ER: Transfection with Sec61ß-GFP plasmid

To image the ER the ER-GFP construct Sec61beta-GFP was used. For high-resolution microscopy, labeling conditions have to be fine-tuned intensively to obtain a staining intensity

high enough to be visible with the used lasers and low enough to still be comparable with other fluorescence dyes used, whose fluorescence intensity may be reduced upon using STED. Fluorescence intensity of ER-GFP could be fine-tuned by using different amounts of plasmid DNA. After optimization of transfection conditions, the ER-network could be nicely imaged (Figure 30).

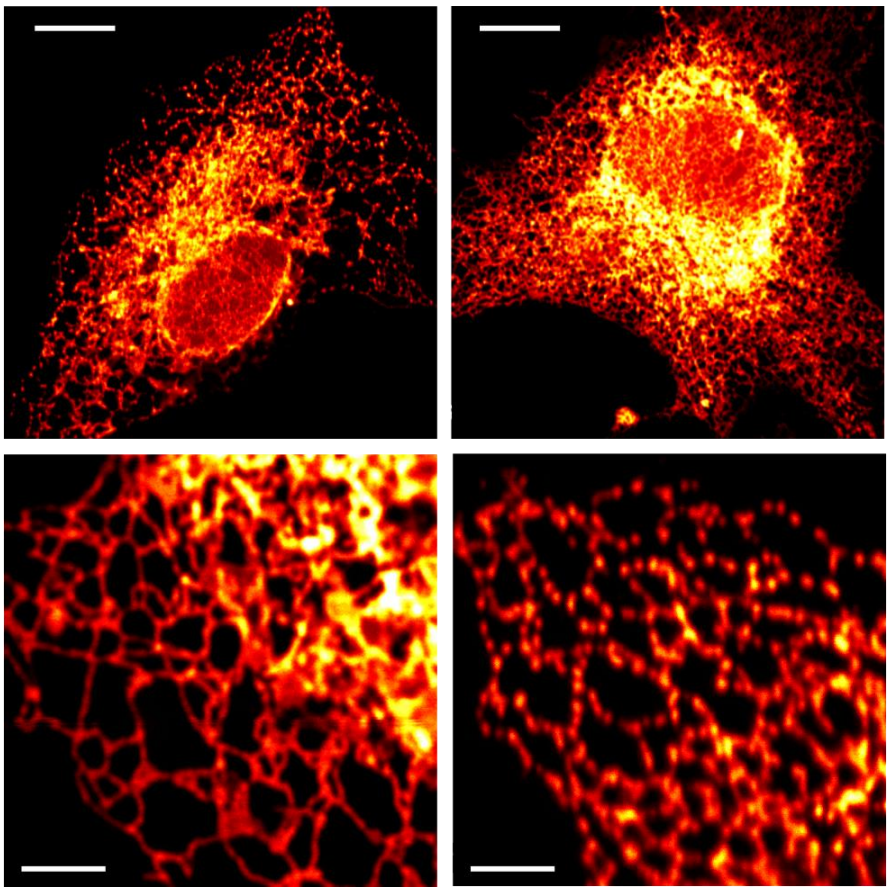

Figure 30: Confocal images of COS-1 cells expressing GFP fused to Sec61beta labeling the ER (ER-GFP). (Red-hot color map visualized fluorescence intensity from dark red (low intensity) to yellow/white (high intensity). (Scale bars: upper images: 10 µm, lower images: 3 µm)

Figure 30 shows that the ER can be nicely visualized with the used microscopy setup, using Sec61beta-GFP. In COS-1 cells one can differentiate between the dense ER around the nucleus consisting of flat membrane sheets (perinuclear region in the upper images) and the peripheral ER forming a continuous network of cylindrical tubules [89] (lower images of Figure 30).

7.2.2. Imaging mitochondria by immunostaining

To get an overview of the mitochondrial distribution and shape in COS-1 cells, mitochondria were first imaged by Tom20 immunostaining. To be able to obtain STED images of Tom20, antibody concentrations had to be optimized of primary and secondary antibody to the extent

that Tom20 staining was dense enough to be highly resolved and bright enough to be STEDed since the STED laser has a high intensity leading to bleaching. Mitochondrial shape and distribution in the whole cell can be seen after optimizing immunostaining conditions in Figure 31.

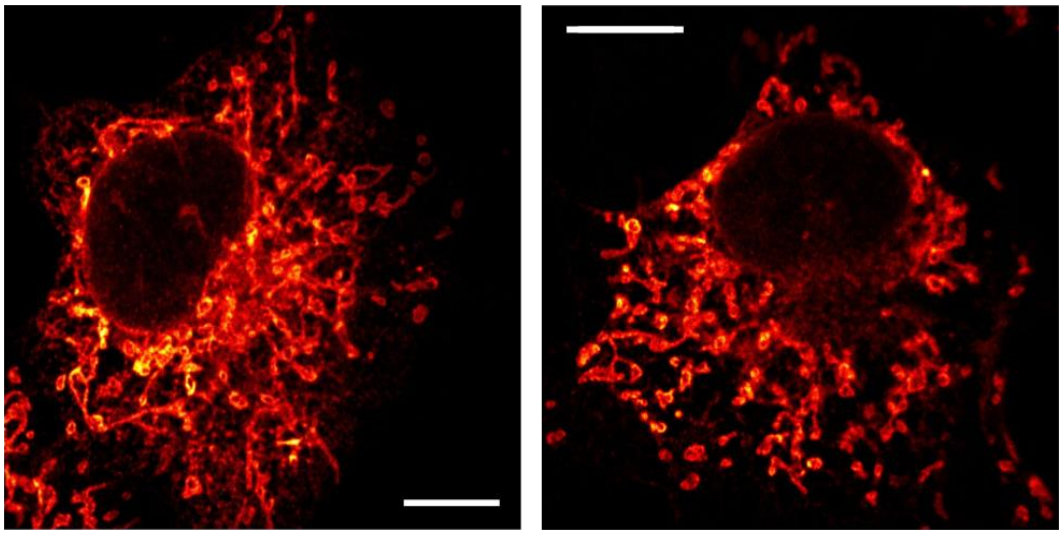

Figure 31: Confocal microscopy of mitochondria in COS-1 cells. Immunostaining with Tom20 primary antibody and DY485XL labeled secondary antibody. (Scale bars: 10 µm, red-hot color map)

Figure 31 shows that in COS-1 cells mitochondria mainly curl in contrast to many other cell types where they mainly exist as long tubules [90, 91]. Here tubules are rather short and mitochondria form donuts and spheres. This can also be seen in close up images (Figure 32).

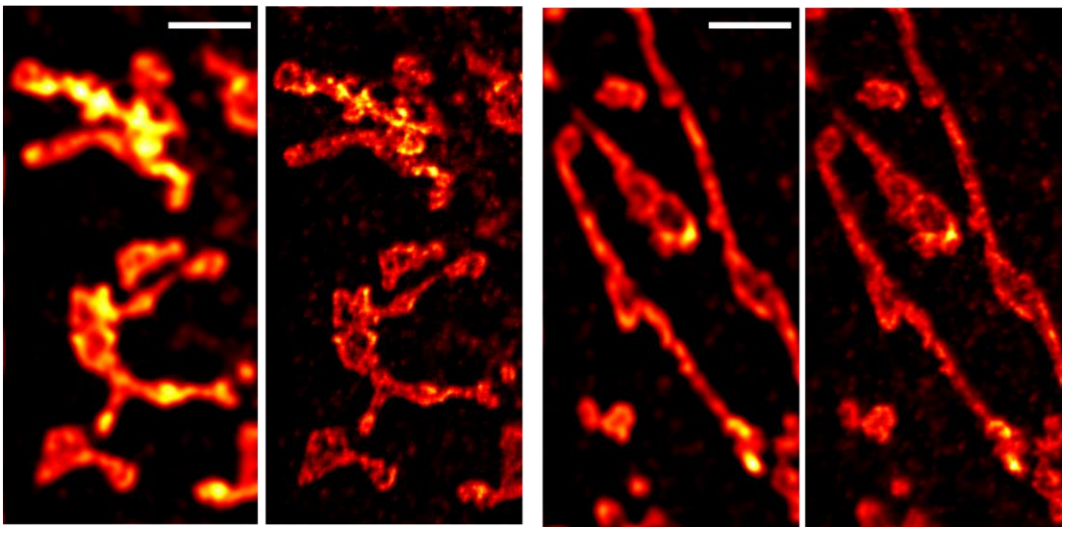

Figure 32: Immunostaining of mitochondria with Tom20-DY485XL. Left image: confocal microscopy, right image: STED microscopy. (Scale bars: 2.5 µm, red-hot color map)

Figure 32 shows a clear improvement of resolution of the STED images in comparison to the confocal images. Mitochondria form different shapes from very branched networks (left) to rather long stretched tubules (right).

7.2.3. Visualization of ER-mitochondria contact sites

By overlaying the images of mitochondria, represented by Tom20 immunostainings, and ER, represented by Sec61beta-GFP, ER-mitochondria contact sites were visualized (Figure 33).

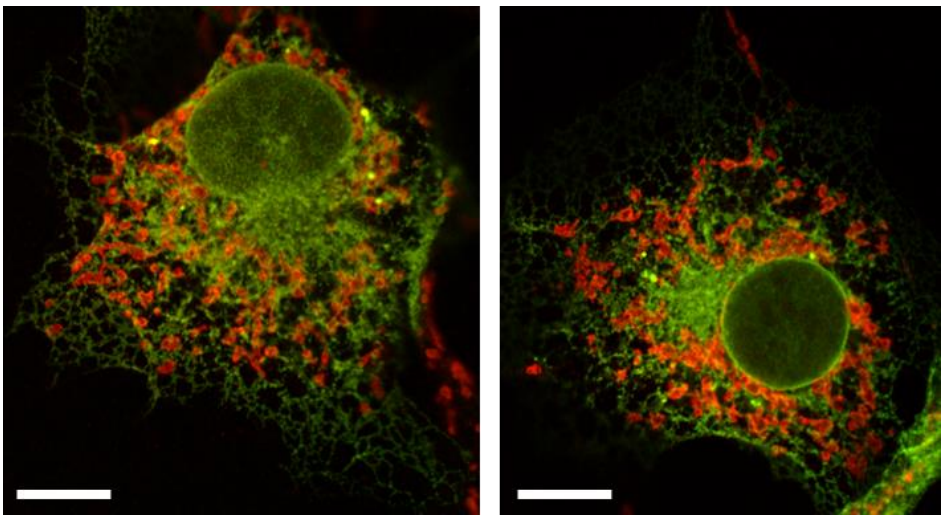

Figure 33: COS-1 cells expressing ER-GFP (green) immunostained with Tom20-DY485XL (red). Overlays of confocal images. (Scale bars: 10 µm)

In the literature ER-mitochondria contact sites are often identified using Sec61beta-GFP in combination with a mitochondrial matrix localized dsRed. Therefore anti-Acat1, an antibody directed against the mitochondrial matrix protein Acat1, was also tested in combination with Sec61beta-GFP (Figure 34).

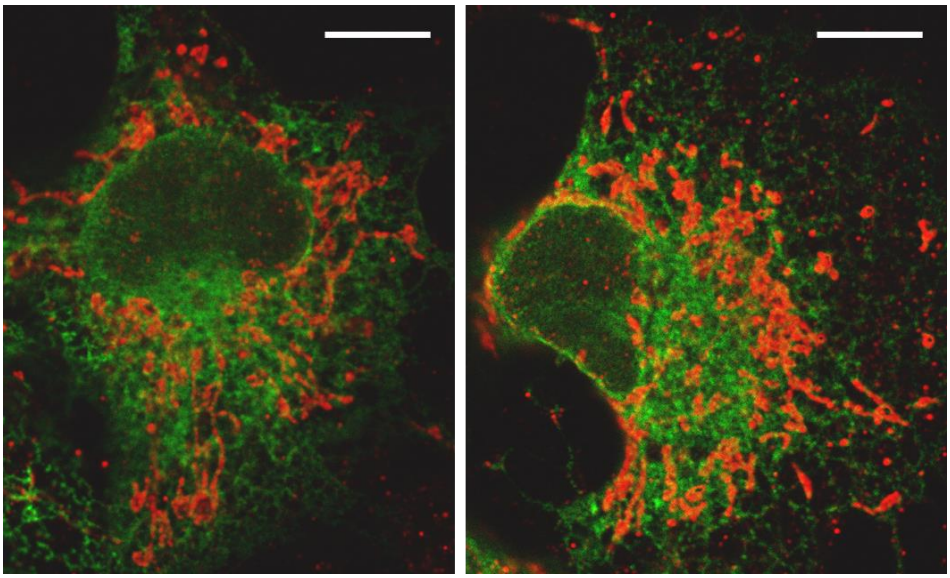

Figure 34: COS-1 cells expressing ER-GFP (green) immunostained with Acat1 primary antibody and Atto565 labeled secondary antibody (red). Overlays of confocal images. (Scale bars: 10 µm)

As expected, Acat1 being a mitochondrial protein, Acat1 immunostaining images of the whole cell show a similar distribution to Tom20 (Figure 33) cells based on confocal images

taken on the whole cell. Figure 35 shows the distribution of Acat1 in a larger scale (STED image) with respect to the ER.

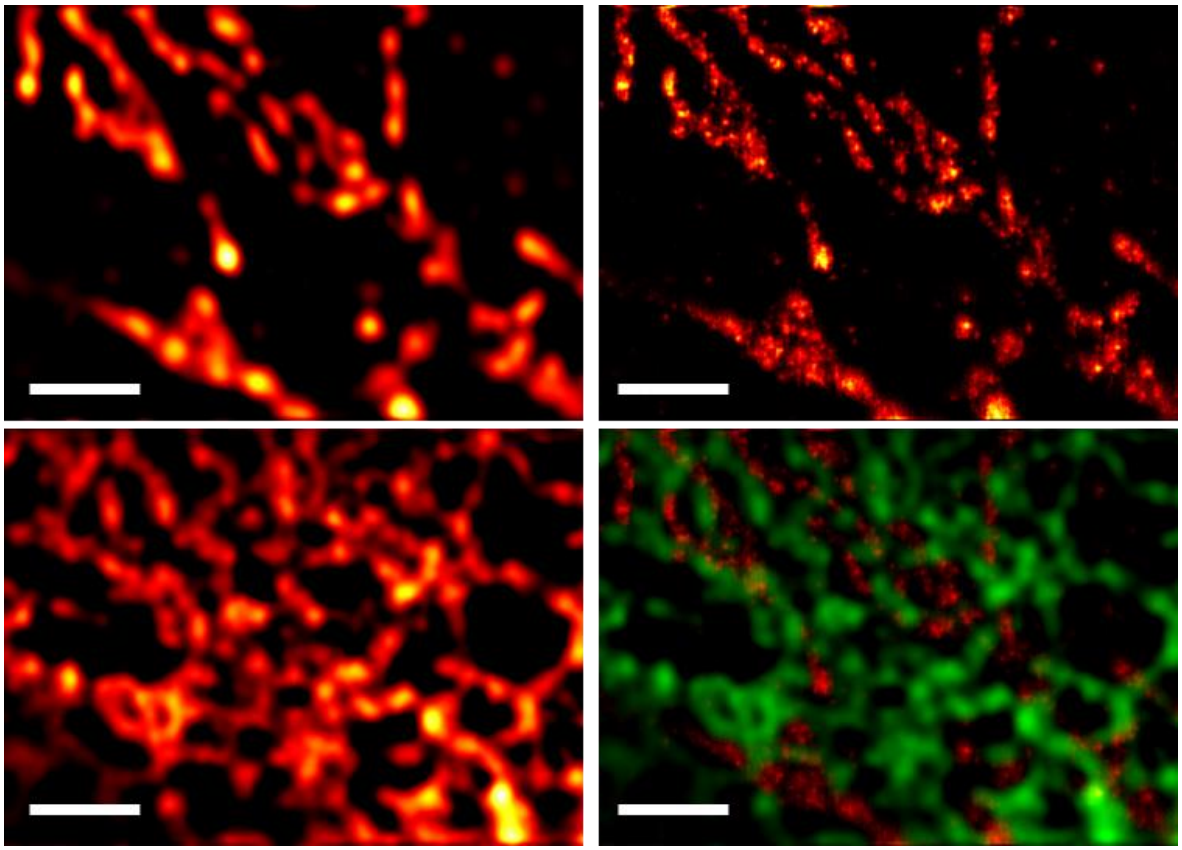

Figure 35: COS-1 cells expressing ER-GFP immunostained with Acat1-Atto565. Upper left: confocal image of Acat1 (red-hot color map), upper right: STED image of Acat1 (red-hot color map), lower left: confocal image of ER-GFP (red-hot color map), lower right: overlay of ER-GFP confocal image (green) and Acat1 STED image (red). (Scale bars: 1.5 µm) (More images can be found in the appendix.)

Acat1 does not colocalize with Sec61beta-GFP at all. This is explained by the fact that Sec61beta, as localized in the ER membrane, does not have the ability to physically interact with a mitochondrial matrix protein like Acat1 since the mitochondrial double membrane keeps the two molecules apart. Since the resolution of the STED microscopy setup is high enough to resolve mitochondria and ER well a colocalization of Acat1 and Sec61beta-GFP cannot be detected. Therefore, the antibody directed against the mitochondrial matrix protein Acat1 cannot be used to identify MAMs since the resolution of the STED microscopy setup is high enough so that mitochondrial matrix and ER membrane do not colocalize at all. Thus, Tom20 being localized in the mitochondrial outer membrane is a better marker for MAM identification because in fact the MOM interacts with the ER membrane at the MAMs. Figure 36 shows Tom20 STED images overlayed with ER-GFP. These images enable to visualize MAMs with enhanced resolution.

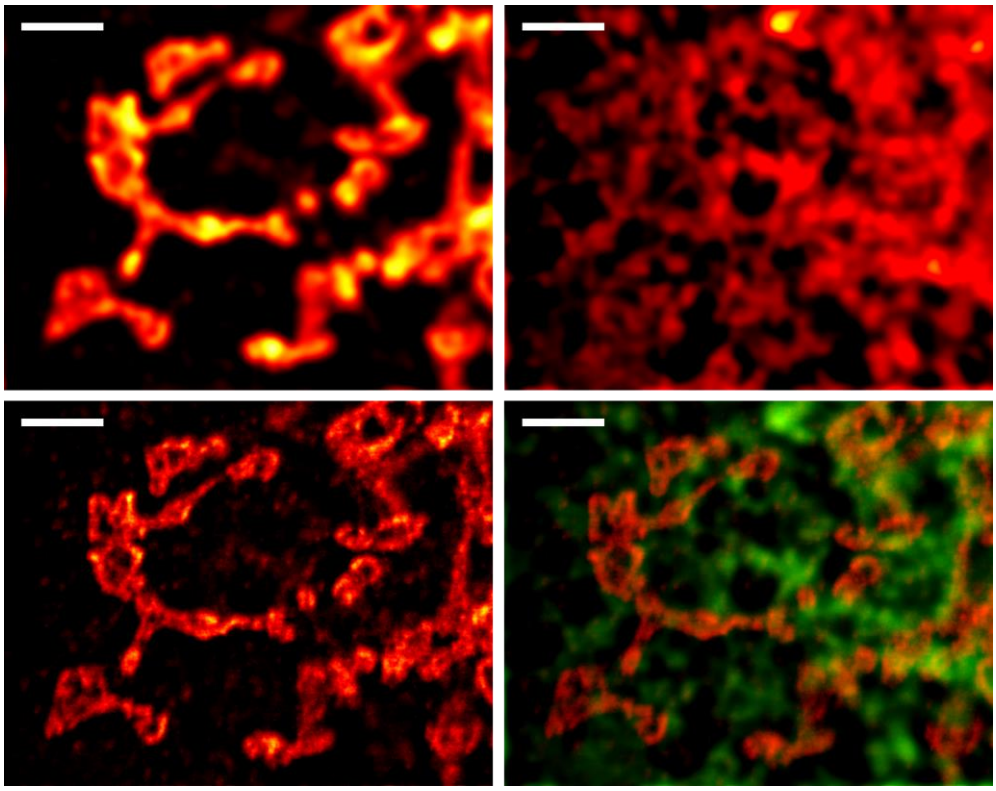

Figure 36: COS-1 cells expressing ER-GFP immunostained with Tom20-DY485XL. Upper left: confocal image of Tom20 (red-hot color map), lower left: STED image of Tom20 (red-hot color map), upper right: confocal image of ER-GFP (red-hot color map), lower right: overlay of ER-GFP confocal image (green) and Tom20 STED image (red). (Scale bars: 2 µm) (More images can be found in the appendix.)

To visualize the difference between Tom20 and Acat1 both proteins were marked with antibodies simultaneously (Figure 37 and Figure 38).

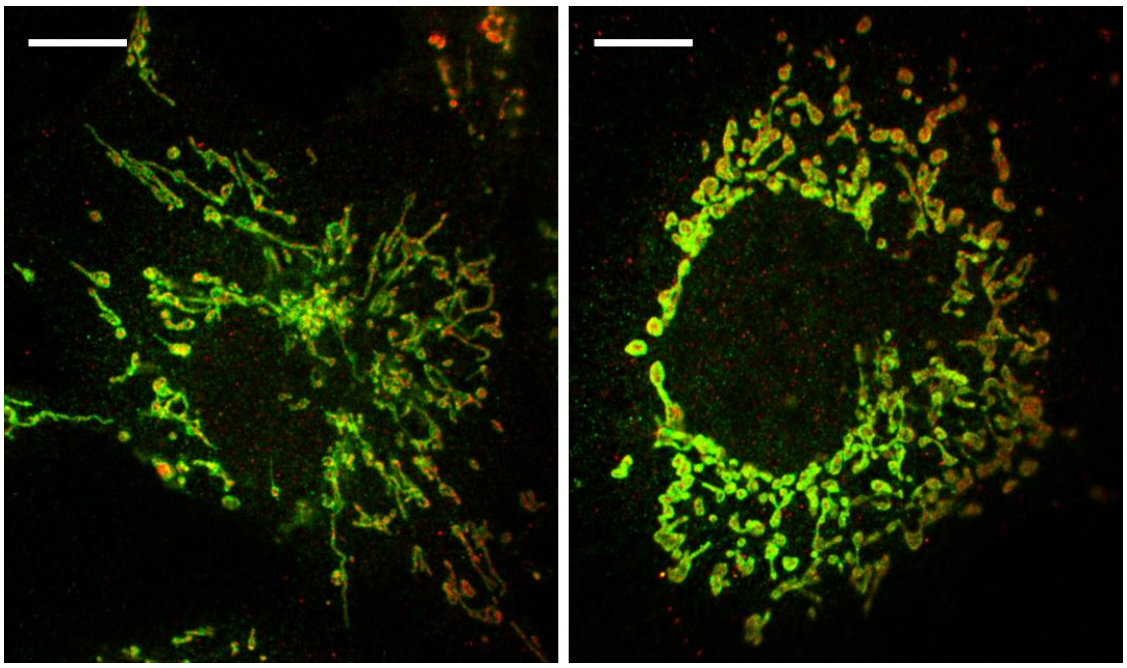

Figure 37: COS-1 cells immunostained with Tom20-DY485XL (green) and Acat1-Atto565 (red). Overlays of confocal images. (Scale bars: 10 µm)

Figure 37 shows the typical mitochondrial distribution in COS-1 cells (as Figure 31) with both immunostained proteins Tom20 (green) and Acat1 (red) localized to mitochondria as expected.

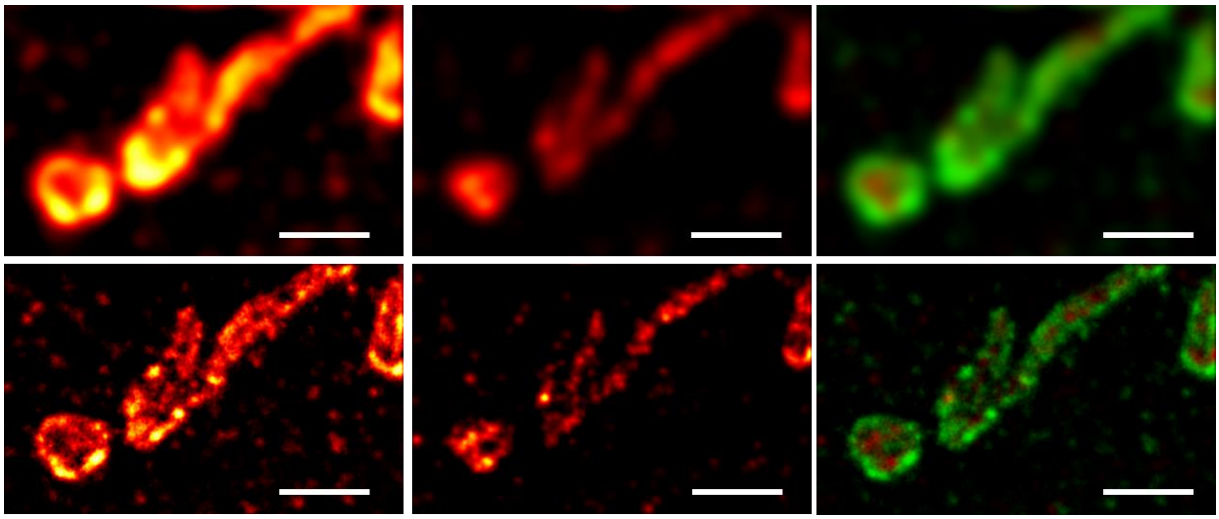

Figure 38: COS-1 cells immunostained with Tom20-DY485XL and Acat1-Atto565. Upper left: confocal image of Tom20 (red-hot color map), lower left: STED image of Tom20 (red-hot color map), upper middle: confocal image of Acat1 (red-hot color map), lower middle: STED image of Acat1 (red-hot color map), upper right: overlay of confocal images of Tom20 (green) and Acat1 (red), lower right: overlay of STED images of Tom20 (green) and Acat1 (red). (Scale bars: 1.5 µm) (More images can be found in the appendix.)

By the improvement of the resolution of STED images in comparison to confocal images (Figure 38) one can identify the cross section of a mitochondrial tubule with Tom20 (green) in the outer mitochondrial membrane and the mitochondrial matrix visualized by the Matrix protein Acat1 (red) in between. These images explain the observation that Acat1 did not colocalize with the ER at all (Figure 35), because Acat1 localized in the mitochondrial matrix is resolved that well that the fact that the mitochondrial matrix does not get into physical contact with the ER membrane because of the MOM in between can be visualized. Therefore, Tom20 was decided to be used as a mitochondrial marker in combination with ER-GFP to identify MAMs.

7.3. Examination of a protein located at ER-mitochondria contact sites: Grp 78

The aim of this study was to get a better idea of the structural organization of proteins located at the MAMs. One of these proteins is the 78 kDa glucose-regulated protein (Grp78), a molecular chaperone located in the ER lumen. It is part of the Ca^{2+}-sensitive chaperone machinery responsible for Ca^{2+} transfer between ER and mitochondria. To gain an overview about the distribution of Grp78 with respect to the ER, confocal images of ER-GFP transfected cells immunostained for Grp78 were taken (Figure 39). Figure 39 gives the idea of

a rather homogenous distribution of Grp78 along the ER. To take a closer look at this, STED images were taken (Figure 40).

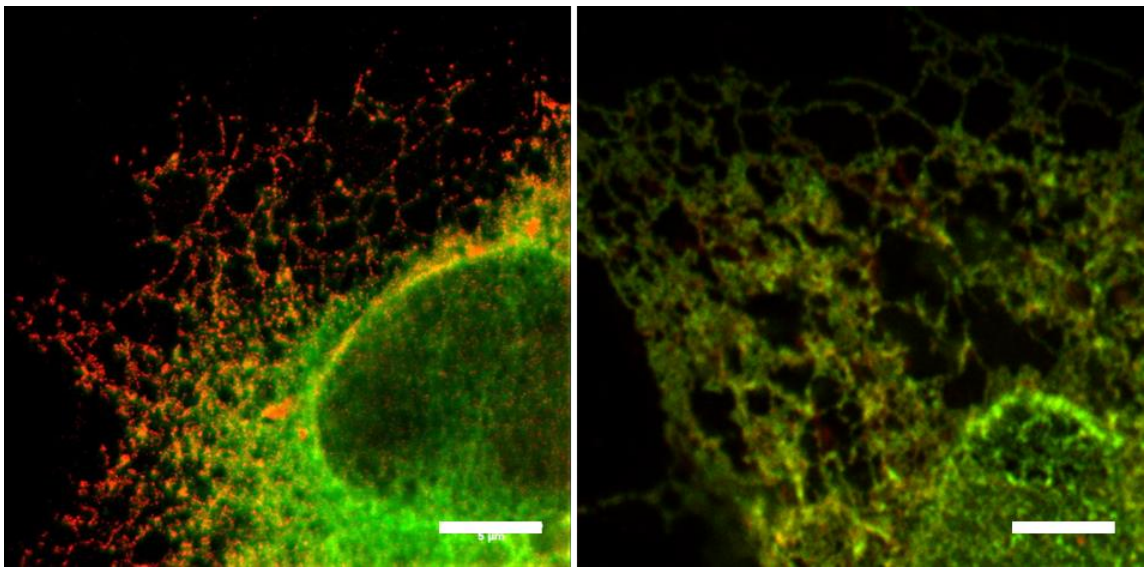

Figure 39: COS-1 cells expressing ER-GFP (green) immunostained with Grp78 primary antibody and Atto565 labeled secondary antibody (red). Overlays of confocal images. (Scale bars: 5 µm)

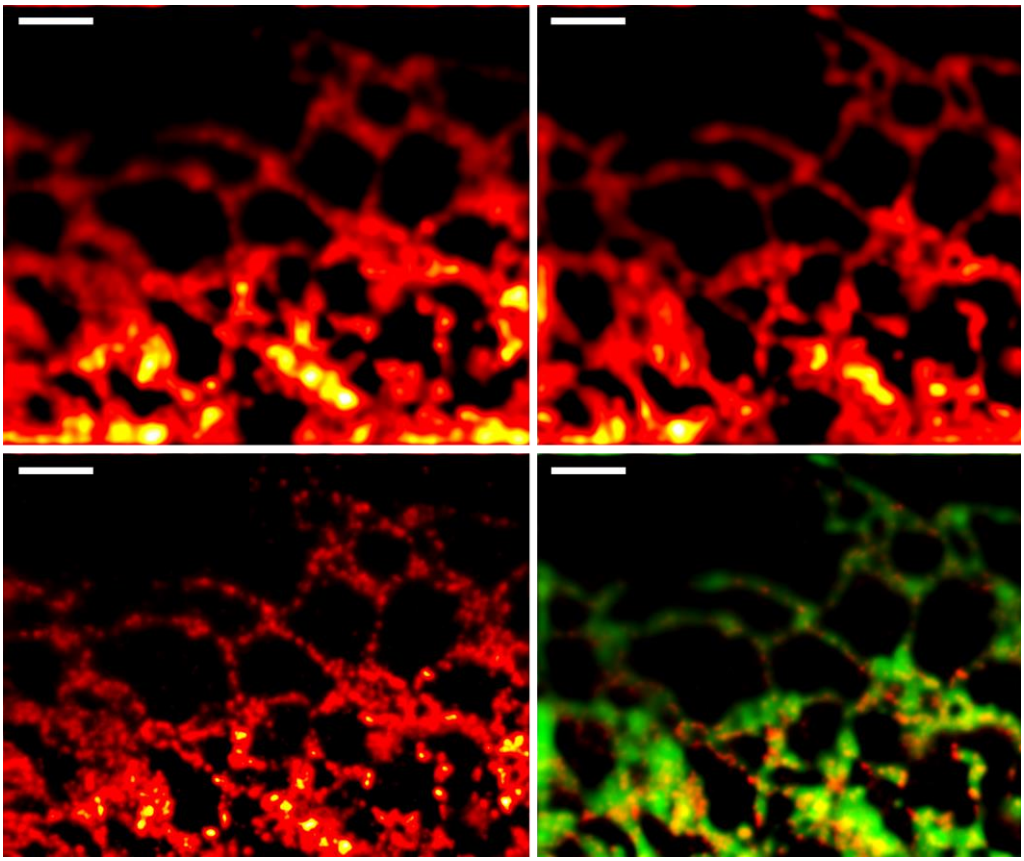

Figure 40: COS-1 cells expressing ER-GFP immunostained with Grp78-Atto565. Upper left: confocal image of Grp78 (red-hot color map), lower left: STED image of Grp78 (red-hot color map), upper right: confocal image of ER-GFP (red-hot color map), lower right: overlay of ER-GFP confocal image (green) and Grp78 STED image (red). (Scale bars: 2 µm)

It is striking that the confocal image of Grp78 (upper left of Figure 40) looks almost the same as the ER-GFP image (upper right of Figure 40). However, resolution improves significantly in the STED image (lower left of Figure 40). Both images confirm the hypothesis that Grp78 is rather homogenously distributed among the ER. This result is rather unexpected since Grp78 was found to be accumulated at the MAMs with biochemical methods.

7.4. Discussion and Outlook

In this study, ER-mitochondria contact sites were imaged by overlaying images of ER and mitochondria of COS-1 cells. Sec61beta-GFP was used to label the ER. To visualize mitochondria two antibodies were tested, one against a protein in the mitochondrial matrix, Acat1, and one against a protein in the MOM, Tom20. Although matrix localized dsRed was used in combination with Sec61beta-GFP in the literature to identify MAMs [8, 87], it was shown here that a matrix localized protein (Acat1) is not suitable for MAM identification using STED microscopy. The reason is that the resolution of the STED setup used in this study is that high that mitochondrial matrix and mitochondrial outer membrane can be differentiated. Thus the matrix localized Acat1 does not colocalize with ER-GFP at all since it does not get into contact with the ER membrane because the MOM is in between. In the literature dsRed was used to label mitochondria in confocal microscopy where the resolution is not as high so that dsRed still colocalizes with ER-GFP identifying MAMs. This shows one of the constraints of confocal microscopy visualizing MAMs: the resolution is too low to actually visualize MAMs because mitochondrial outer membrane and matrix cannot be resolved and thus a MAM protein cannot be located exactly enabling to identify if a protein really localizes to the MAM.

In the STED experiments performed here, it was decided to use Tom20 as a mitochondrial marker for MAM identification since it is localized in the MOM which gets into direct physical contact with the ER membrane at the MAM. By imaging Tom20 with STED microscopy, resolution could be improved in comparison to confocal images being able to identify cross sections of mitochondrial tubules with Tom20 in the MOM “on the top” and “on the bottom” with the mitochondrial matrix in between. Furthermore, it was possible to obtain high resolution images of the MAM protein Grp78. Grp78 could be shown to exactly colocalize with the ER. STED images of Grp78 show the distribution of individual Grp78 molecules among the ER. Surprisingly, the distribution of Grp78 looks rather homogeneous among the ER. Since Grp78 is supposed to be enriched at ER-mitochondria contact sites, one would have expected some molecule domains or clusters at potential MAMs. In contrast,

looking at confocal images from the literature imaging ER, mitochondria and e.g. the MAM proteins Mff1 or Miro1, they always appeared directly localizing to the contact sites maybe as clusters or higher concentrations but not distributed over the whole organelle [8, 84]. In order to make a solid statement about the distribution of Grp78 at the MAM it would be necessary to obtain 3-color high resolution images of ER, mitochondria, and the MAM proteins of interest. These are not trivial to produce. To obtain a good visual overview of the structural organization of the MAM, the resolution of the STED images would have to be improved to about 20 nm, because the distance between ER and mitochondria at the MAM has been estimated to be between 10 and 25 nm [12]. The resolution of STED microscopy has been pushed to 15-20 nm [92]. However, in order to reach such a high resolution one needs very good sample preparations with a high labeling density and a fluorescence intensity, which is high enough to be STEDed with high STED laser power without bleaching. Since it was not possible in this study to obtain 3-color images, results from the literature namely that Grp78 is accumulated at ER-mitochondria interaction sites could not be confirmed by imaging data. Actually, this study shows rather the opposite namely that Grp78 seems to be distributed homogenously along the ER. The presence of Grp78 has so far only been concluded from biochemical studies isolating MAMs but not by microscopy images. However, some publications can only find Grp78 to be “moderately enriched in the MAM fraction” [14]. This may be an explanation for our observations namely that Grp78 is actually rather expressed ubiquitously. The slight accumulation in the MAM may just not be visible in the microscopy images. But to our knowledge no publication exists where the resolution of fluorescent MAM images is high enough to show a structural distribution of proteins at ER-mitochondria contact sites. One of the restraints in imaging MAMs is that there is no good bona fide marker for the contact sites. Drp1 and Mff have been observed to localize to contact sites [11] but they do not localize to all contacts and they also localize to peroxisomes as well (unpublished data of Friedman et al., information from communication). Another restraint is that both organelles, ER and mitochondria, are quite dynamic and thus the best way of imaging a MAM protein of interest would be in live cells over time along with ER and mitochondrial markers. But taking 3-color images of live cells with high resolution STED microscopy is so far not possible.

One problem in this study for the generation of 3-color images was that the intensity of Tom20-DY485XL immunostaining fluorescence was oftentimes too low to perform STED microscopy in ER-GFP transfected cells. Surprisingly, fluorescence was higher in cells that were not transfected. Thus, it seems as if the transfection procedure may affect Tom20

immunostaining. Transfection reagents like Lipofectamine 2000 affect the cell membrane to make it permeable for DNA. Thus it may also have an influence on the mitochondrial outer membrane and impair its immunostaining. Since Lipofectamine 2000 is a quite harsh transfection reagent, milder reagents like jetPRIME (Polyplus) or FuGENE (Roche) were also tested. But unfortunately these did not give significantly better results. For double staining images of only ER and mitochondria another antibody could be used for Tom20 immunostaining than for images also including Grp78. The antibody against Grp78 was an antibody from rabbit. Thus, a mouse antibody had to be used for Tom20 (Abcam). This antibody did not lead to as nice results as a rabbit Tom20 antibody (Santa Cruz), which was used for ER/mitochondria images. But the rabbit Tom20 antibody could not be used in combination with the Grp78 rabbit antibody. As a consequence, another strategy, which could lead to 3-color images would be to use mouse antibodies for the MAM proteins of interest in combination with the rabbit Tom20 antibody. Once it is possible to obtain high quality 3-color images of the MAM, the idea would be to image as many MAM proteins as possible in order to get an idea about the structural organization of ER-mitochondria contact sites. To further study the Ca^{2+} transfer function of the MAM two interesting proteins to analyze would be VDAC, resident in mitochondria, and IP3R, residing in the ER. These two proteins are most important for Ca^{2+} transfer since these are the two protein channels mediating the ion exchange. For further analysis of the lipid synthesis machinery at the MAM one could for example image the phosphatidylserine synthase-1 (PSS-1) or FACL4 (fatty acid-CoA ligase type4). It would also be very interesting to get a better visual idea of the MAM proteins regulating mitochondrial dynamics like Drp-1, important for mitochondrial fission, Mfn, responsible for mitochondrial fusion, and Miro, mediating mitochondrial movement (described in chapter I.2.2.3).

In summary, in this study an imaging strategy of ER-mitochondria contact sites with high resolution microscopy was established. Labeling ER with Sec61beta-GFP and mitochondria with Tom20 immunostaining, it was possible to identify MAMs at a higher resolution than in publications where MAM imaging has so far only been performed with confocal microscopy. Furthermore, STED images of Grp78, a protein proposed to reside at MAMs, could be obtained enabling to visualize the distribution of Grp78 with respect to the ER. Applying the here established imaging strategy of ER-mitochondria contact sites with high resolution microscopy in combination with several MAM proteins of interest will enable to get deeper structural insights into the organization of those proteins keeping ER and mitochondria in close contact.

III. Materials and Methods

8. Cell culture procedures

8.1. Cultivation of cell lines

Cancer cell lines SiHa and CaSki as well as COS-1 cells (fibroblast-like cell line derived from monkey kidney tissue) [93] were cultured in Dulbecco's Modified Eagle Medium (DMEM) (Sigma) supplemented with 10% heat-inactivated fetal calf serum (FCS) (Linaris) and 1% Penicillin/Streptomycin (Invitrogen). HPV16-immortalized keratinocytes carrying the E6 and/or E7 oncogene were grown in Keratinocyte-SFM medium supplemented with bovine pituitary gland extract and rhEGF (recombinant human epidermal growth factor receptor) (Life Technologies). Cells were cultivated in cell culture flasks until a confluency of about 90% was reached and then passaged or seeded for experiments. Human neonatal Epidermal Keratinocytes (Life Technologies), referred to as primary keratinocytes (pK), were cultivated in EpiLife medium (Life Technologies) containing 60 µM calcium supplemented with Human Keratinocyte Growth Supplement (Life Technologies). pK were passaged before a confluency of 70% was reached in order to avoid cell differentiation. All cell lines were kept in an incubator at 37°C, 5% CO2 and 95% humidity.

8.2. Passaging and seeding of cells

For cell passage, first, the culture medium was removed and cells were washed with PBS (phosphate buffered saline) (Invitrogen). Then cells were detached from the culture vessel with 0.25% trypsin-EDTA (Invitrogen). To speed up the process, cells in trypsin were incubated at 37°C for a few minutes until all cells were floating. Trypsin was inactivated by adding an equal amount of 10% FCS in PBS and cells were transfered into a falcon tube and pelleted for 10 min at 300 x g and room temperature. Then cells were washed by resuspension in PBS and repeated centrifugation. Afterwards cell were resuspended in medium and for maintenance culture cells were reseeded at a ratio of 1:10 or 1:20 in new medium and further cultivated.

To passage primary keratinocytes, cells were washed with Versene (EDTA solution, Invitrogen) prior to trypsin treatment. Then cells were detached with 0.05% trypsin as described above. Afterwards cells were washed twice with PBS and transferred into a fresh culture flask at a ratio of no more than 1:3.

For experimental set-ups, the cell concentration was determined by counting cells with a Neubauer hemocytometer. Thus the number of cells per ml was identified and the volume containing the required number of cells could be calculated.

8.3. Transfection of siRNA

For siRNA-mediated knock-down of Bcl-xL, 5 x 10^5 cells were seeded into petri dishes with a diameter of 8.5 cm and incubated over night. The next day cells were 20 – 30% confluent. Cell culture medium was removed, cells were washed with PBS, and 4.7 ml Optimem (reduced serum media, Invitrogen) were added. Cells were transfected using Lipofectamine 2000 transfection reagent (Invitrogen). 6 µl Lipofectamine were diluted in 600 µl Optimem and incubated for 5 min at room temperature. siRNA by Silencer Select directed against human Bcl-xL (Ambion, s1921) was used to knock down Bcl-xL. As a control Silencer Select Negative Control #1 siRNA (Ambion) was used. siRNA was ultimately transfected at a concentration of 2 nM. siRNA stocks were diluted at a concentration of 20 µM. Thus, 0.6 µl siRNA stock were diluted in 600 µl Optimem and then mixed with the Lipofectamine/Optimem mixture. siRNA and Lipofectamine were incubated together for 20 min at room temperature and then the 1.2 ml mixture were added to the cells and distributed evenly. After 6 hours in the cell incubator, 6 ml of DMEM containing 20% FBS were added to the petri dish. On the next day, media was changed to new DMEM including 10% FBS and 1% Penicillin/Streptomycin. Experiments were performed with knock-down cells after 48 h.

8.4. Transfection of expression plasmids

To visualize the ER, COS-1 cells were transfected with the pAc-GFPC1-Sec61beta plasmid [86] (Addgene, plasmid 15108). Sec61beta is a component of the protein translocation apparatus of the ER membrane. In cells expressing Sec61beta fused to green fluorescent protein (GFP) the ER can be visualized. 40 000 COS-1 cells were seeded on 30 mm glas coverslips in 6-well plates and let adhere over night. Per well 0.05 µg plasmid-DNA and 1 µl Lipofectamine 2000 (Invitrogen) were used. Culture medium was removed and 1 ml fresh DMEM, 10% FCS were added per well. For the transfection of each well 1 µl Lipofectamine was mixed with 25 µl Optimem (Invitrogen) and incubated for 5 min at room temperature. 0.05 µg plasmid DNA was mixed with 25 µl Optimem and the Lipofectamine/Optimem mix was added to the DNA. This mixture was incubated for 20 min at room temperature. Then those 50 µl were added to the cells, distributed evenly and after 6 hours the media was changed to DMEM, 10% FCS, 1% Penicillin/Streptomycin. The next day cells were fixed and immunostained according to chapter 12. Immunocytochemistry.

9. Analysis of proteins

Solutions for protein analysis

RIPA buffer	20 mM Tris pH 7.5, 150 mM NaCl, 1 mM EGTA, 1 mM Na_2EDTA, 1% sodium deoxycholate, 1% NP-40
6 x sample buffer	0.424 g Trizma base, 2.6 ml glycerol, 1 g DTT, 60 µl 10% Bromphelol blue, 200 µl 20% SDS → fill up with water to 7 ml
Lower Tris (1.5 M Tris-HCl, pH 8.8, 0.4% SDS)	dissolve 18.17 g Trizma base, add concentrated HCl to pH 8.8, 2 ml 20% SDS → fill up with water to 100 ml
Upper Tris (0.42 M Tris-HCl, pH 6.8, 0.4% SDS)	dissolve 6.06 g Trizma base, add concentrated HCl to pH 6.8, 2.4 ml 20% SDS → fill up with water to 120 ml
Running buffer	60g Trizma base, 288 g glycine, 100mL 20% SDS → fill up with water to 2 l
Cathode buffer	25 mM Tris, 40 mM Glycin, 10% methanol, pH 9.4
Anode buffer I	0.3 M Tris, 10 % methanol, pH 10.4
Anode buffer II	25 mM Tris, 10% methanol
10 x TBS	0.5 M Tris, 1.5 M NaCl, pH 7.5
1 x TBST	1 x TBS pH 7.5, 0.1% (v/v) Tween 20

Primary antibodies: anti-Bim (Calbiochem), anti-Bcl-2 (BD Biosciences), anti-Bid (Santa Cruz), anti-Mcl-1 (BD Biosciences), anti-Bax (Cell Signaling), anti-Bak (Cell Signaling), anti-Actin (Millipore).

9.1. Protein extraction

Cells were collected, washed with PBS and total protein extracts were prepared by lysing cells for 30 min on ice with RIPA buffer containing complete protease inhibitor cocktail (Roche). Protein samples were cleared from cell debris by centrifugation and the supernatants were stored at -80°C until protein quantification. Protein concentrations of supernatants were

quantified calorimetrically with Protein Assay Dye Reagent Concentrate (Bio-Rad) comparing unknown samples with a BSA standard curve according to manufacturer's instructions. Protein samples were mixed in a proportion of 1:6 with 6x sample buffer, incubated at 95°C for 10 min, and 50 µg of total protein lysate were separated by SDS-polyacrylamide gel electrophoresis (SDS-PAGE) and analyzed by Western Blotting.

9.2. SDS-polyacrylamide gel electrophoresis (SDS-PAGE)

Proteins were separated by size via SDS-PAGE. Proteins with a size between 12 and 45 kDa were separated with SDS-PAGE gels containing 15% acrylamide. Proteins were focused with a stacking gel and then separated in the resolving gel. 1.5 mm thick gels were casted with the Mini-PROTEAN system from Biorad. Compositions for two gels were as follows:

Resolving Gel:

Components	Volume [ml]
H_2O	4.6
30% Acrylamide-Bis Mix	10.0
Lower Tris	5.0
10% SDS	0.2
10% ammonium persulfate	0.2
TEMED	0.01

Stacking Gel:

Components	Volume [ml]
H_2O	5.5
30% Acrylamide-Bis Mix	1.3
Upper Tris	1.0
10% SDS	0.08
10% ammonium persulfate	0.08
TEMED	0.012

Next to a protein standard size marker (PageRuler) 50 µg protein sample was applied to the SDS-PAGE gel per well. Gels were run in 1 x running buffer at 80 V for 20 – 30 min until the

sample had migrated through the stacking gel. Then voltage was increased to 120 V for further protein separation.

9.3. Immunoblotting and Western blot analysis

After protein separation by SDS-PAGE gel electrophoresis, proteins were transferred to a PVDF membrane with a semi-dry approach using the Trans-Blot Turbo machine by Bio-Rad. First, the gel was incubated in cathode buffer for 10 min at room temperature to remove the SDS. The PDVF membrane was activated in methanol for 1 – 2 min, rinsed in water, and then equilibrated in anode buffer II for 2 min. Whatman papers were soaked in anode buffers I and II and in cathode buffer before assembling the "transfer sandwich" in the following order:

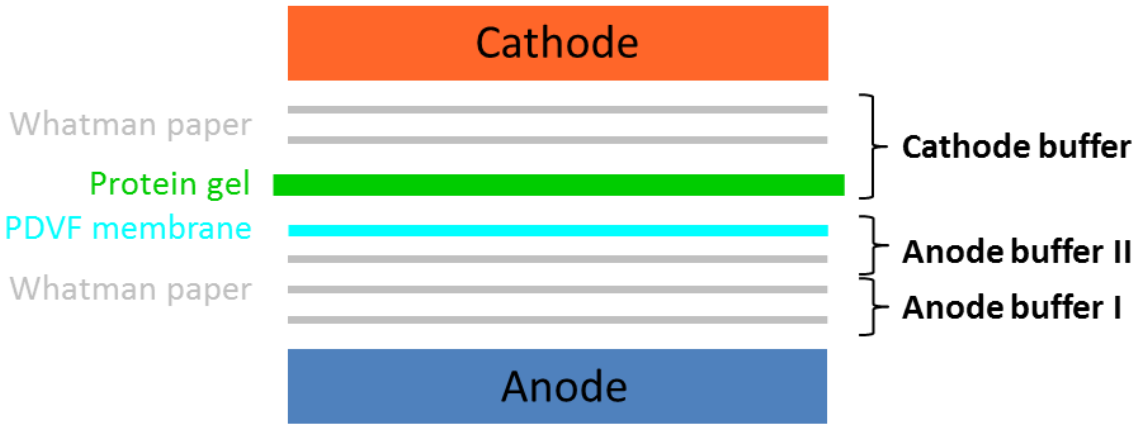

Figure 41: Immunoblotting set-up with the Trans-Blot Turbo machine, Bio-Rad (semi-dry approach). Whatman filter papers, acrylamide gel and PDVF membrane were equilibrated in the indicated buffers.

Protein transfer was performed with a 30 min standard procedure. After the transfer, PVDF membranes were blocked with 5% milk in TBST for 1 h at room temperature. Then the respective primary antibody was diluted in 5% milk in TBST and was incubated at 4°C over night. Afterwards, membranes were washed three times for 10 min with TBST. Then the respective secondary antibody conjugated with HRP (horse radish peroxidase) was diluted in 5% milk in TBST and the membrane was incubated for 1 h at room temperature. Membranes were washed for five to six times for 10 min with TBST. Then ECL reagent was applied and proteins were detected using x-ray films.

10. BH3 profiling and Bim/Bid dose-response curves with JC-1

For BH3 profiling a protocol from Ryan et al. [34] was adapted. After BH3 peptide treatment mitochondrial membrane potential loss was determined with the fluorescent dye JC-1. BH3 peptides (Bim, Bid, Bad, Bik, Noxa A, Hrk, Puma, and Bmf) were purchased from AnaSpec. Stock solutions at a concentration of 10 mM were prepared in H_2O or DMSO according to manufacturer's recommendation (Bid, Noxa A, Hrk, Bmf in H_2O and Bim, Bad, Bik, Puma in DMSO) and stored at -80°C. Stocks of 20 mg/ml oligomycin (Sigma), 5% digitonin (Sigma), and 75 µM JC-1 (Biomol) in DMSO were stored at -20°C.

At the beginning of the assay a peptide treatment plate was first set up in a 96 well-plate format for faster treatment addition later on in the experiment. Peptides were mixed with T-EB (300 mM Trehalose, 10 mM hepes-KOH pH 7.7, 80 mM KCl, 1 mM EGTA, 1 mM EDTA, 0.1% BSA, 5 mM Na succinate) to 2x of the final peptide concentration and 50 µl was pipetted in each well. As a positive control for the JC-1 assay CCCP (Carbonyl cyanide *m*-chlorophenyl hydrazone) was mixed with T-EB to 2x the final concentration (4 µM, final concentration in the assay: 2 µM) and 50 µl were pipetted in a well. As solvent control treatment wells contained 49 µl TEB and 1 µl DMSO or H_2O. The final peptide concentration in the BH3 profiling assays with all peptides was 100 µM. For the Bid and Bim dose-response curves also lower concentrations were used as indicated in the figures. The adherent cells from our experimental model system were brought into suspension by trypsinization and washed with T-EB before resuspending them at 4x their final density. In the 96-well plate format each well contained approximately 25 000 cells. One volume of the 4x cell suspension was added to one volume of a 4x dye solution containing 4 µM JC-1, 40 µg/ml oligomycin, 0.02% digitonin, and 10 mM 2-mercaptoethanol in T-EB. 50 µl of this 2x cell/dye suspension were added to each well of a black 96-well plate with transparent bottom (Thermo Scientific). The time for cell permeabilization and dye equilibration before adding treatments was about 20 min. The 50 µl from the treatment plate were added to each well of the black plate with a multichannel pipette and mixed with the pipette. JC-1 fluorescence loss as an indicator for mitochondrial membrane potential loss was measured in a Synergy 2 multireader (BioTek) (Excitation: 560 ± 20 nm, Emission: 620 ± 40 nm) at 25°C every 5 min. Since the difference between different treatments could be seen best at 20 min the % of mitochondrial membrane potential loss was calculated for the fluorescence values (in relative fluorescence units, rfu) at 20 min:

$$\%\ \text{membrane potential loss} = \frac{\text{rfu (solvent)} - \text{rfu (treatment)}}{\text{rfu (solvent)}} \times 100\%$$

11. Cell viability assays

11.1. Sytox assay

For the Sytox assay 10 000 cells were seeded per well of a transparent 96-well plate and let adhere over night. The next day, cells were treated with TNF, Cycloheximide or both. Final TNF concentrations were 4.3 ng/ml and final Cycloheximide concentrations 5 µg/ml. Drugs were incubated for 10 hours. Then Sytox was added at a final concentration of 0.2 µM and incubated for 1 hour before measuring fluorescence at 485 nm with a Synergy 2 multireader (BioTek).

11.2. Caspase activity assay

Caspase activity was determined with the Caspase-Glo 3/7 Assay by Promega. Approximately 2000 cells were seeded in 25 µl culture media in each well of a black 384-well plate with transparent bottom (Fisher Scientific) and let adhere over night. Apoptosis was induced by removing 17 µl of media and adding 17 µl Camptothecin to a final concentration of 2 µM or 8.33 µl of TNF and 8.33 µl of Cycloheximide to a final volume of 4.3 ng/ml an 5 µg/ml respectively (final volume 25 µl). Cells were incubated with Camptothecin or TNF/Cycloheximide for 24 hours in cell culture conditions. To determine caspase activity 25 µl Caspase-Glo 3/7 Reagent was added to each well and incubated at room temperature for 2 hours. The luminescence corresponding to caspase activity was measured with a Synergy 2 multireader (BioTek).

12. Immunocytochemistry

For immunocytochemistry cells were grown on 30 mm glass coverslips in 6-well plates. 40 000 cells were seeded per well and let adhere over night. The next day, cells were either transfected with the ER-GFP plasmid (see 8.4 Transfection of expression plasmids) or directly fixed. Fixation was performed in 3 steps: First cells were incubated in 4% paraformaldehyde in PBS at room temperature for 10 min. Then they were incubated in -20°C cold methanol for 5 min and afterwards in -20°C acetone for 2 min. Afterwards the cells were washed with PBS (Invitrogen). Cell membranes were permeabilized with 0.3% Triton-X in PBS for 10 min at room temperature. To avoid non-specific binding to the cell surface, cells were blocked with 3% BSA in 0.3% Triton-X in PBS (blocking solution) for 45 min. Then the primary antibody was diluted in blocking solution and incubated for 1 h at room temperature. To remove unbound antibody, cells were washed with PBS for 10 min. Then the secondary antibody was diluted in blocking solution and incubated for 1 h in the dark at room

temperature. After this, cells were washed with PBS at 4°C over night. The next day, cells were mounted on glass slides with Mowiol-DABCO (see below).

Primary antibodies

Immunogen	Animal produced in	Company	Order Number	Dilution used
Tom20	Rabbit	Santa Cruz	sc-11415	1:100
Tom20	Mouse	Abcam	ab56783	1:30
Acat1	Rabbit	Sigma	HPA004428	1:20
Grp78	Rabbit	Abcam	ab21685	1:20

Secondary antibodies

Immunogen	Fluorescent dye	Company	Dilution used
Mouse	Dyomics-485XL	Dyomics (485-41)	1:20
Rabbit	Dyomics-485XL	Self coupled to dye by Hell group	1:50
Rabbit	Atto-565	Self coupled to dye by Hell group	1:50 (Grp78) 1:30 (Acat1)

Production of Mowiol-DABCO

6 ml distilled water were mixed with 6 g glycerol and 2.4 g 4-88 polyvinilalcohol. This mixture was incubated for 2 hours at room temperature. Then 12 ml 100 mM Tris-buffer pH 8.5 were added and stirred for one day. 0.6 g (2.5% w/v) DABCO (1,4-diazobicyclo[2.2.2]octane were added and dissolved. The mixture was centrifuged for 15 min at 5000 rpm and the solution was aliquoted and stored at -20°C.

13. STED microscopy

Image acquisition was performed in collaboration with Dr. Jasmin Zahn (Optical Nanoscopy Group, DKFZ). The STED microscope setup used for this study was custom-built. Pulsed excitation of the Atto565 fluorescent label was attained using a high-repetition rate laser source PicoTA (PicoQuant) at a wavelength of λ_{exc} = 532 nm, synchronized with the STED-laser via a photodiode (Alphalas). GFP and DY485XL were excited by the 470 nm line from a pulsed high-repetition rate laser diode source (PicoQuant). Fluorescence inhibition at λ_{STED} = 647 nm was accomplished using an actively mode locked (APE) Ar-Kr laser (spectra Physics-Division of Newport Corporation). Beams were combined using acousto-optical

tunable filters (AOTF) (Crystal Technologies) and coupled into a microscope stand (DMI 4000B, Leica Microsystems CMS GmbH) including a three axis piezo stage-scanner (PI) and an ACS APO, 63x/1.30NA oil immersion lens (Leica Microsystems CMS GmbH). AOTFs enable blanking of the lasers and allow the power of each laser beam to be controlled independently. Furthermore, they permit selecting counter-propagating fluorescence returning from the confocal microscope. The collected fluorescence was passed through an additional band-pass filter (580/40 for Atto565 / DY485XL and 510/40 for GFP (AHF Analysentechnik)) and was detected confocally with a single-photon counting module (SPCM-AQR-13-FC, PerkinElmer). The scanner fly backs were blanked via the line signal from the Imspector data acquisition software. A vortex phase plate (RPC Photonics) was used in the STED beam path to generate a donut shaped focal intensity distribution [94].

14. Image processing

Image processing was conducted by Dr. Jasmin Zahn (Optical Nanoscopy Group, DKFZ). Images were processed using Imspector software (www.imspector.de). STED images were deconvolved using a Gauß filter.

IV. Appendix

15. Further images of ER-mitochondria contact sites

15.1. ER-GFP and Acat1

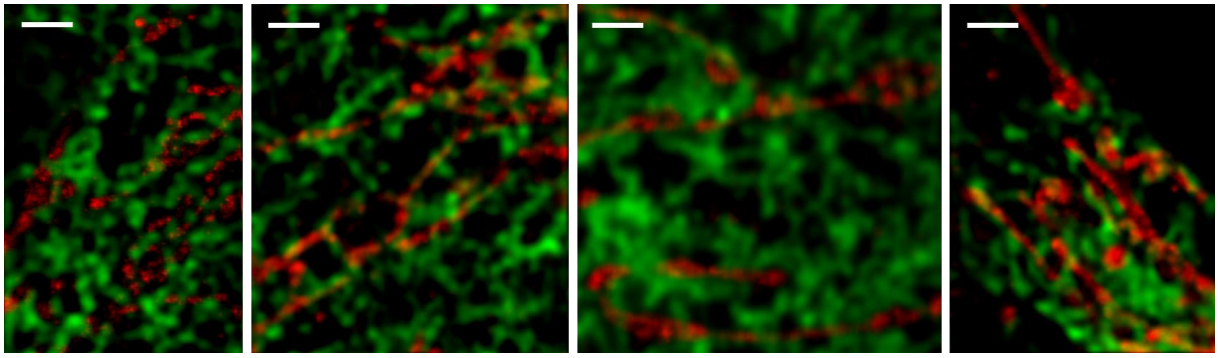

Figure 42: COS-1 cells expressing ER-GFP immunostained with Acat1-Atto565. Overlays of ER-GFP confocal images (green) and Acat1 STED images (red). (Scale bars: 1.5 µm)

15.2. ER-GPF and Tom20

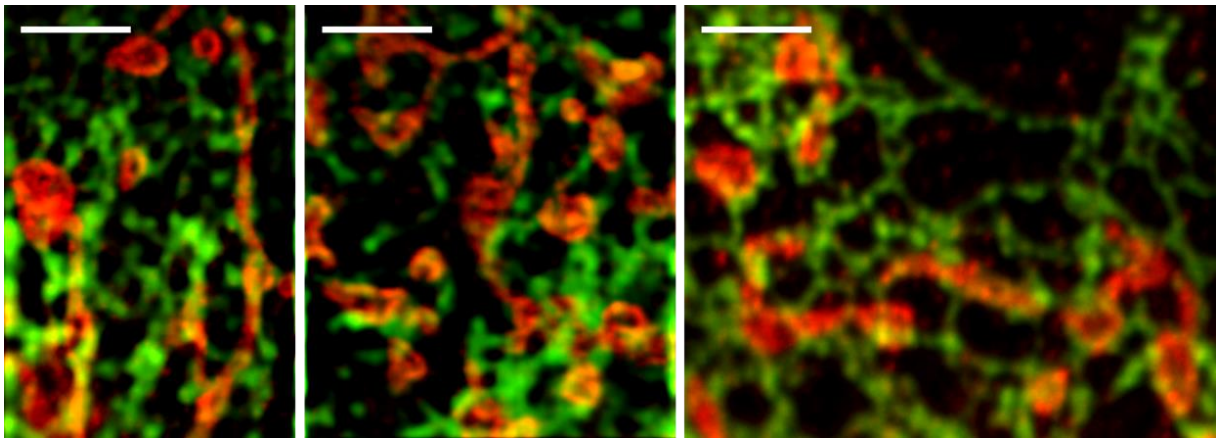

Figure 43: COS-1 cells expressing ER-GFP immunostained with Tom20-DY485XL. Overlays of ER-GFP confocal images (green) and Tom20 STED images (red). (Scale bars: 3 µm)

15.3. Tom20 and Acat1

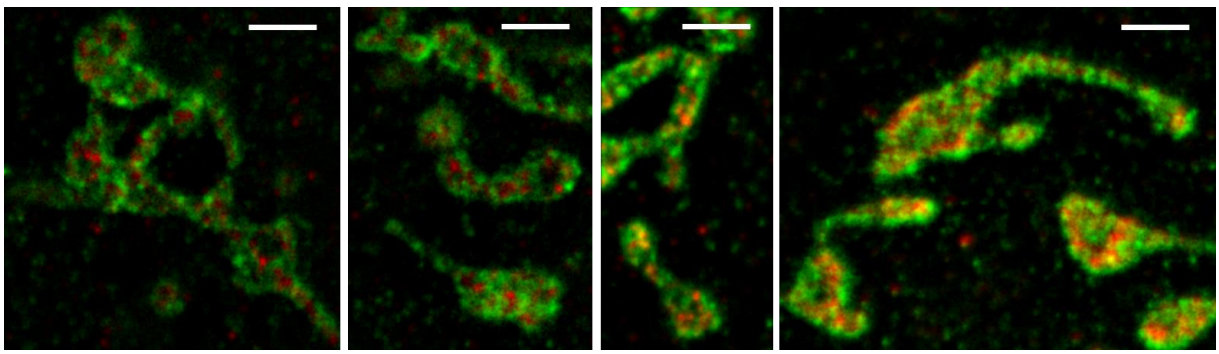

Figure 44: COS-1 cells immunostained with Tom20-DY485XL (green) and Acat1-Atto565 (red). Overlays of STED images. (Scale bars: 1.5 µm)

V. References

1. Bruce Alberts, A.J., Julian Lewis, Martin Raff, Keith Roberts, Peter Walter, *Molecular Biology of the Cell*. 2002, Garland Science: New York.
2. http://micro.magnet.fsu.edu/cells/mitochondria/images/mitochondriafigure1.jpg.
3. McBride, H.M., M. Neuspiel, and S. Wasiak, *Mitochondria: more than just a powerhouse.* Curr Biol, 2006. **16**(14): p. R551-60.
4. Nunnari, J. and A. Suomalainen, *Mitochondria: in sickness and in health.* Cell, 2012. **148**(6): p. 1145-59.
5. Tait, S.W. and D.R. Green, *Mitochondria and cell death: outer membrane permeabilization and beyond.* Nat Rev Mol Cell Biol, 2010. **11**(9): p. 621-32.
6. Chinnery, P.F. and G. Hudson, *Mitochondrial genetics.* Br Med Bull, 2013. **106**: p. 135-59.
7. Hollenbeck, P.J. and W.M. Saxton, *The axonal transport of mitochondria.* J Cell Sci, 2005. **118**(Pt 23): p. 5411-9.
8. Friedman, J.R., et al., *ER tubules mark sites of mitochondrial division.* Science, 2011. **334**(6054): p. 358-62.
9. Vance, J.E., *Phospholipid synthesis in a membrane fraction associated with mitochondria.* J Biol Chem, 1990. **265**(13): p. 7248-56.
10. Hayashi, T., et al., *MAM: more than just a housekeeper.* Trends Cell Biol, 2009. **19**(2): p. 81-8.
11. Kornmann, B., *The molecular hug between the ER and the mitochondria.* Curr Opin Cell Biol, 2013. **25**(4): p. 443-8.
12. Giorgi, C., et al., *Structural and functional link between the mitochondrial network and the endoplasmic reticulum.* Int J Biochem Cell Biol, 2009. **41**(10): p. 1817-27.
13. Szabadkai, G., et al., *Chaperone-mediated coupling of endoplasmic reticulum and mitochondrial Ca2+ channels.* J Cell Biol, 2006. **175**(6): p. 901-11.
14. Hayashi, T. and T.P. Su, *Sigma-1 receptor chaperones at the ER-mitochondrion interface regulate Ca(2+) signaling and cell survival.* Cell, 2007. **131**(3): p. 596-610.
15. Pizzo, P. and T. Pozzan, *Mitochondria-endoplasmic reticulum choreography: structure and signaling dynamics.* Trends Cell Biol, 2007. **17**(10): p. 511-7.
16. Swayne, T.C., et al., *Role for cER and Mmr1p in anchorage of mitochondria at sites of polarized surface growth in budding yeast.* Curr Biol, 2011. **21**(23): p. 1994-9.
17. Pinton, P., et al., *Calcium and apoptosis: ER-mitochondria Ca2+ transfer in the control of apoptosis.* Oncogene, 2008. **27**(50): p. 6407-18.
18. Karbowski, M., et al., *Spatial and temporal association of Bax with mitochondrial fission sites, Drp1, and Mfn2 during apoptosis.* J Cell Biol, 2002. **159**(6): p. 931-8.
19. Boehning, D., et al., *Cytochrome c binds to inositol (1,4,5) trisphosphate receptors, amplifying calcium-dependent apoptosis.* Nat Cell Biol, 2003. **5**(12): p. 1051-61.
20. Jayaraman, T. and A.R. Marks, *T cells deficient in inositol 1,4,5-trisphosphate receptor are resistant to apoptosis.* Mol Cell Biol, 1997. **17**(6): p. 3005-12.
21. Oakes, S.A., et al., *Proapoptotic BAX and BAK regulate the type 1 inositol trisphosphate receptor and calcium leak from the endoplasmic reticulum.* Proc Natl Acad Sci U S A, 2005. **102**(1): p. 105-10.
22. White, C., et al., *The endoplasmic reticulum gateway to apoptosis by Bcl-X(L) modulation of the InsP3R.* Nat Cell Biol, 2005. **7**(10): p. 1021-8.
23. Pinton, P., C. Giorgi, and P.P. Pandolfi, *The role of PML in the control of apoptotic cell fate: a new key player at ER-mitochondria sites.* Cell Death Differ, 2011. **18**(9): p. 1450-6.
24. Scorrano, L., et al., *BAX and BAK regulation of endoplasmic reticulum Ca2+: a control point for apoptosis.* Science, 2003. **300**(5616): p. 135-9.

25. Chami, M., et al., *Bcl-2 and Bax exert opposing effects on Ca2+ signaling, which do not depend on their putative pore-forming region.* J Biol Chem, 2004. **279**(52): p. 54581-9.
26. Wozniak, A.L., et al., *Requirement of biphasic calcium release from the endoplasmic reticulum for Fas-mediated apoptosis.* J Cell Biol, 2006. **175**(5): p. 709-14.
27. Igney, F.H. and P.H. Krammer, *Death and anti-death: tumour resistance to apoptosis.* Nat Rev Cancer, 2002. **2**(4): p. 277-88.
28. Schmitz, I., S. Kirchhoff, and P.H. Krammer, *Regulation of death receptor-mediated apoptosis pathways.* Int J Biochem Cell Biol, 2000. **32**(11-12): p. 1123-36.
29. Zimmermann, K.C., C. Bonzon, and D.R. Green, *The machinery of programmed cell death.* Pharmacol Ther, 2001. **92**(1): p. 57-70.
30. Del Gaizo Moore, V. and A. Letai, *BH3 profiling--measuring integrated function of the mitochondrial apoptotic pathway to predict cell fate decisions.* Cancer Lett, 2013. **332**(2): p. 202-5.
31. Danial, N.N., *BCL-2 family proteins: critical checkpoints of apoptotic cell death.* Clin Cancer Res, 2007. **13**(24): p. 7254-63.
32. Certo, M., et al., *Mitochondria primed by death signals determine cellular addiction to antiapoptotic BCL-2 family members.* Cancer Cell, 2006. **9**(5): p. 351-65.
33. Youle, R.J. and A. Strasser, *The BCL-2 protein family: opposing activities that mediate cell death.* Nat Rev Mol Cell Biol, 2008. **9**(1): p. 47-59.
34. Ryan, J.A., J.K. Brunelle, and A. Letai, *Heightened mitochondrial priming is the basis for apoptotic hypersensitivity of CD4+ CD8+ thymocytes.* Proc Natl Acad Sci U S A, 2010. **107**(29): p. 12895-900.
35. Garcia-Saez, A.J., *The secrets of the Bcl-2 family.* Cell Death Differ, 2012. **19**(11): p. 1733-40.
36. Garcia-Saez, A.J., et al., *Permeabilization of the outer mitochondrial membrane by Bcl-2 proteins.* Adv Exp Med Biol, 2010. **677**: p. 91-105.
37. Adams, J.M. and S. Cory, *The Bcl-2 apoptotic switch in cancer development and therapy.* Oncogene, 2007. **26**(9): p. 1324-37.
38. Hanahan, D. and R.A. Weinberg, *The hallmarks of cancer.* Cell, 2000. **100**(1): p. 57-70.
39. Tsujimoto, Y., et al., *Cloning of the chromosome breakpoint of neoplastic B cells with the t(14;18) chromosome translocation.* Science, 1984. **226**(4678): p. 1097-9.
40. Cory, S. and J.M. Adams, *The Bcl2 family: regulators of the cellular life-or-death switch.* Nat Rev Cancer, 2002. **2**(9): p. 647-56.
41. Kelly, G.L. and A. Strasser, *The essential role of evasion from cell death in cancer.* Adv Cancer Res, 2011. **111**: p. 39-96.
42. Kondo, S., et al., *Mutations of the bak gene in human gastric and colorectal cancers.* Cancer Res, 2000. **60**(16): p. 4328-30.
43. Tagawa, H., et al., *Genome-wide array-based CGH for mantle cell lymphoma: identification of homozygous deletions of the proapoptotic gene BIM.* Oncogene, 2005. **24**(8): p. 1348-58.
44. Mestre-Escorihuela, C., et al., *Homozygous deletions localize novel tumor suppressor genes in B-cell lymphomas.* Blood, 2007. **109**(1): p. 271-80.
45. Soengas, M.S., et al., *Inactivation of the apoptosis effector Apaf-1 in malignant melanoma.* Nature, 2001. **409**(6817): p. 207-11.
46. Jeffers, J.R., et al., *Puma is an essential mediator of p53-dependent and -independent apoptotic pathways.* Cancer Cell, 2003. **4**(4): p. 321-8.
47. Hanahan, D. and R.A. Weinberg, *Hallmarks of cancer: the next generation.* Cell, 2011. **144**(5): p. 646-74.

48. Bedikian, A.Y., et al., *Dacarbazine with or without oblimersen (a Bcl-2 antisense oligonucleotide) in chemotherapy-naive patients with advanced melanoma and low-normal serum lactate dehydrogenase: 'The AGENDA trial'.* Melanoma Res, 2014.
49. Chen, L., et al., *Differential targeting of prosurvival Bcl-2 proteins by their BH3-only ligands allows complementary apoptotic function.* Mol Cell, 2005. **17**(3): p. 393-403.
50. Walensky, L.D., et al., *A stapled BID BH3 helix directly binds and activates BAX.* Mol Cell, 2006. **24**(2): p. 199-210.
51. Oltersdorf, T., et al., *An inhibitor of Bcl-2 family proteins induces regression of solid tumours.* Nature, 2005. **435**(7042): p. 677-81.
52. Billard, C., *BH3 mimetics: status of the field and new developments.* Mol Cancer Ther, 2013. **12**(9): p. 1691-700.
53. Shoemaker, A.R., et al., *A small-molecule inhibitor of Bcl-XL potentiates the activity of cytotoxic drugs in vitro and in vivo.* Cancer Res, 2006. **66**(17): p. 8731-9.
54. Moody, C.A. and L.A. Laimins, *Human papillomavirus oncoproteins: pathways to transformation.* Nat Rev Cancer, 2010. **10**(8): p. 550-60.
55. Stanley, M.A., M.R. Pett, and N. Coleman, *HPV: from infection to cancer.* Biochem Soc Trans, 2007. **35**(Pt 6): p. 1456-60.
56. Doorbar, J., *Molecular biology of human papillomavirus infection and cervical cancer.* Clin Sci (Lond), 2006. **110**(5): p. 525-41.
57. zur Hausen, H., *Papillomaviruses and cancer: from basic studies to clinical application.* Nat Rev Cancer, 2002. **2**(5): p. 342-50.
58. Hwang, E.S., T. Nottoli, and D. Dimaio, *The HPV16 E5 protein: expression, detection, and stable complex formation with transmembrane proteins in COS cells.* Virology, 1995. **211**(1): p. 227-33.
59. Zhang, B., D.F. Spandau, and A. Roman, *E5 protein of human papillomavirus type 16 protects human foreskin keratinocytes from UV B-irradiation-induced apoptosis.* J Virol, 2002. **76**(1): p. 220-31.
60. DiMaio, D. and D. Mattoon, *Mechanisms of cell transformation by papillomavirus E5 proteins.* Oncogene, 2001. **20**(54): p. 7866-73.
61. McDougall, J.K., *Immortalization and transformation of human cells by human papillomavirus.* Curr Top Microbiol Immunol, 1994. **186**: p. 101-19.
62. Werness, B.A., A.J. Levine, and P.M. Howley, *Association of human papillomavirus types 16 and 18 E6 proteins with p53.* Science, 1990. **248**(4951): p. 76-9.
63. Dyson, N., et al., *The human papilloma virus-16 E7 oncoprotein is able to bind to the retinoblastoma gene product.* Science, 1989. **243**(4893): p. 934-7.
64. Thomas, M. and L. Banks, *Inhibition of Bak-induced apoptosis by HPV-18 E6.* Oncogene, 1998. **17**(23): p. 2943-54.
65. Duensing, S. and K. Munger, *Mechanisms of genomic instability in human cancer: insights from studies with human papillomavirus oncoproteins.* Int J Cancer, 2004. **109**(2): p. 157-62.
66. Yuan, C.H., M. Filippova, and P. Duerksen-Hughes, *Modulation of apoptotic pathways by human papillomaviruses (HPV): mechanisms and implications for therapy.* Viruses, 2012. **4**(12): p. 3831-50.
67. Cai, Q., et al., *Human papillomavirus early proteins and apoptosis.* Arch Gynecol Obstet, 2013. **287**(3): p. 541-8.
68. Vogt, M., et al., *Inhibition of Bax activity is crucial for the antiapoptotic function of the human papillomavirus E6 oncoprotein.* Oncogene, 2006. **25**(29): p. 4009-15.
69. Aguilar-Lemarroy, A., et al., *Restoration of p53 expression sensitizes human papillomavirus type 16 immortalized human keratinocytes to CD95-mediated apoptosis.* Oncogene, 2002. **21**(2): p. 165-75.
70. Niebler, M., et al., *Post-translational control of IL-1beta via the human papillomavirus type 16 E6 oncoprotein: a novel mechanism of innate immune escape*

mediated by the E3-ubiquitin ligase E6-AP and p53. PLoS Pathog, 2013. **9**(8): p. e1003536.
71. Rincon-Orozco, B., et al., *Epigenetic silencing of interferon-kappa in human papillomavirus type 16-positive cells.* Cancer Res, 2009. **69**(22): p. 8718-25.
72. Meissner, J.D., *Nucleotide sequences and further characterization of human papillomavirus DNA present in the CaSki, SiHa and HeLa cervical carcinoma cell lines.* J Gen Virol, 1999. **80 (Pt 7)**: p. 1725-33.
73. Pattillo, R.A., et al., *Tumor antigen and human chorionic gonadotropin in CaSki cells: a new epidermoid cervical cancer cell line.* Science, 1977. **196**(4297): p. 1456-8.
74. Friedl, F., et al., *Studies on a new human cell line (SiHa) derived from carcinoma of uterus. I. Its establishment and morphology.* Proc Soc Exp Biol Med, 1970. **135**(2): p. 543-5.
75. Deng, J., et al., *BH3 profiling identifies three distinct classes of apoptotic blocks to predict response to ABT-737 and conventional chemotherapeutic agents.* Cancer Cell, 2007. **12**(2): p. 171-85.
76. Ryan, J. and A. Letai, *BH3 profiling in whole cells by fluorimeter or FACS.* Methods, 2013. **61**(2): p. 156-64.
77. McKenzie, M.D., et al., *Proapoptotic BH3-only protein Bid is essential for death receptor-induced apoptosis of pancreatic beta-cells.* Diabetes, 2008. **57**(5): p. 1284-92.
78. Albihn, A., et al., *Camptothecin-induced apoptosis is enhanced by Myc and involves PKCdelta signaling.* Int J Cancer, 2007. **121**(8): p. 1821-9.
79. Akao, Y., et al., *Ceramide accumulation is independent of camptothecin-induced apoptosis in prostate cancer LNCaP cells.* Biochem Biophys Res Commun, 2002. **294**(2): p. 363-70.
80. Sarosiek, K.A., et al., *BID preferentially activates BAK while BIM preferentially activates BAX, affecting chemotherapy response.* Mol Cell, 2013. **51**(6): p. 751-65.
81. Du, J., et al., *Resistance to apoptosis of HPV 16-infected laryngeal cancer cells is associated with decreased Bak and increased Bcl-2 expression.* Cancer Lett, 2004. **205**(1): p. 81-8.
82. Allen-Hoffmann, B.L., et al., *Normal growth and differentiation in a spontaneously immortalized near-diploid human keratinocyte cell line, NIKS.* J Invest Dermatol, 2000. **114**(3): p. 444-55.
83. Helle, S.C., et al., *Organization and function of membrane contact sites.* Biochim Biophys Acta, 2013. **1833**(11): p. 2526-41.
84. Kornmann, B., C. Osman, and P. Walter, *The conserved GTPase Gem1 regulates endoplasmic reticulum-mitochondria connections.* Proc Natl Acad Sci U S A, 2011. **108**(34): p. 14151-6.
85. Hell, S.W. and J. Wichmann, *Breaking the diffraction resolution limit by stimulated emission: stimulated-emission-depletion fluorescence microscopy.* Opt Lett, 1994. **19**(11): p. 780-2.
86. Voeltz, G.K., et al., *A class of membrane proteins shaping the tubular endoplasmic reticulum.* Cell, 2006. **124**(3): p. 573-86.
87. Friedman, J.R., et al., *ER sliding dynamics and ER-mitochondrial contacts occur on acetylated microtubules.* J Cell Biol, 2010. **190**(3): p. 363-75.
88. Vives-Bauza, C., et al., *PINK1-dependent recruitment of Parkin to mitochondria in mitophagy.* Proc Natl Acad Sci U S A, 2010. **107**(1): p. 378-83.
89. Pendin, D., J.A. McNew, and A. Daga, *Balancing ER dynamics: shaping, bending, severing, and mending membranes.* Curr Opin Cell Biol, 2011. **23**(4): p. 435-42.
90. Wurm, C.A., et al., *Nanoscale distribution of mitochondrial import receptor Tom20 is adjusted to cellular conditions and exhibits an inner-cellular gradient.* Proc Natl Acad Sci U S A, 2011. **108**(33): p. 13546-51.

91. Neumann, D., et al., *Two-color STED microscopy reveals different degrees of colocalization between hexokinase-I and the three human VDAC isoforms.* PMC Biophys, 2010. **3**(1): p. 4.
92. Donnert, G., et al., *Macromolecular-scale resolution in biological fluorescence microscopy.* Proc Natl Acad Sci U S A, 2006. **103**(31): p. 11440-5.
93. Gluzman, Y., *SV40-transformed simian cells support the replication of early SV40 mutants.* Cell, 1981. **23**(1): p. 175-82.
94. Chojnacki, J., et al., *Maturation-dependent HIV-1 surface protein redistribution revealed by fluorescence nanoscopy.* Science, 2012. **338**(6106): p. 524-8.

Acknowledgments – Danksagung

I would like to thank my supervisor Prof. Dr. Ana Garcia-Saez for giving me the opportunity to work in her group. Thank you Ana, for all your advice and your time, for valuable discussions, and all your help. I appreciate the encouragement to work on different projects enabling me to learn many different methods.

I would like to thank my group for all their help and support during my PhD time. A special thanks goes to Carolin Stegmüller for excellent technical support. I also very much appreciate the collaboration with Dr. Stephanie Bleicken and for the opportunity to support her project with experiments leading to a joint publication. But moreover, I would like to thank her for all the advice in the laboratory especially on protein purification but also for all the valuable discussions about my other projects and especially for her help reviewing my manuscript on the BH3 profiling project. Furthermore, I would like to thank Raquel Salvador for our collaboration supporting my project with Western blots of the Bcl-2 proteins. I would also like to thank all the other group members for generating a productive work atmosphere, helpful discussions and all their support: Dr. Katia Consentino, Eduard Hermann, Dr. Yamunadevi Subburaj, Dr. Begona Ugarte, Joseph Unsay, and Dr. Monika Zelman.

Furthermore, I would like to thank my collaborators. For the collaboration in the BH3 profiling project I would like to thank the members of the Infection and Cancer group, Division of Viral Transformation Mechanisms at the DKFZ, Heidelberg, Dr. Bladimiro Rincon-Orozco and Prof. Dr. Frank Rösl. A special thanks goes to Regina Ly for excellent technical support. I would also like to thank the lab members who supported me with all kinds of help in the lab and a nice working atmosphere: Dr. Martina Niebler, Dr. Vlada Kogosov, Dr. Rainer Zawatsky and Daniel Hasche. I would also like to thank my collaborators of the Division of Optical Nanoscopy at the DKFZ, Heidelberg, especially Dr. Jasmin Zahn for all her work on the microscope and image analysis. A sincere thanks to Prof. Dr. Stefan Hell for enabling the collaboration and thus giving me the opportunity to get an exciting insight into the world of high resolution microscopy. Furthermore, I am very grateful for all the help of Dr. Johann Engelhard always handling and managing all kinds of problems with the STED setup. But I am especially thankful to the group of Optical Nanoscopy for integrating me into their group when my group left to Tübingen. I am not only grateful for a nice place to work but especially for making me part of their group supporting me during the writing process of my thesis, giving me new energy during enjoyable breaks, lunches, and Weißwurst, cake, and breakfast parties.

I would also like to thank Dr. Karsten Thierbach from the BZH, Biochemistry Center of the University of Heidelberg for all his help and know-how for the work with yeast in the fight to purify Mitofusins which unfortunately did not make it into my thesis.
My sincere thanks also goes to PD Dr. Karsten Rippe and Prof. Dr. Thomas Söllner. Thank you very much, Karsten, for all your advice and support. Thank you very much, Thomas, especially for all your advice and time discussing about purification of Mitofusins. Furthermore I would like to thank Prof. Dr. Stephan Frings and Dr. Rainer Zawatsky for being part of my defense committee.
I would also like to thank my students Felix Wertek, Vasha Liluashvili, and Lucia Cocera for all their hard work and support of my projects.
I thank the DKFZ graduate school for selecting me into their program and proving me with a PhD stipend.
Last but not least my personal gratitude goes to my friends and family. Thank you so much for making my time as a PhD student enjoyable, helping me through tough times, giving me advice and support and being there for me when I needed you. Thank you Yamuna, Babi, Vipin, Bella, Franzi, Jenny, Ansam, Marie, Kerstin, Anke, Yasser, Stefan and especially Jasmin. I would particularly like to thank Sigrid not only for being a great friend but also for all her help revising my thesis and always motivating me to go on when I was about to give up. My special thanks goes to my family who is always there for me. Mama und Papa, ich kann mir keine besseren Eltern vorstellen. Durch euch habe ich es hierher geschafft. Mit euch kann ich meine Freuden und mein Leid teilen, ihr habt mich zu dem gemacht, was ich bin und ihr seid immer für mich da. Dafür bin ich euch unendlich dankbar! And what would I do without my sister? Jenny, keiner versteht mich wie du, mit dir kann ich lachen und weinen. Ich bin so unendlich froh, dass es dich gibt und dass wir unseren Lebensweg gemeinsam bestreiten. Danke, dass du bist, wie du bist und mich einfach immer und in allem unterstützt.

With the help of all those people I made it until the end of my PhD. Thank you for your motivation, inspiration and help!